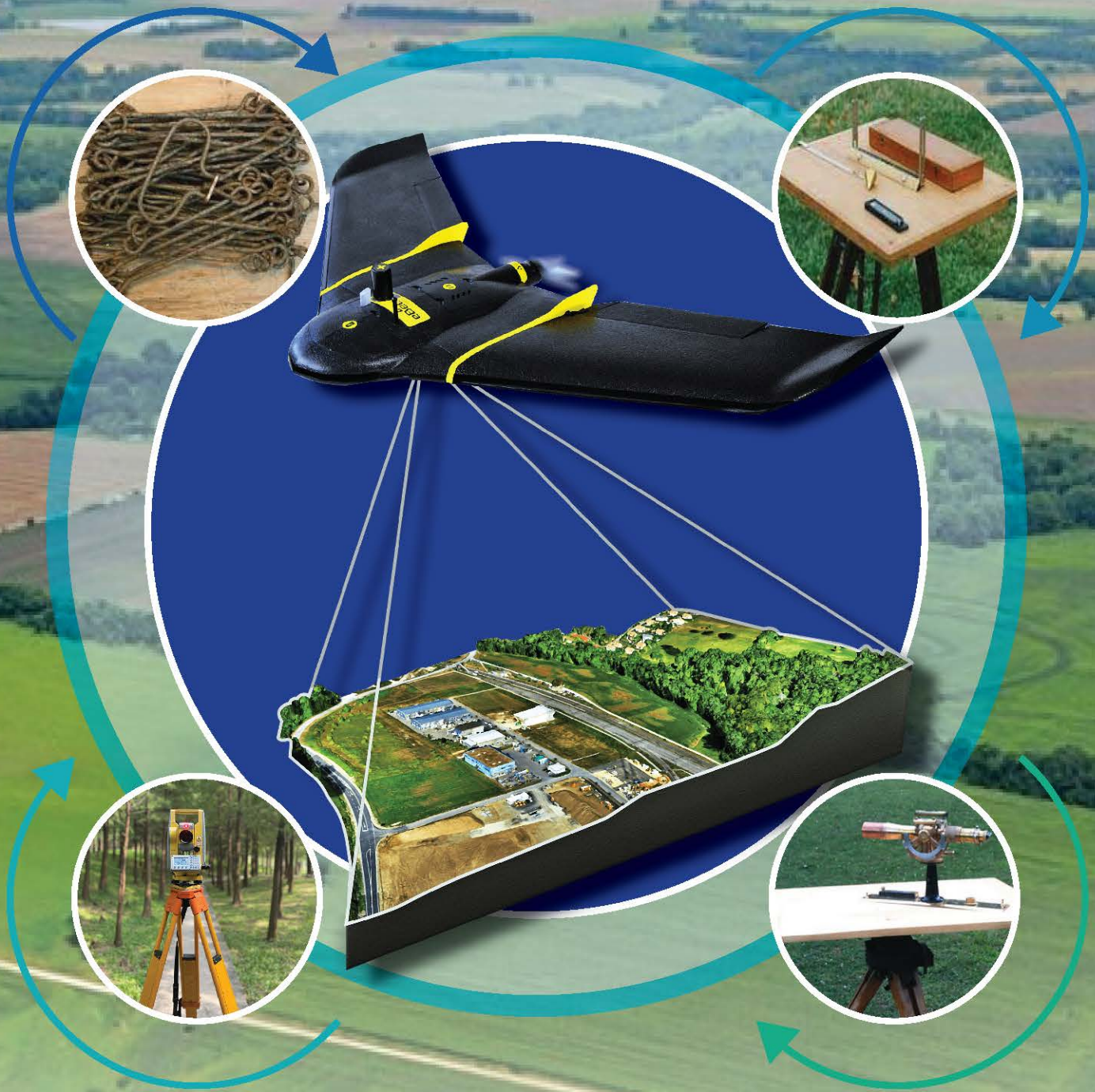


JOURNAL ON GEOINFORMATICS

Nepal

Number: 24

Jestha 2082 (May 2025)





Land Ownership Certificate distribution by Rt. Hon. Prime Minister at Gauradaha Municipality, Jhapa.



Delegation team from Korea Land and Geospatial InformatiX Corporation (LX) to Survey Department.



FIG president Diane A Dumashie visiting Survey Department.



Deputy Director General Mr. Susheel Dangol, Director Mr. Tanka Prasad Dahal, Survey Officers Girija Pokharel, Kapil Katuwal and Sahadev Ghimire organizing orientation program about international boundary at Koshi Province for APF staff.

Journal on Geoinformatics

Nepal

Number : 24

Jestha 2082 BS
May 2025 AD

Annual publication of Survey Department, Government of Nepal

The content and the ideas of the articles are solely of authors.

Published by:
Government of Nepal
Ministry of Land Management, Cooperatives & Poverty Alleviation
Survey Department
Min Bhawan, Kathmandu
Nepal

No. of copies : 500

© *Copyright reserved by Survey Department*

FOREWORDS



Survey Department with great honor present the 24th issue of the *Journal on Geoinformatics Nepal*, the esteemed annual publication of the Department. Over the years, this journal has served as an invaluable platform for knowledge sharing, research dissemination, and technological advancements in geoinformatics, contributing to the development and modernization of spatial sciences in Nepal.

Geoinformatics has evolved rapidly, transforming the way we collect, analyze, and utilize geospatial data for national planning, environmental sustainability, disaster management, and infrastructure development. As Nepal continues to embrace digital transformation, the integration of geospatial technology has become more essential than ever in supporting evidence-based decision-making and fostering innovation across various sectors. In this regard, the Survey Department, as the National Mapping Agency, has been continuously working to define a spatial reference frame, conduct large-scale topographic mapping, and perform cadastral mapping using UAV technology and orthophotos.

This issue showcases a diverse range of articles from experts, researchers, and practitioners in the field, reflecting the latest advancements in land surveying, GIS applications, remote sensing technologies, and spatial data management. These contributions reinforce our collective commitment to harnessing geoinformatics for sustainable development and technological progress.

I extend my sincere appreciation to all the authors, reviewers, and editorial team members whose dedication has made this publication possible. Your efforts ensure that *Journal on Geoinformatics Nepal*

remains a vital resource for professionals and academics engaged in geospatial sciences.

As we move forward, let us continue to collaborate, innovate, and advance the field of geoinformatics in Nepal. I encourage readers to engage with the insights presented in this issue and contribute further to this ever-evolving discipline.

Thank you for your continued support, and I look forward to witnessing the positive impact of geospatial technologies in shaping Nepal's future.

Enjoy Reading!

Thank you!

Prakash Joshi

Director General

lightjoshiji@gmail.com

EDITORIAL



Dear Readers,

It is with great pleasure that we present to you the 24th issue of the Journal on Geoinformatics Nepal, the annual publication of the Survey Department. Over the years, this journal has served as a platform to showcase groundbreaking research, technological advancements, and insightful discussions in the field of geoinformatics, contributing to the ongoing evolution of spatial science in Nepal and beyond.

This edition brings together a diverse collection of articles from esteemed professionals, researchers, and academics, highlighting the latest innovations, challenges, and applications of geospatial technology. From land surveying methodologies to remote sensing advancements, spatial data infrastructure, and GIS applications in various sectors, the contributions in this issue reflect the dynamic progress of geoinformatics and its role in shaping informed decision-making.

As technology continues to reshape the way we understand and interact with our environment, the Survey Department remains committed to fostering knowledge, collaboration, and the dissemination of valuable research within the geospatial community. We extend our heartfelt gratitude to all the contributors, reviewers, and editorial team members whose dedication has made this publication possible.

We invite you to explore the articles within this issue, engage with the insights presented, and join us in advancing the future of geoinformatics in Nepal. Your continued support and contributions inspire us to push the boundaries of knowledge and innovation.

Thank you for being a part of this journey, and we look forward to your valuable feedback and engagement in future editions.

Warm regards,

Karuna K.C.

Editor-in Chief,

Jestha, 2082 (May 2025)

Advisory Council



Prakash Joshi
Chairperson



Karuna K.C.
Member



Susheel Dangol
Member



Krishna Prasad Sapkota
Member



Narayan Regmi
Member

Editorial Board



Karuna K.C.
Editor-in-Chief



Bikash Kumar Karna (Ph.D.)
Member



Tanka Prasad Dahal
Member



Damodar Dhakal
Member

Product Price

Maps

Page 67

Control Points

Page 67

CORS Station Data

Page 67

Geoid Data

Page 67

Price of Aerial Photograph

Page 32

Land Use Digital Data

Page 32

Price of Printed Maps

Page 32

Digital Orthophoto Image Data

Page 32

Digital Topographical Data

Page 32

LiDAR Data

Page 32

List of Paper Reviewer

Susheel Dangol

Ajit Kunwar

Bikash Kumar Karna (Ph. D.)

Harisharan Nepal

Khim Lal Gautam

Sanjeevan Shrestha

Sudip Shrestha

Cover Concept

Technological development of
cadastral survey

Features

Articles

- 1 **Accuracy Assessment of Open-Source DEM: A Case for Nepal**
Tanka Prasad Dahal & Susheel Dangol
Page 1
- 2 **Comparative Assessment of Archaeological Scene Reconstruction Using Iphone LIDAR Scanner**
Binod Prasad Bhatta, Abishek Shah, Man Kumari Chaulagain, Aagya Dhungana, Lalit Mandal, Punam Koirala, Shangharsha Thapa & Uma Shankar Panday
Page 9
- 3 **Comparison of Deep Learning Models with Different Backbones for Building Footprints Extraction in Dense Residential Areas of Bhaktapur**
Abin Prajapati & Romik Gosai
Page 21
- 4 **Evaluating Machine Learning Algorithms for Forest Cover Extraction in Kailali, Nepal**
Sudarshan Kumar Gautam, Sanjeevan Shrestha, Subhadra Joshi & Jeshan Pokharel
Page 33
- 5 **Flood Hazard Modelling Assessment Using Deep Learning and Earth Observation**
Binita Shahi, Arjun Poudel, Ashmeera Dahal & Sandesh Upadhyaya
Page 41

Contents

Contents

Professional Organization Pages	Nepal Remote Sensing and Photogrammetric Society Page 68
	Nepal Surveyor's Association (NESA) Page 76
	Nepal Geomatics Engineering Society (NGES) Page 104
Regular Column	Forewords Page iii
	Editorial Page v
	Obituary Page 20
	Call for Papers Page 48
	Calender of International Events Page 58
Informations	Instruction and Guidelines for Authors Regarding Manuscript Preparation Page 62

Contents

6	Integrating GIS and AHP for Forest Fire Risk Mapping in Kailali, Nepal <i>Ganesh Pandey & Daman Neupane</i> Page 49
7	Developing New National Geodetic Reference Frame of Nepal <i>Narayan Regmi, Sandesh Upadhyaya, Manisha Thapa, Shiva Prasad Lamsal & Suraj Bahadur KC</i> Page 59
8	Multi-Modal Image Synthesis with Attention Conditional GANs: SAR, Optical, and DEM <i>David Nhemaphuki, Ajay Kumar Thapa & Umesh Bhurtyal</i> Page 69
9	Present Land Use and Land Use Zoning of Kushma Municipality: A Comparative Assessment with Cadastral Superimpose <i>Sushmita Subedi, Roman Pandit, Manoj G.C. & Indra Subedi</i> Page 77
10	Remeasuring Annapurna I: Geospatial Innovation and the Quest for Precision <i>Er. Khim Lal Gautam & Suraj Bahadur K.C.</i> Page 93

Accuracy Assessment of Open-Source DEM: A Case for Nepal

Tanka Prasad Dahal¹ & Susheel Dangol¹
tpdahal@gmail.com, Susheel.dangol@nepal.gov.com
¹Survey Department

KEYWORDS

Accuracy Assessment, Open Source, DEM

ABSTRACT

Digital representation of the earth topography is called Digital Elevation Model (DEM). DEMs are very useful for disaster assessment, 3D modelling, infrastructure planning and other development activities. There are various satellite systems providing the DEMs with different spatial resolution freely. This study assesses the reliability of the freely available DEMs while using those data for decision making. Reference elevation point data are taken from the topographical base map of the respective area. Statistical calculation was carried out for the testing reliability of the data. Root Mean Square Error (RMSE), Standard Deviation and Mean deviation are calculated to conduct the accuracy assessment. From the study, it is seen that, ALOS PRISM DEM of 30m resolution gave the precise result based on RMSE with the value of 5.9m in comparison to other five DEMs used in this study.

1. INTRODUCTION

“A map is a symbolized representation of geographic reality, representing selected features or characteristics, resulting from the creative effort of its author’s execution of choices, and is designed for use when spatial relationships are of primary relevance.” (ICA, 2003). With the views that the map should include traditional and modern maps, real and virtual maps like web maps, 3D maps, animated maps and globe etc., new definition of map was given by Lapaine *et al.* (2021) as “A map is a medium designed for communication of generalized spatial information and relationships”.

Maps can serve as data brain for different applications (Li *et al.*, 2024). Map represents

the ground features in pictorial format through symbols. Map can have 2-dimensional or 3-dimensional or both information. Planimetric maps only have 2D information whereas topographical maps holds both 2D and 3D features. 2D maps only gives the information of “x” and “y” position of the objects and the 3D gives the “z” value as well. In 2D maps, the details are represented with symbols. On the other hands, 3D information is shown with different forms like contour, hachure, hill shade, spot height, TIN, DEM. 3D maps gives the perspective of 3 dimensions even the landscape is shown in 2-dimensional media (Christian, 2002).

The topography of earth surface can be

represented digitally in the form of Digital Elevation Model (DEM), Triangulated Irregular Network (TIN) and contour based model (Jalal *et al.*, 2020). DEM comprises of two main categories: one is Digital Terrain Model (DTM) which represent earth surface without any natural or manmade structure and another is Digital Surface Model (DSM) which represent ground surface as well as all natural and manmade structured on the ground (Abili, 2021).

The paper is the study on accuracy assessment of different open-source DEM.

2. SOURCE OF DEM

DEM is the representation of squared cells called as pixel where each pixel has elevation value (Manuel, 2004). It is the symbolization of height information of the earth surface (Hasan, 2019) or the digital representation of the ground topography which can be created with different technology and methods with varying accuracies depending on the method adopted (Farah *et al.*, 2008; Mukherjee *et al.*, 2013) and every methods has its own advantages and disadvantages (Elsonbaty *et al.*, 2023).

2.1. Generation of DEM

Traditional methods like levelling, topographical mapping with total station, stereo photographs were used to generate DEM (Abili, 2021; Hasan, 2019). However, these kinds of traditional methods are expensive whereas DEM generation from GNSS technology gives cost effective solution among other advanced technologies like laser scanning, radar interferometry etc. (Farah *et al.*, 2008). Emerging UAV technology together with photogrammetry can also generate cost effective and accurate DTM (Jiménez-Jiménez *et al.*, 2021). DEM can also be generated automatically from aerial and satellite images by image processing methodologies (Krupnik, 2000).

Height information can be derived from the contour lines of topographic maps, spot heights, photogrammetry and also field surveys and generate the DEM from this information (Jalal *et al.*, 2020). Contours have the properties of consecutive equivalence in height information along its line and also the topological property, they are considered as suitable feature lines to generate DEMs (Li *et al.*, 2017). Basically, DEMs can be generated from contour lines of topographic maps, field surveys, stereo photographs/photogrammetry, radar interferometry and laser altimetry (Manuel, 2004).

2.2. Open-source DEM

Besides generation of DEM from secondary data or field observation, there are also freely available DEM available which were generated from different methods. The Shuttle Radar Topographic Mission (SRTM) of 30m x 30m resolution is the most popular Global DEM freely available from the National Aeronautics and Space Administration (NASA) and TerraSAR-X with approximate resolution of 90m x 90 m) is another freely available DEM which represents the bare Earth surface. (Jalal *et al.*, 2020). Advanced Land Observation Satellite Phased Array L-band Synthetic Aperture Radar (ALOS PALSAR 12.5 m) is the most precise GDEM which is freely available (Halim *et al.*, 2019). ASTER and SRTM DEM are most widely used DEMs and ALOS AW3D30 and TanDEM-X are gaining popularity in different field (Han *et al.*, 2021; Liu *et al.*, 2022).

3. ACCURACY ASSESSMENT REVIEW

Quantitative analysis like statistics and accuracy metrics, and qualitative analysis like visual inspection are often used for DEM accuracy evaluation (Wise, 2007). However, the quality of DEM is defined by different factors like terrain type, algorithm, grid spacing & characteristics as well as sensor

types (Hebeler & Purves, 2009) and also the result of quality assessment depends on source of data, resolution of DEM, distribution of GCP used as reference and topography (Toz & Erdogan, 2008). Further, large number of reference check points with high accuracy are required to compute the DEM RMSE with some reliability (Aguilar *et al.*, 2007). Elsonbaty *et al.* (2023) accessed five freely available DEMs, ASTER GDEM2, SRTM 90 m, SRTM 30 m, Sentinel 1, and TanDEM-X 90 m with the reference of GNSS observation. Statistical evaluation of the five DEMs shows the Root Mean Square (RMSE) of ± 20.25 m, ± 3.56 m, ± 57.68 m, ± 10.21 m, and ± 5.89 m for Advanced Spaceborne Thermal Emission and Reflection Radiometer (ASTER), SRTM 30, SENTINEL 1, TanDEM-X, and SRTM3 respectively showing the highest accuracy of SRTM 90 among the five (Elsonbaty *et al.*, 2023). Study by Jalal *et al.* (2020) shows the RMSE of ± 7.3 m, ± 7.6 m and ± 6.5 m checked with the reference of 12 fixed Ground Control Points (GCPs) for the ALOS PALSAR (12.5 m), the SRTM (30 m) and the TerraSAR-X respectively.

Similarly, comparison of freely created DEM from Google Earth, SRTM 30 and ASTER GDEM shows the RMSE of ± 6.9 m, ± 5.5 m and ± 4.8 m respectively for the case of Iraq (Hasan, 2019). Accuracy assessment of open source DEMs, SRTM 30, ALOS and ASTER GDEM showed the RMSE of ± 4.63 m, ± 5.25 and ± 11.18 m in the study area of Adama City, Ethiopia showing the higher accuracy of SRTM in comparison to ALOS DEM and ASTER GDEM (Abili, 2021). Similar type of study between ASTER and SRTM DEM shows the RMSE of 12.62 m and 17.76 m respectively for both (Mukherjee *et al.*, 2013). Accuracy assessment of ALOS W3D30, ASTER GDEM and SRTM 30 done for the case of Nigeria shows the high accuracy of ALOS W3D30 with the RMSE value of 5.4 m against 7.47m and 20.03 m RMSE of SRTM and ASTER

respectively (Apeh *et al.*, 2019). Accuracy assessment of open source global DEM against GNSS levelling shows that TanDEM-X shows the smallest RMSE of 2.574 m compared to SRTM30, SRTM90, ASTER, GMTED10, and ALOS W3D with RMSE of 2.968 m, 3.006 m, 3.217 m, 2.975 m, and 2.876 m respectively (Abd Rahman *et al.*, 2022) Similarly, accuracy assessment of ALOS AW3D30 and ALOS PRISM against contour data shows that AW3D30 DSM presents two or three times lower Root Mean Square Error (RMSE) than the respective DSMs from ALOS PRISM images (Konstantinos, 2020).

Though there are many research on examination of vertical accuracy of DEM, there is always enough scope of research since the accuracy vary for different landscape (Mukherjee *et al.*, 2013). Also, majority of the research on assessment of accuracy of DEM are based on point type reference data rather than linear and surface data expanding the scope of more research with standardized assessment methods (Mesa-Mingorance & Ariza-López, 2020)

4. METHODOLOGY

Kavrepalanchok district of Nepal was selected for the study (Figure 1). Openly accessible global DEM for the study area were downloaded from different source. Contour and spot height from existing base map of 1:25000 scale was used as reference data for validation.

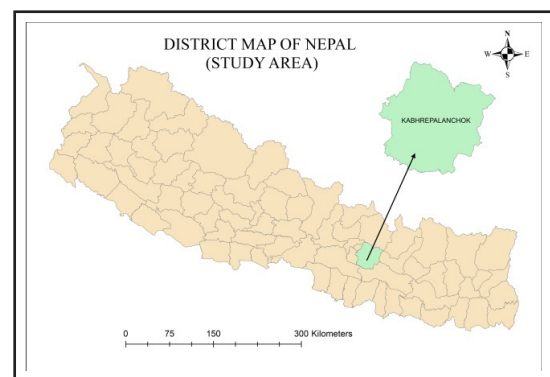


Figure 1: Study Area Map

4.1. Open-Source DEM Used for Analysis

Six open-source DEM were used for this study. The DEM used were ALOS PALSAR (12.5 m), CartoDEM V3 R1 (30 m), ASTER GDEM V2 (30 m), SRTM (30m), ALOS PRISM (30m), TanDEM-X (90 m). The major characteristics are shown in Table 1

Table 1: Specifications of DEM use for study

S. No.	DEM	Method of DEM	Vertical Datum	Spatial Resolution
1	PALSAR	RADAR	EGM96	12.5 m
2	Carto DEM	Optical Sterio	WGS84	1 arc second
3	PRISM	Optical Sterio	EGM96	1 arc second
4	SRTM	RADAR	EGM96	1 arc second
5	ASTER	Optical Sterio	EGM96	1 arc second
6	TanDEM-X	RADAR	WGS84	3 arc second

4.2. Methodology

DEM of the study area were downloaded. For the validation of the height value, reference points were collected from the topographical base map. The validation points were selected on the basis of contour value and the spot height shown in the topographical maps. The height generated for validation points were converted to global datum as per the datum of the DEM to be validated. For every point selected for validation, height value from DEM was extracted. Then after, statistical analysis was done to find the RMSE and deviations. The flow diagram of methodology is shown in Figure 2.

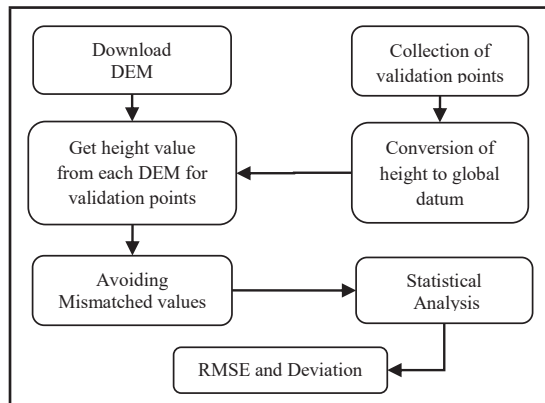


Figure 2 : Study Methodology

4.3. Data Analysis

Total 44 reference points for validation were extracted from 1:25000 scale topographical base map. Data analysis was carried out in GIS environment using reference points as vector data and DEMs as raster data. The extraction of height from DEMs to reference data was carried out using Extract Multi Values to Points tool available in ArcGIS 10x. Since vertical datum of openly accessible DEMs were not same, 'GeoidEval utility' was used for online calculation of Geoid undulation for conversion from orthometric height to Ellipsoid height (WGS84). Minimum elevation is 367 m and maximum elevation is 2682 m.

The statistical calculation for the mean deviation and RSME was done using MS-Excel. The scatter plot and charts were also produced by using Excel. During the calculation of RMSE, the difference value of map height to the DEMs height greater than 20 meters are assumed to be gross errors and hence, those points are removed during calculation assuming that height of the building and vegetation should not be more than 20m for those sample areas.

5. RESULT AND DISCUSSION

RMSE for each DEM, mean deviation of height derived from DEM and reference as well as standard deviation for the same values were calculated. Table 2 shows the results of statistical analysis.

Table 2: Statistical analysis result.

S.N.	DEM	RMSE	Mean Deviation	Standard Deviation
1	PALSAR	6.4	5.64	5.81
2	Cartosat	11.4	5.79	7.59
3	SRTM	6.6	5.26	6.13
4	ASTER	12.5	10.22	7.85
5	PRISM	5.9	5.28	6.58
6	TanDEM	11.3	8.03	8.22

The analysis shows that, among six DEMs the least RMSE value is 5.9m for ALOS PRISM 30m spatial resolution. Similarly,

least mean deviation is 5.26 m for SRTM and least standard deviation is 5.81m for ALOS PALSAR.

The scatter plot for all reference data and height from DEMs shown that there is a good linear relationship between them. The Figure 3 showed the linear relationship between the reference elevation data and each DEM in Nepal.

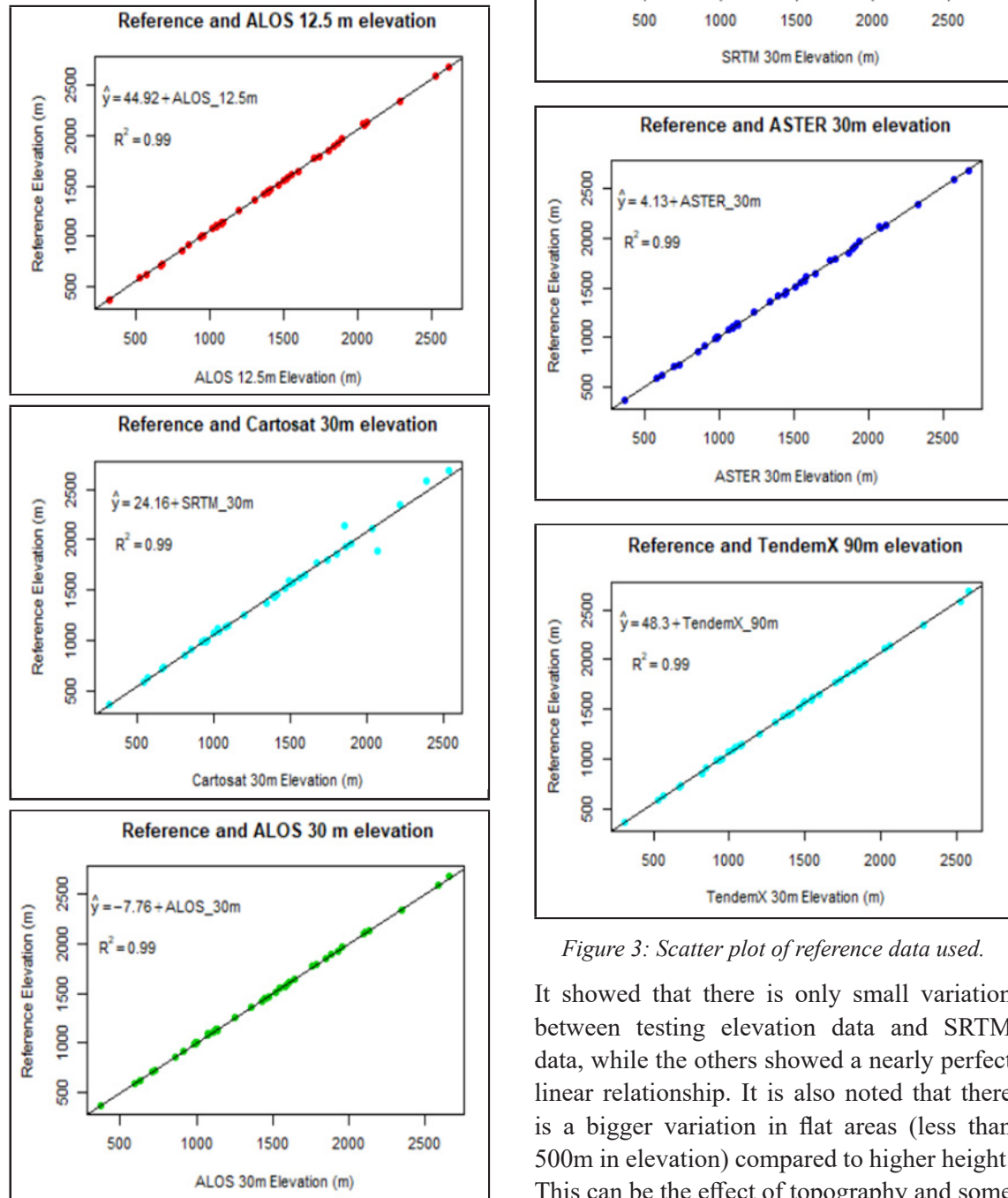


Figure 3: Scatter plot of reference data used.

It showed that there is only small variation between testing elevation data and SRTM data, while the others showed a nearly perfect linear relationship. It is also noted that there is a bigger variation in flat areas (less than 500m in elevation) compared to higher height. This can be the effect of topography and some

errors in the DEM. 99% of variations in the model can be explained by DEMs ($R^2 = 0.99$), which showed that there is a very small difference between openly accessible DEMs and assumed true values.

6. CONCLUSION & RECOMMENDATIONS

There are various satellite systems which provide openly accessible global DEMs generated by various technologies. The validation samples are taken from the topographical base map of scale 1:25000. The height provided in different DEMs are in different vertical datum those heights are converted to ellipsoidal height using Online geoid calculations using the GeoidEval utility with geoid undulation for each reference sample points based on latitude and longitude.

The RMSE calculation shows that the ALOS PRISM DEM 30m spatial resolution having RMSE value 5.9m is the best DEM among the six DEMs for study area. RMSE value of the ALOS PALSAR having 6.4 seems to be less accurate than the ALOS PRISM DEM having 12.5m spatial resolution. This study is expected to provide the public users as a reference so that they can choose the “best” openly accessible DEMs as per requirement. Further, secondary data extracted from the topographical base maps were used for validation of DEMs. However, it is recommended to use primary field data for validation of the DEMs which is better compared to the use of validation points from topographical map of scale 1:25000.

REFERENCES

- Abd Rahman, M. F., Din, A. H. M., Abd Hamid, A. I., Alihan, N. S. A., Yazid, N. M., Ansar, A. M. H., Pa’Suya, M. F., Yamen, S. N. M., Khalid, N. F., & Junid, M. A. H. (2022). Accuracy Assessment of Open-source Global Digital Elevation Models (GDEMs) with Global Navigation Satellite System (GNSS) Levelling. *IOP Conference Series: Earth and Environmental Science*, 1064, 012018.
- Abili, H. Z. (2021). Comparison of Vertical Accuracy of Open-Source Global Digital Elevation Models: A Case Study of Adama City, Ethiopia. *Turkish Journal of Computer and Mathematics Education (TURCOMAT)*, 12(4), 1731-1744.
- Aguilar, F. J., Agüera, F., & Aguilar, M. A. (2007). A Theoretical Approach to Modeling the Accuracy Assessment of Digital Elevation Models. *Photogrammetric Engineering & Remote Sensing*, 73(12), 1367-1379.
- Apeh, O. I., Uzodinma, V. N., Ebinne, E. S., Moka, E. C., & Onah, E. U. (2019). Accuracy Assessment of ALOS W3d30, ASTER GDEM and SRTM30 DEM: A Case Study of Nigeria, West Africa. *Journal of Geographic Information System*, 11(2), 111-123.
- Christian, H. (2002). 3D Map Presentation: A Systematic Evaluation of Important Graphic Aspects. *Proceedings of ICA Mountain Cartography Workshop" Mount Hood, 11*.
- Elsonbaty, L., Fawzy, H. E.-D., Moghazy, H. M., Rashed, G., & Hamed, M. (2023). Vertical Accuracy Assessment for Open-Source Digital Elevation Models using GPS Control Points and Watershed Basins Delineation Using GIS. *Alexandria Engineering Journal*, 84, 47-58.
- Farah, A., Talaat, A., & Farrag, F. (2008). Accuracy Assessment of Digital Elevation Models using GPS. *Artificial Satellites*, 43(4), 151-161.

- Halim, S. M. A., Green, M. F. P., Narashid, R. H., & Din, A. H. M. (2019). Accuracy Assessment of TanDEM-X 90 m Digital Elevation Model in East of Malaysia Using GNSS/Levelling. 2019 IEEE 10th Control and System Graduate Research Colloquium (ICSGRC),
- Han, H., Zeng, Q., & Jiao, J. (2021). Quality Assessment of TanDEM-X DEMs, SRTM and ASTER GDEM on Selected Chinese Sites. *Remote Sensing*, 13(7), 1304.
- Hasan, R. H. (2019). Evaluation of the Accuracy of Digital Elevation Model Produced from Different Open Source Data. *Journal of Engineering*, 25(8), 100-112.
- Hebeler, F., & Purves, R. S. (2009). The Influence of Elevation Uncertainty on Derivation of Topographic Indices. *Geomorphology*, 111(1), 4-16. <https://doi.org/https://doi.org/10.1016/j.geomorph.2007.06.026>
- ICA. (2003). Strategic Plan 2003-2011. In. https://ica.org/files/documents/reference_docs/ICA_Strategic_Plan_2003-2011.pdf: International Cartographic Association.
- Jalal, S. J., Musa, T. A., Ameen, T. H., Din, A. H. M., Aris, W. A. W., & Ebrahim, J. M. (2020). Optimizing the Global Digital Elevation Models (GDEMs) and Accuracy of Derived DEMs from GPS Points for Iraq's Mountainous Areas. *Geodesy and Geodynamics*, 11(5), 338-349. <https://doi.org/https://doi.org/10.1016/j.geog.2020.06.004>
- Jiménez-Jiménez, S. I., Ojeda-Bustamante, W., Marcial-Pablo, M. d. J., & Enciso, J. (2021). Digital Terrain Models Generated with Low-cost UAV Photogrammetry: Methodology and Accuracy. *ISPRS International Journal of Geo-Information*, 10(5), 285.
- Konstantinos, G. N. (2020). Accuracy Assessment of ALOS AW3D30 DSM and Comparison to ALOS PRISM DSM Created with Classical Photogrammetric Techniques. *European Journal of Remote Sensing*, 53, 1-14. <https://doi.org/10.1080/22797254.2020.1774424>
- Krupnik, A. (2000). Accuracy Assessment of Automatically Derived Digital Elevation Models from SPOT Images. *Photogrammetric Engineering and Remote Sensing*, 66(8), 1017-1023.
- Lapaine, M., Midtbø, T., Gartner, G., Bandrova, T., Wang, T., & Shen, J. (2021). Definition of the Map. *Advances in Cartography and GIScience of the ICA*, 3, 1-6.
- Li, B., Guo, Y., Zhou, J., Tang, Y., Dong, Q., & Li, Z. (2024). Development and Prospects of High Definition Map for Intelligent Vehicle. *Geomatics and Information Science of Wuhan University*, 49(4), 491-505. <https://doi.org/10.13203/j.whugis20230287>
- Li, X., Shen, H., Feng, R., Li, J., & Zhang, L. (2017). DEM Generation from Contours and a Low-Resolution DEM. *ISPRS Journal of Photogrammetry and Remote Sensing*, 134, 135-147. <https://doi.org/https://doi.org/10.1016/j.isprsjprs.2017.09.014>
- Liu, X., Ran, M., Xia, H., & Deng, M. (2022). Evaluating Vertical Accuracies of Open-Source Digital Elevation Models over Multiple Sites in China Using GPS Control Points. *Remote Sensing*, 14(9), 2000.

- Manuel, P. (2004). Influence of DEM Interpolation Methods in Drainage Analysis. *GIS Hydro*, 4.
- Mesa-Mingorance, J. L., & Ariza-López, F. J. (2020). Accuracy Assessment of Digital Elevation Models (DEMs): A Critical Review of Practices of the Past Three Decades. *Remote Sensing*, 12(16), 2630.
- Mukherjee, S., Joshi, P. K., Mukherjee, S., Ghosh, A., Garg, R. D., & Mukhopadhyay, A. (2013). Evaluation of Vertical Accuracy of Open Source Digital Elevation Model (DEM). *International Journal of Applied Earth Observation and Geoinformation*, 21, 205-217. <https://doi.org/https://doi.org/10.1016/j.jag.2012.09.004>
- Toz, G., & Erdogan, M. (2008). DEM (Digital Elevation Model) Production and Accuracy Modeling of DEMs from 1: 35.000 Scale Aerial Photographs. *The International Archives of the Photogrammetry Remote Sensing and Spatial Information Sciences*, 37, 775-780.
- Wise, S. M. (2007). Effect of Differing DEM Creation Methods on the Results from a Hydrological Model. *Computers & Geosciences*, 33(10), 1351-1365. <https://doi.org/https://doi.org/10.1016/j.cageo.2007.05.003>



Author's Information

Name	: Tanka Prasad Dahal
Academic Qualification	: Master's Degree in Land Administration, Kathmandu University
Current Designation	: Director
Work Experience	: 29 years

Comparative Assessment of Archaeological Scene Reconstruction Using Iphone LIDAR Scanner

Binod Prasad Bhatta¹, Abishek Shah¹, Man Kumari Chaulagain¹, Aagya Dhungana¹, Lalit Mandal¹,
Punam Koirala¹, Shangharsha Thapa², Uma Shankar Panday¹

¹Department of Geomatics Engineering, Kathmandu University, Dhulikhel, Nepal
(prasad.binodbhatta11@gmail.com, sahabishek5@gmail.com, chaulagainasmita7@gmail.com,
agyadhungana94@gmail.com, lalitkumarmandal0000@gmail.com, poonamokoirala333@gmail.com,
uspanday@ku.edu.np)

²Lund University, Sweden (shangharsha.thapa@nateko.lu.se)

KEYWORDS

iPhone, LiDAR, point cloud, mesh, 3D reconstruction, archaeology

ABSTRACT

Archaeological sites hold immense economic value for Nepal, contributing to income and overall economic growth. These sites are susceptible to damage from both human activities and natural factors, needing swift and cost-effective reconstruction efforts. In addressing this challenge, 3D scene reconstruction emerges as a crucial reverse engineering method. Various techniques, such as LiDAR and Photogrammetry, are used for this purpose. While LiDAR offers precise models, its high cost has limited its accessibility. A notable development in this context has been achieved due to the introduction of consumer-grade LiDAR sensors, particularly with the integration of such sensors into iPhones. The primary focus of this research revolves around assessing the efficacy of consumer-grade LiDAR sensors in archaeological scene reconstruction. Utilizing the SiteScape and 3D Scanner apps, several tests with various settings were conducted to generate point clouds of the studied archaeological structures. The obtained point clouds were analyzed to assess point density variations across various application settings. Meshes were generated from these point clouds and the measurements were then taken from digital meshes which are compared with in-situ measurements, allowing for the calculation of relative error. Measurements obtained through SiteScape displayed a maximum difference of 4.17% and a minimum difference of 0.05%. In contrast, the 3D Scanner exhibited a maximum difference of 6.22% and a minimum difference of 0.09%. The findings suggest that the SiteScape app provides a higher point density and a higher accuracy than the 3D Scanner.

1. INTRODUCTION

Archaeology is the study of human cultures using material evidence to explain the origins and development of civilizations (Hussain & Will, 2021). Archaeological sites are subjected to deterioration due to

natural calamities as well as anthropogenic causes (Linn, 2018) like air temperature (A. El-Gohary, 2010), wind erosion (Delgado Rodrigues & Gil Saraiva, 1985), earthquake (Ignatavičius & Ignatavičius, 2005). The historical monuments are of significant source

of income and economic growth through national and international tourism in Nepal. Thus, it requires high-paced reconstruction but the process is generally delayed due to a lack of archaeological framework and manpower required to reconstruct traditional artifacts (KC et al., 2019).

3D model reconstruction is considered the most important information of reverse engineering required for the reconstruction of such sites (Intwala & Magikar, 2016). The image-based 3D reconstruction method has been used in reconstruction scenarios, including earthquake mitigation, construction monitoring, and the development of buildings (Han et al., 2022). The traditional method, image-based 3D reconstruction technique is time-consuming for the image processing, and its ability to effectively simulate situations has become a bottleneck that prevents it from being used in emergency situations (Han et al., 2022). Thus, the development of accessible and cost effective method to carry out the reconstruction of the archaeological framework has become necessary. Light Detection and Ranging (LiDAR) and Unmanned Aerial Vehicle (UAV) photogrammetric data capture are desirable over conventional survey due to their efficiency and accuracy over large areas (Jakovljevic et al., 2019; Khanal et al., 2020; Kovanič et al., 2023)

A single narrow-beam laser and a receiver system make up a LiDAR system. An optical pulse created by the laser is transmitted, reflected by a target, and then sent back to the receiver. The receiver measures the pulse's complete travel time, from the beginning to the end calculating the distance between launches, and determining the 3D coordinates of locations (Pajankar et al., 2019). LiDAR is a powerful tool to help uncover possible archaeological structures and its reconstruction. Therefore, it is possible to obtain a 3D reconstruction based on LiDAR data (Cheng et al., 2013; Forlani et al., 2006; Khanal et al., 2020; Wu et al., 2018). Nevertheless the high cost (in the range of 60k-80k €) of such integrated LiDAR systems

makes their regular use only possible for very large projects (Zaczek-peplinska & Kowalska, 2022).

In 2020, Apple Inc. released the first phone with integrated built-in LiDAR depth sensors and an improved augmented reality (AR) application programming interface (API). In order to compete with the existing hardware solutions for survey operations requiring just moderate accuracy, a comparatively cheap alternative was devised. Nonetheless, in Archaeological sector, the use of iPhone's LiDAR performance and precision of the acquired 3D point clouds has not been very well studied and documented (Teppati Losè et al., 2022). Thus, this study aims to address the gap and analyze the effectiveness of the consumer grade LiDAR in archaeological scene reconstruction.

The main objective of the study was to evaluate the efficacy of iPhone's LiDAR in documenting the 3D structure for archaeological scene reconstruction. Additionally, the study aimed to compare scanning apps; SiteScape & 3D Scanner. The different scanning modes offered by the selected apps were also studied.

2. MATERIALS AND METHODS

2.1 Study Area

The archaeological structures were selected from the Panauti Municipality, Nepal. It is located 32 km southeast of the capital city, Kathmandu. The municipality has been listed as a probable site for UNESCO world heritage since 1996 (UNESCO, n.d.), which specifically concentrates on the reconstruction of archaeologically significant sites. Panauti being a historically important city consisted of a variety of Hindu and Buddhist monuments of different sizes and surface complexities (UNESCO, n.d.). Archaeological structures selected are shown in Figure 1.

Three structures based on the type of structures were selected for this study. The structure types for the monuments include stone surface, brick surface, and wooden carved surface. The study

structures were categorized as case study 1, case study 2, and case study 3 for combination of stone and brick structure, brick structure and carved-wooden structure respectively.

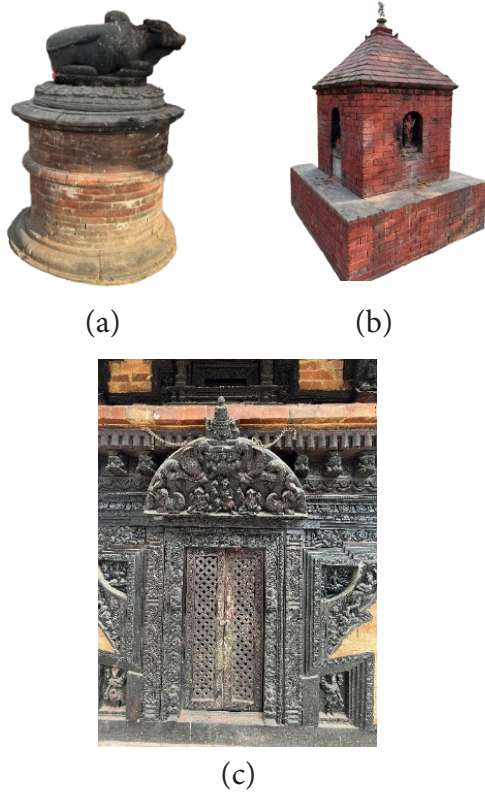


Figure 1: Study Structures a) Combination of stone and brick, b) Brick structure c) Carved-wooden structure

2.2 Methods

The major stage of the methodology were: Data Capturing, Data Collection, Data Preparation, and Data Analysis. The study was carried out in three archaeological structures. They were scanned with the scanning apps which directly provided the point clouds. The point density is compared between the scanning apps. 3D mesh was also generated using the point clouds obtained. The dimension measurement (such as length, breadth and height) was carried out in the mesh and it was compared with the in-situ measurements. Figure 2 shows overall methodological process of comparative assessment of archaeological scene reconstruction using iPhone's LiDAR.

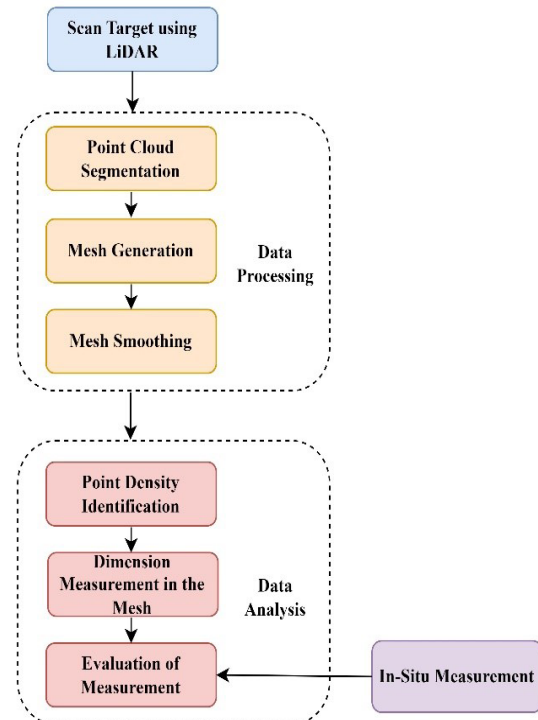


Figure 2: Methodological flowchart

2.2.1 Scan Target Using LiDAR

The applications SiteScope and the 3D scanner app which are available in iPhone 14 pro apple stores were utilized for the study. The iPhone was placed at a distance of 2-3 meters from the structure being scanned to capture the data. The scanning process involved moving the iPhone in a clockwise direction to cover the entire structure as shown in Figure 3.

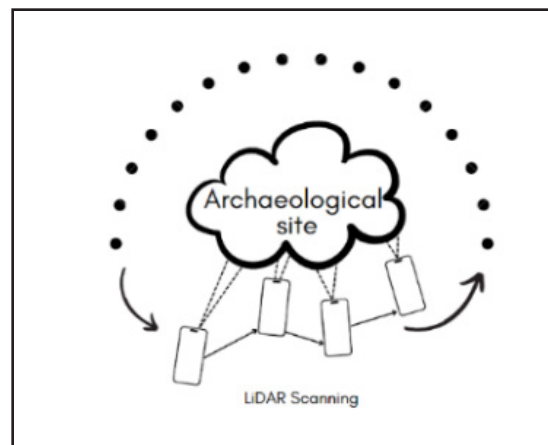


Figure 3: Data Collection process using LiDAR Method

The following settings were incorporated to collect the data from these applications:

Scan settings of SiteScape

- High Point Density, High point Size (SiteScape1)
- High Point Density, Low Point Size (SiteScape2)
- Low Point Density, High Point Size (SiteScape3)
- Low Point Density, Low Point Size (SiteScape4)
- Medium Point Density, Medium Point Size (SiteScape5)

Scan Settings of 3D Scanner

- Low Confidence, 5 mm Resolution (3D Scanner1)
- High Confidence, 5 mm Resolution (3D Scanner2)
- Medium Confidence, 5 mm Resolution (3D Scanner3)

2.2.2 Point Cloud Segmentation

The point cloud files were exported in .e57 format and .las format for the SiteScape and 3D Scanner App respectively which provided the point clouds data directly.

The point clouds obtained from both techniques were added in Cloud Compare software. The point clouds contained points that covered background noises. So, the clipping of point clouds was accordingly done to achieve only targeted structure.

2.2.3 Mesh Generation

Mesh was generated from the obtained point clouds. The normal tools and Poisson surface reconstruction plugin was used to generate the mesh.

The normal tool calculates point cloud's normal as it represented the local surface of that point and its neighbors. The model was first put through this process since the amount

of noise and the number and proximity of neighboring structures could alter how this surface appears in the final model.

Poisson surface reconstruction plugin was used to generate the mesh. In Poisson surface reconstruction, main parameter was "Octree Depth" as the deeper (i.e. greater) the value, finer will be the result, but requires more time and memory.

In the next step, Input Density as SF operation was done in Cloud Compare which facilitates removing unnecessary portion from the previously generated mesh.

2.2.4 Mesh Smoothing

The generated mesh was smoothen to make the mesh finer in visual appearance. To smoothen the mesh generated, Laplacian smoothing tool was used. In this, value 20 was provided for iteration and 0.2 for smoothing factor.

2.2.5 Point Density Identification

The point densities in a specific portion of the structures, such as a 1m x 1m area in case Study 2, Case Study 3 and the upper part of the case study 1 was clipped as shown in Figure 5 and studied. The results for point density are presented in the results section.

2.2.6 Dimension Measurements in the Mesh

Measurements were initially taken on the ground using a measuring tape. The same measurements were replicated on a digital mesh, employing a "point picking" tool to determine distances between two points. To ensure accuracy, the average of measurements was calculated for both length and height.

2.2.7 Evaluation of the Measurements

The measurements obtained from the mesh were compared with the in-situ measurements. Following relation was used to compute the relative error percentage:

Relative Error (R.E.) in %

$$\frac{\text{InSitu Measurement}-\text{Measurement made on mesh}}{\text{InSitu Measurement}} * 100\%$$

3. RESULTS AND DISCUSSION

3.1 Result

The mesh of the each structures were obtained as depicted in Figure 4. The point density in different scan settings were studied and also the difference in the dimension measured between in-situ measurements and the measurements achieved from mesh were studied.

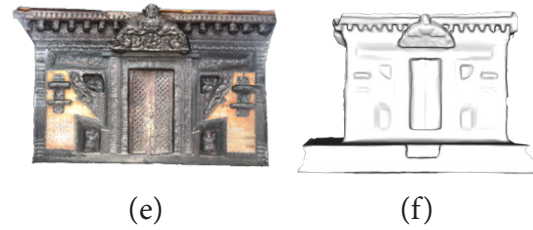
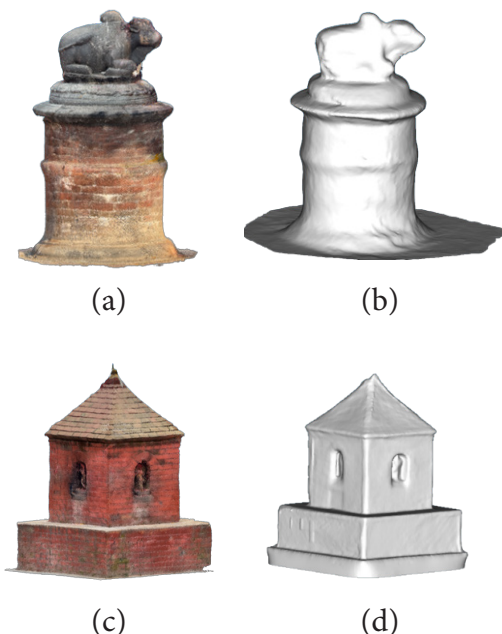
3.1.1 Mesh of the Structures

Sample representations of the generated meshes are shown in Figure 4 for each of the archaeological structures. The parameters that were used to generate the mesh has been shown in below in Table 1.

Table 1: Parameters for mesh generation

Plugins	Parameters	
Normals	Local Surface Model	Plane
	KNN Value	8
PoissonRecon	Octree Depth	10

The meshes generated from SiteScape data displayed RGB color, while those from the 3D Scanner App lacked RGB color and were initially rendered in green. Subsequently, a color scale with intensity values ranging from 0 to 1 is applied to represent the meshes in white hues.



3.1.2 Point Density Comparison

Application	Settings	Point density (upper part of sculpture, Figure 5)
SiteScape	SiteScape1	6808918
	SiteScape2	5654703
	SiteScape3	3065422
	SiteScape4	1870084
	SiteScape5	3710338
3D Scanner	3D Scanner1	16329
	3D Scanner2	15300
	3D Scanner3	14912

The first analysis done on this study was comparison of the point density in the point clouds obtained using different settings SiteScape1, SiteScape2, SiteScape3, SiteScape4, SiteScape5, 3D Scanner1, 3D Scanner2, and 3D Scanner3.

The density of points in different scanning modes of the SiteScape application varied for the same structures. Similarly, the point density obtained from 3D Scanner had lower point density compared to SiteScape. The following sections briefly describes the point density comparisons in different case studies.

Case Study 1: Combination of stone and brick



Figure 5: segmented point cloud of Case Study 1: SiteScape (Left), 3D Scanner (Right)

The case study 1 corresponds to the Stone Sculpture (Nandi) which was constructed using stone. A stone was skillfully carved to create a sculpture of Nandi, which is a significant figure in Hindu culture as the mount of Lord Shiva. The stone sculpture exhibits fine texturing and detailing. However, during the segmentation process for this structure, the desired dimensions of 1m*1m were not achieved. Consequently, the upper part of the sculpture was separated, as illustrated in the Figure 5. It's worth noting that the segmentation was uniformly applied across all scanning modes.

Table 2: Comparison of Point Density of Case Study 1 in different scan mode

Application	Settings	Point density (upper part of sculpture, Figure 5)
SiteScape	SiteScape1	6808918
	SiteScape2	5654703
	SiteScape3	3065422
	SiteScape4	1870084
	SiteScape5	3710338
3D Scanner	3D Scanner1	16329
	3D Scanner2	15300
	3D Scanner3	14912

When analyzing point density, SiteScape outperformed the 3D Scanner in terms of providing a denser point cloud. Among the different scanning settings, SiteScape1 yielded the highest number of points, while SiteScape4 produced the lowest point count. On the other hand, within the 3D Scanner data, 3D Scanner1 generated the most points 16,329 while 3D Scanner3 produced the fewest points.

Case Study 2: Brick structure

The case study 2 corresponds to the Indreshwor temple which was constructed using bricks, and small stone sculptures of the goddess were placed inside the temple. Firstly 1m*1m area was segmented from the existing point cloud to identify point density. When examining the point density, in various settings using SiteScape and 3D Scanner, the following outcomes were observed.

SiteScape1 offered the highest point density, while SiteScape3 had the lowest point density. Notably, the 3D Scanner only produced point densities in the thousands. 3D Scanner2 yielded a higher density of points, whereas 3D Scanner1 produced the lowest point density. In comparison to the SiteScape app, 3D Scanner provided much less point density in 3 different settings.

Table 3: Comparison of Point Density of Case Study 2 in different scan mode

Application	Settings	Point density (per sq. m)
SiteScape	SiteScape1	1738367
	SiteScape2	1525050
	SiteScape3	340808
	SiteScape4	911772
	SiteScape5	723185
3D Scanner	3D Scanner1	8462
	3D Scanner2	8706
	3D Scanner3	8511

Case Study 3: Carved-wooden structure

The case study 3 corresponds to the wooden carved door. Firstly 1m*1m area was segmented from the existing point cloud to identify point density. In this case as well, SiteScape has resulted far denser points than that of 3D Scanner. The result shows that the SiteScape2 has maximum point density that accounts for 1688775 points while SiteScape3 provided the least point density. Studying the point densities from the 3D Scanner, it shows the point densities again in only thousands. Maximum point density was achieved in 3D Scanner1 and least point density has been obtained in 3D Scanner3.

Table 4: Comparison of Point Density of Case Study 3 in different scan mode

Application	Settings	Point density (per sq. m)
SiteScape	SiteScape1	692455
	SiteScape2	1688775
	SiteScape3	397468
	SiteScape4	699230
	SiteScape5	1185659

3D Scanner	3D Scanner1	9544
	3D Scanner2	8868
	3D Scanner3	8373

3.1.3 Evaluation of the dimension measurements

Second analysis done in this research was comparison of the measurements in different settings of the scanning apps, SiteScape1, SiteScape2, SiteScape3, SiteScape4, SiteScape5, 3D Scanner1, 3D Scanner2 and 3D Scanner3. The measurements done in the mesh using point picking tool was compared with the in-situ measurements. The measurements obtained from in-situ and computed from mesh are shown in Table 5, Table 6, Table 7 along with the relative errors found in the measurements from the mesh.

Case Study 1: Combination of stone and brick

The assessment of the case study 1 included using a tape measure to measure both the circular section and height, yielding a circumference (CF) of 3.28 meters and a height (H) of 1.05 meters.

Following this, within the mesh created from point clouds obtained from both applications, multiple measurements of the same dimensions were measured. The average of the multiple measurements were calculated and are presented in Table 5 along with the relative errors in the measurements.

Table 5: Comparison of dimensions of digital meshes with in situ measurements of Case Study 3

Measurement Modes	CF (m.)	H (m.)	R.E. of CF (%)	R.E. of H (%)
In Situ Measurements	3.28	1.050	-	-
	SiteScape			
SiteScape1	3.159	1.020	3.67	2.85
SiteScape2	3.264	1.024	0.48	2.44
SiteScape3	3.260	1.023	0.60	2.56
SiteScape4	3.245	1.034	1.07	1.52
SiteScape5	3.143	1.024	4.17	2.52

	3D Scanner			
3D Scanner1	3.136	1.024	4.38	2.46
3D Scanner2	3.127	1.006	4.67	4.21
3D Scanner3	3.076	1.014	6.22	3.48

The results clearly show that SiteScape provides greater accuracy in comparison to the 3D Scanner application. When evaluating circumference measurements, SiteScape2 displayed the highest accuracy with only a 0.48% error, while 3D Scanner3 exhibited the largest error at 6.22%. Regarding height measurements, SiteScape4 demonstrated the least error, specifically 1.52%, whereas 3D Scanner2 showed the highest error at 4.21%.

Case Study 2: Brick structure

In this case, length and height were measured by using tape which resulted in 1.832 meter length and 1.067 meter height.

Following table provides the comparison of the measurements with in-situ measurements.

Table 6: Comparison of dimensions of digital meshes with in situ measurements of Case Study 2

Measurement Modes	Length (m.)	Height (m.)	R. E. of length (%)	R. E. of height (%)
In Situ Measurements	1.832	1.067	-	-
	SiteScape			
SiteScape1	1.827	1.065	0.27	0.19
SiteScape2	1.834	1.064	0.11	0.28
SiteScape3	1.831	1.068	0.05	0.09
SiteScape4	1.817	1.054	0.82	1.22
SiteScape5	1.829	1.062	0.16	0.47
	3D Scanner			
3D Scanner1	1.768	1.061	3.49	0.56
3D Scanner2	1.849	1.065	0.93	0.19
3D Scanner3	1.809	1.068	1.26	0.09

The results clearly indicate that SiteScape offers superior accuracy compared to the 3D Scanner application. When evaluating length measurements, SiteScape3 displayed the greatest accuracy with a mere 0.05% error, and SiteScape4 exhibited highest at 0.82%, while 3D Scanner1 showed the highest error

at 3.49%. Regarding height measurements, SiteScape3 exhibited the least error at 0.09%, whereas 3D Scanner1 demonstrated the highest error at 0.56%.

Case Study 3: Carved-wooden structure

In this case, length and height were measured using tape which resulted in 2.57 meter length and 1.312 meter height.

Following table provides the comparison of the measurements with in-situ measurements.

Table 7: Comparison of dimensions of digital meshes with in situ measurements of Case Study 3

Parameters	Length (m.)	Height (m.)	R.E. of Length (%)	R. E. of Height (%)
In Situ Measurements	2.57	1.312	-	-
	SiteScape			
SiteScape1	2.568	1.311	0.06	0.05
SiteScape2	2.559	1.316	0.44	0.33
SiteScape3	2.567	1.310	0.12	0.14
SiteScape4	2.572	1.310	0.09	0.19
SiteScape5	2.560	1.320	0.39	0.60
	3D Scanner			
3D Scanner1	2.551	1.284	0.73	2.16
3D Scanner2	2.552	1.283	0.71	2.18
3D Scanner3	2.551	1.288	0.73	1.83

This results clearly indicates that SiteScape provide better accuracy compared to the 3D Scanner application. When evaluating length measurements, SiteScape1 displayed the highest accuracy with only a 0.06% error, while 3D Scanner1 and 3D Scanner2 exhibited the largest error at 0.73%. In terms of height measurements, SiteScape1 demonstrated the least error, specifically 0.05%, and the highest error at 0.60%, while 3D Scanner2 showed the highest error at 2.18%.

3.2 Discussion

In this study, we examined two distinct LiDAR apps by generating mesh using various modes within those applications and subsequently comparing their dimensions with in-situ

measurements. The relative error in accuracy assessment was affected by discrepancies in point selection, as different individuals marked distinct points while evaluating the mesh dimensions. This introduced uncertainty in the measurements in the mesh, also the results varied based on the textures and materials of the structures under consideration which is in alignment with (Kovanič et al., 2023).

The primary difficulties associated with employing the iPhone's LiDAR approach lie in the data acquisition phase, where the obtained point clouds exist in an arbitrary coordinate system. Despite having location services enabled during data acquisition, it did not impart any location information, leading to the use of an arbitrary coordinate system. Even though the data captured was in arbitrary coordinate system, it did not affect the accuracy drastically. Additionally, capturing detailed information about the upper parts of structures with greater heights proved challenging with the iPhone. Consequently, point clouds may not be generated for the upper section of monuments, resulting in the creation of voids in the mesh. Mokroš et al., (2021) highlight the potential of Apple's technology for scanning geomorphological formations, but also identify several issues and challenges. Mokroš et al., (2021) emphasize the importance of data collection methods in ensuring its completeness. The Apple device's scanning distance was less than 3 m, compared to terrestrial laser scanners that can reach up to 200 m. This is a significant limitation to the technology's use.

It was found that the higher number of point density was obtained from SiteScape's point cloud rather than the point clouds of 3D Scanner is in alignment with the result obtained in (Vacca, 2023). SiteScape achieves this by conducting repeated acquisitions in the same area, thereby increasing the number of points observed. Meanwhile, 3D Scanner provided least number of point clouds as 3D Scanner app does not increase the number

of points when the operator scans the same area multiple times, resulting to a less noisy point cloud (Teppati Losè et al., 2022). The limited points in the 3D scanner's point cloud contributed to a less accurate results.

The result above signifies SiteScape app offers superior geometrical accuracy as the measurements provide the precise results than the 3Dscanner app (Kartini et al., 2022). However, the meshes generated through SiteScape app are visually appealing due to the inclusion of RGB values providing colored textures, and displaying distinct variations in texture and intricate patterns carved in the monuments. However, the mesh generated exhibit blurriness, making it challenging to achieve a clear visualization of the study area. On the other hand, the meshes obtained from the 3D Scanner app appear less sharp and lack the actual color representation as the object was scanned for a longer duration for covering the whole scene of monuments (i.e., no RGB values), reducing their suitability for visualization purposes in scene reconstruction.

Despite the SiteScape app providing superior accuracy, the dimensions from meshes generated by both applications do not deviate significantly from the in situ measurements. The analysis suggested that both applications produced sufficiently significant outcomes, making them suitable for practical modeling for scene reconstruction. (Vacca, 2023) findings suggest that Apple LiDAR sensors are a valuable tool for creating 3D models of architectural and cultural heritage, contributing to metric documentation and asset knowledge. This match with the results obtained in the context of archeological scene reconstruction.

4. CONCLUSION AND RECOMMENDATION

The main goal of this research was to compare the consumer grade LiDAR sensor and its usability for reconstructing archaeological scenes. Both applications examined in this study allow for the direct export of generated point clouds and potential meshes in different

formats. The iPhone's consumer-grade LiDAR, characterized by its accessibility, affordability, and user-friendly interface, becomes a convenient option for individuals with limited training, providing a simplified approach to scene reconstruction compared to Terrestrial Laser Scanning (TLS).

The study seeks to quantitatively evaluate commonly used apps and LiDAR devices, highlighting their potential benefits while identifying potential limitations. Although both apps demonstrated enhanced performance in diverse application scenarios, SiteScape consistently produced satisfactory reconstructions across all tested cases using the specified settings.

For future research, it is recommended to incorporate Ground Control Points (GCP) markers to improve point picking accuracy and minimize human errors. The inclusion of Model-to-Model comparison (M3C2 algorithms) in Cloud Compare could provide additional insights. Additionally, proposing a comparative analysis between Apple's LiDAR and TLS is suggested for the purpose of data validation and accuracy verification.

REFERENCES

- A. El-Gohary, M. (2010). The Environmental Factors Affecting the Archaeological Buildings in Egypt. *The Conference Book of the General Union of Arab Archeologists*, 13(13), 72–73. <https://doi.org/10.21608/cguaa.2010.37727>
- Cheng, L., Tong, L., Chen, Y., Zhang, W., Shan, J., Liu, Y., & Li, M. (2013). Integration of LiDAR data and optical multi-view images for 3D reconstruction of building roofs. *Optics and Lasers in Engineering*, 51(4), 493–502. <https://doi.org/https://doi.org/10.1016/j.optlaseng.2012.10.010>
- Delgado Rodrigues, J., & Gil Saraiva, A. (1985). Experimental and theoretical approach to the study of the mechanism of wind erosion of stone in monuments. *5th Int. Cong. on Deterioration and*

Conservation of Stone, March 2015, 167–175.

- Forlani, G., Nardinocchi, C., Scaioni, M., & Zingaretti, P. (2006). Complete classification of raw LIDAR data and 3D reconstruction of buildings. *Pattern Analysis and Applications*, 8(4), 357–374. <https://doi.org/10.1007/s10044-005-0018-2>
- Han, S., Huo, L., Wang, Y., Zhou, J., & Li, H. (2022). Rapid reconstruction of 3d structural model based on interactive graph cuts. *Buildings*, 12(1). <https://doi.org/10.3390/buildings12010022>
- Hussain, S. T., & Will, M. (2021). Materiality, Agency and Evolution of Lithic Technology: an Integrated Perspective for Palaeolithic Archaeology. *Journal of Archaeological Method and Theory*, 28(2), 617–670. <https://doi.org/10.1007/s10816-020-09483-6>
- Ignatavičius, Č., & Ignatavičius, G. (2005). Investigation of damage and microclimate deterioration caused by dampness in the palace of signatories to the declaration of independence. *Indoor and Built Environment*, 14(1), 89–95. <https://doi.org/10.1177/1420326X05050503>
- Intwala, A. M., & Magikar, A. (2016). A review on process of 3D Model Reconstruction. *International Conference on Electrical, Electronics, and Optimization Techniques, ICEEOT 2016, December*, 2851–2855. <https://doi.org/10.1109/ICEEOT.2016.7755218>
- Jakovljevic, G., Govedarica, M., Alvarez-Taboada, F., & Pajic, V. (2019). Accuracy assessment of deep learning based classification of LiDAR and UAV points clouds for DTM creation and flood risk mapping. *Geosciences (Switzerland)*, 9(7). <https://doi.org/10.3390/geosciences9070323>
- Kartini, G. A. J., Gumilar, I., Abidin, H. Z., & Yondri, L. (2022). the Comparison of Different Lidar Acquisition Software on Ipad Pro M1 2021. *International Archives of the Photogrammetry, Remote Sensing and Spatial Information Sciences - ISPRS Archives*, 48(2/W1-2022), 117–120. <https://doi.org/10.5194/isprs-archives-XLVIII-2-W1-2022-117-2022>
- KC, A., Sharma, K., & Pokharel, B. (2019). Reconstruction of heritage structures in Nepal after 2015 Gorkha, Nepal earthquake. *12th Canadian Conference on Earthquake Engineering, June*.
- Khanal, M., Hasan, M., Sterbentz, N., Johnson, R., & Weatherly, J. (2020). Accuracy comparison of aerial lidar, mobile-terrestrial lidar, and UAV photogrammetric capture data elevations over different terrain types. *Infrastructures*, 5(8). <https://doi.org/10.3390/INFRASTRUCTURES5080065>
- Kovanič, L., Topitzer, B., Peťovský, P., Blišťan, P., Gergeľová, M. B., & Blišťanová, M. (2023). Review of Photogrammetric and Lidar Applications of UAV. *Applied Sciences (Switzerland)*, 13(11). <https://doi.org/10.3390/app13116732>
- Linn, R. (2018). Identifying and Evaluating Deterioration Factors Which Affect Archeological Sites: The Case Study of Hippos. *Journal of Eastern Mediterranean Archaeology & Heritage Studies*.
- Mokroš, M., Mikita, T., Singh, A., Tomašík, J., Chudá, J., Wężyk, P., Kuželka, K., Surový, P., Klimánek, M., Zięba-Kulawik, K., Bobrowski, R., & Liang, X. (2021). Novel low-cost mobile mapping systems for forest inventories as terrestrial laser scanning alternatives. *International Journal of Applied Earth Observation and Geoinformation*, 104, 102512. <https://doi.org/10.1016/j.jag.2021.102512>
- Pajankar, N. N., Sawale, Y., Navghare, P. S. A., Harinkhede, A., & Pachare, A. (2019).

LIDAR : Advanced Method Of Survey And Mapping. 31–34.

Panauti travel - Lonely Planet | Nepal, Asia. (n.d.). Retrieved December 25, 2022, from <https://www.lonelyplanet.com/nepal/around-the-kathmandu-valley/panauti>

Teppati Losè, L., Spreafico, A., Chiabrandò, F., & Giulio Tonolo, F. (2022). Apple LiDAR Sensor for 3D Surveying: Tests and Results in the Cultural Heritage Domain. *Remote Sensing*, 14(17). <https://doi.org/10.3390/rs14174157>

UNESCO (n.d.). *The early medieval architectural complex of Panauti - UNESCO World Heritage Centre*. Retrieved December 25, 2022, from <https://whc.unesco.org/en/tentativelists/839/>

Vacca, G. (2023). 3D Survey with Apple LiDAR Sensor—Test and Assessment for Architectural and Cultural Heritage. *Heritage*, 6(2), 1476–1501. <https://doi.org/10.3390/heritage6020080>

Wu, Q., Yang, H., Wei, M., Remil, O., Wang, B., & Wang, J. (2018). Automatic 3D reconstruction of electrical substation scene from LiDAR point cloud. *ISPRS Journal of Photogrammetry and Remote Sensing*, 143, 57–71. <https://doi.org/https://doi.org/10.1016/j.isprsjprs.2018.04.024>

Zaczek-peplinska, J., & Kowalska, M. E. (2022). *Works Evaluation of the LiDAR in the Apple iPhone 13 Pro for use in Inventory Works (11458) Janina Zaczek-Peplinska and Maria Kowalska (Poland) FIG Congress 2022 Volunteering for the future - Geospatial excellence for a better living Warsaw, Poland, . September 2022*, 11–15.



Author's Information

Name	: Binod Prasad Bhatta
Academic Qualification	: BE in Geomatics Engineering
Organization	: Kathmandu University
Current Designation	: Researcher
Work Experience	: 1 years
Published paper/article	: 3



Obituary



All the officials of Survey Department pray to the almighty for eternal peace to the departed soul of the following officials of the department and this department will always remember the contribution they have made during their service period in this department.



Sahadev Subedi
Chief Survey Officer
Survey Office, Dillibazar, Kathmandu
17 January 2025



Santosh Kumar Mahaseth
Assistant Surveyor
Survey Office, Gaushala, Mahottar
26 January 2025



Ramesh Raj Rajbhandari
Then Chief Survey Officer
10 April 2025



Kusum Lal Mandal
Office Helper
Survey Office, Saptari
11 May, 2025

Comparison of Deep Learning Models with Different Backbones for Building Footprints Extraction in Dense Residential Areas of Bhaktapur

Abin Prajapati¹ & Romik Gosai¹
abinprajapati@gmail.com, romikgosai2057@gmail.com
¹Smart Engineering Consultant Pvt Ltd,

KEYWORDS

Building Extraction, Transfer Learning, Dense Residential Area, Semantic Segmentation

ABSTRACT

The rapid advancements of Artificial Intelligence, particularly deep learning, has enhanced features extraction mainly building footprints. However, models trained on developed countries struggle to perform better while testing on the datasets of high-density residential areas of developing countries like Nepal. This research aims to improve the performance of the models by developing and utilizing a region-specific dataset for Bhaktapur. Initially, models like Unet, PSPNet and LinkNet with different backbone architectures like resnet18, resnet34, resnet50, and vgg19 were trained on the Massachusetts dataset and the performance was poor when tested with the dense residential areas of Bhaktapur datasets. To address this issue, new datasets of Bhaktapur were introduced for high density residential area where houses are closely attached. The datasets were prepared by digitizing each house on the high resolution orthomosaics which was then converted to mask. Subsequently, the orthomosaic was patches into 300 x 300 with the corresponding mask. These patches were split into training, validation and testing datasets. Models with different backbones were trained with custom datasets applying data augmentation techniques, including random clipping of 256 x 256, flipping and rotation to prevent overfitting and make the model more robust to variations in real world data. The models with different backbones were validated and tested, and the best performance was with LinkNet model with vgg19 backbone with an IoU of 94.29% and F1 Score of 98.29%, demonstrating good results for dense residential areas. This study highlights the importance or need of region based custom datasets to improve the accuracy of deep learning segmentation models for building extractions, mainly on unique urban structure which can be useful for urban spatial planning, and disaster risk management and monitoring.

1. INTRODUCTION

Building is the most important features that form the urban fabric. The distribution of buildings is changing due to urbanization and population growth, leading to an urban crawl on the peri-urbanization areas leading to high

density residential areas. The changes in the spatial distribution of the building are very essential for the study of urban settlements, demographics, and so on (Li et al., 2019) . Traditional methods consume more time and effort to track the spatial distribution changes

that necessitate the automated techniques for fast, accurate and error-free data.

The development of Machine Learning (ML) and Deep learning (DL) techniques, particularly Convolutional Neural Networks (CNN) and Artificial Neural Networks (ANN) are exponentially growing and also high accuracy for features extraction buildings have been demonstrated by different researchers using different deep learning approaches. Many researches on building footprints using deep learning for very high resolution (VHR) were carried out and a variety of new methods has been proposed which is beneficial for urban planning, disaster management, population estimation, and environment management (Feng et al., 2023). In the early stages, building footprints extraction were based on traditional image processing methods like edge, object and shadow-based methods (Ziaei et al., 2014). Chen et al. (2018) proposed an indices for edge regularity and shadow line which was employed in three machine learning classifiers: Adaboost, Support Vector Machine and Random Forest. Ok et al. (2013) proposed a fuzzy landscape modeling for directional spatial relationship between building and its corresponding shadows and GrabCut partitioning on VHR satellite images. These studies were based on the traditional methods to detect buildings. Nowadays, different deep learning approach have been used to segment building with higher segmentation accuracy.

Ronneberger et al. (2015) introduced U-Net architecture, designed for medical image segmentation, which was then widely used for building footprints extraction. Rastogi et al., (2022) introduced a novel CNN architecture, UNet-AP, which demonstrated superior performance than SegNet and UNet in terms of mean intersection over union. Similarly, residual U-Net model proposed by H. Wang & Miao (2022) for building footprint extraction claims to be a superior model than SegNet,

FastFCN, Web-Net and DeepLabV3+. Some researchers have explored a variety of encoder-decoder architectures. For instance, Bakirman et al. (2022) compared different pretrained encoder with imagenet and concluded that the Unet++ architecture using SE-ResneXt101 encoder outperformed other models like Unet, DeepLabv3+, FPN and PSPNet. Similarly, Alsabhan & Alotaiby (2022) demonstrated the potentiality of automatic building footprint extraction using artificial intelligence in high-density residential areas using Unet model with resnet50 backbone.

Despite the advancements, numerous researches have been conducted on public datasets from developed countries such as Massachusetts, WHU, Inria, Waterloo. Kang et al. (2019) and Atik et al. (2022) performed experiments on Massachusetts, WHU aerial imagery, and Inria datasets for building segmentation. He et al. (2022) presented Waterloo building dataset with spatial resolution of 12cm which covers the area of Ontario, Canada for building footprints extraction. Atik et al., (2022) compared DeepLabV3 architecture with resnet-18, resnet-50, Xception, and mobilenetv2 backbones in Massachusetts, WHU and Inria datasets in which resnet-50 outperforms other backbones in terms of F1 score and IoU score. B-FGC-Net has improved accurate extraction compared to Unet, Linknet and SegNet models in WHU and Inria building datasets (Y. Wang et al., 2022). Vincent M & P (2024) proposes a Mask-RCNN models which perform better than YOLO models in WHU and Inria datasets. They are limited to urban topography of developed countries which fail to capture the urban complexity and architectural diversity of dense urban of Nepal, particularly Nepal.

Our main contributions can be outlined as follows:

- Testing of dense residential areas on the model trained with Massachusetts datasets.

- Introduced new dataset of Bhaktapur which is a high-density residential area for building footprints extraction. This dataset captures house structure of developing nation, particularly Nepal, with attached buildings with tin, clay tiles and concrete roofs.
- Comparative study of different backbone architecture on performance of semantic models like Unet, Linknet and PSPnet with different backbones like resnet18, resnet34, resnet50, and vgg19 during building extraction.

2. METHODOLOGY

2.1 Study Area

Bhaktapur Municipality is one of the oldest city of Nepal. It is smallest municipality of Nepal with an area of 6.88km² with population

density of 12,070 per km² and lies at 1330 meters above the sea level. Geographically it extends from 27.66 ° North to 27.69 ° North and 85.399 ° East to 85.448 ° East. It is surrounded by 3 municipalities of Bhaktapur district, namely Changuanarayan Municipality, Suryabinayak Municipality and Madhyapur Thimi Municipality.

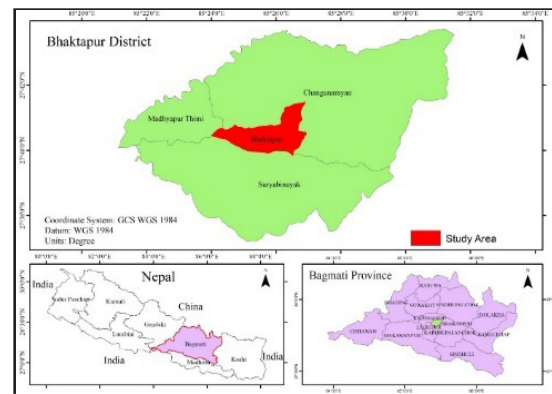


Figure 1: Study Area

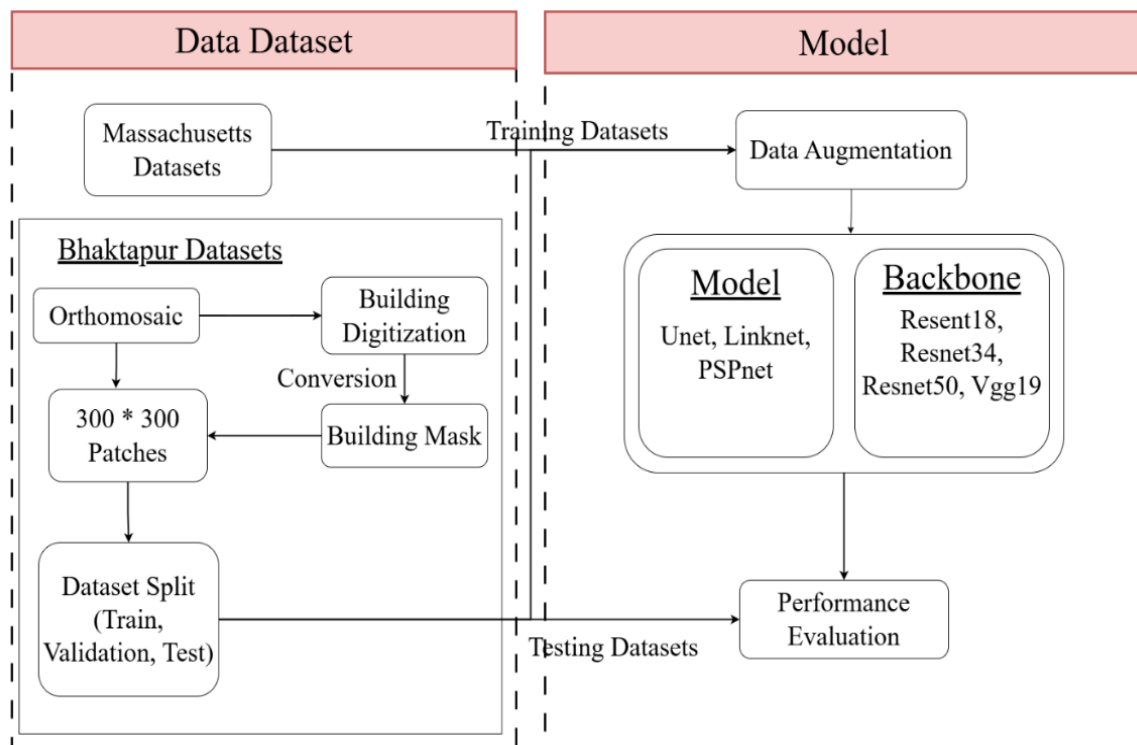


Figure 2: Methodology

2.2 Data Preparation

Massachusetts dataset of image 1500 x 1500 were split into 300 x 300 image size for both image and mask.

Digitization of the building's polygon were performed on the orthomosaic of Bhaktapur. The buildings features were converted to the mask images and split into 300 x 300 patches aligned corresponding to the RGB image which was uploaded in *Bhaktapur Building Dataset*¹. Subsequently, these datasets were split into training, validation, and testing datasets in 7:1.5:1.5 ratio for enough data to train a model and unbiased validation and testing of the model. ¹<https://www.kaggle.com/datasets/romikgosai/bhaktapur-building-dataset>

2.3 Model and Metrics

2.3.1 Models

2.3.1.1 Unet with Resnet Backbone

Figure 3 represents the deep learning architecture of Unet with Resnet backbone having encoder and decoder for semantic segmentation. The encoder utilizes a Resnet backbone with multiple layers. In encoder part, initially convolutional layer of 7 x 7 were applied to input image to extract low-level features and increase the number of channels. Then four layers of Resnet backbone were applied where residual blocks were applied in each layer to enhance feature learning and prevent vanishing gradients, followed by max pooling operations which decreases the spatial resolution. The extracted features are passed to decoder for up sampling to segment map. Decoder restore spatial resolution of the segmentation map by up sampling. Up-convolutional layers are applied to increase the feature map dimensions which are followed by concatenation that copy feature maps from encoder to retain spatial features. Finally, 1 x 1 convolutional layer refines feature

representations to generate the final output segmentation map.

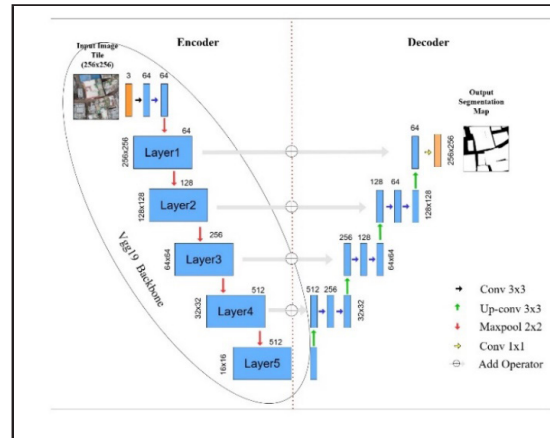


Figure 3: Architecture of Unet with Resnet backbone

2.3.1.2 Linknet with resnet Backbone

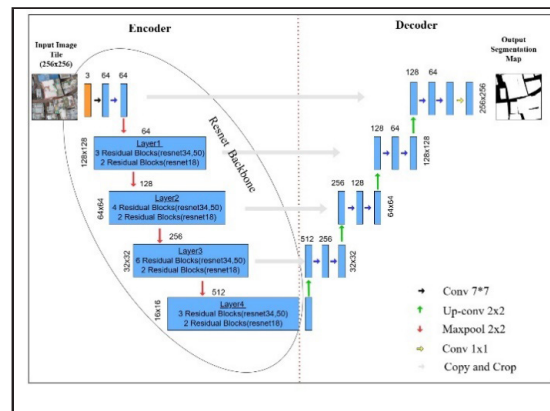


Figure 4: Architecture of Linknet with Vgg19

Figure 4 illustrates the deep learning architecture of Linknet with Vgg19 backbone, comprising of an encoder and decoder for building segmentations. In the encoder part, the encoder begins with 3 x 3 convolutional layer applied to the input image to extract low level features and increase the number of channels. It consists of the five layers utilizing Vgg19 backbone in which each layer consists of convolutional layer followed by 2x2 max pooling operations that decreases the spatial resolution and increases the feature depth. Decoder restore spatial resolution by up sampling the encoded features. Feature

map dimensions are increased by applying up-convolutional layers and add operator facilitates feature fusion across different layers. Finally, final output segmentation is generated by refining the feature representations by applying 1 x 1 convolutional layer.

2.3.1.3 PSPNet with Backbone

Pyramid Scene Parsing Network (PSPNet) was introduced to extract global and local information about the overall scene. As in figure 5, backbones are utilized to extract features from the input image. Pyramid Pooling module process generated feature map by gathering multiscale information, integrating four parallel feature representations at different scales. Subsequently, the processed features are up sampled to original resolution and a final convolution are applied which refines the output.

Three semantic segmentation models-Unet, PSPNet, and LinkNet were developed and trained with the custom dataset. Backbones were integrated with the models in which backbones serve as encoder and decoder components were composed of the respective model. Backbones has pre-trained networks which extract hierarchical features from input data that can learn the intricate patterns. Integration of backbones with the semantic models improve performance, avoid overfitting, and makes training faster.

In this study, for semantic segmentation of

building footprints, the experiments were conducted with three models: Unet, PSPNet and Linknet with different backbones like resnet18, resnet34, resnet50, and vgg19. A default learning rate of 0.0001 was used for the stable and gradual updates to the model's weights. Further, an Adam optimizer, which iteratively updates the weights of networks leading to faster convergence and sigmoid activation function for binary classification were used. Different numbers of epochs were investigated to get the optimum value for training in the model training process i.e. the highest accuracy was obtained within 100 epochs for all models. That's why 100 epochs were used for training. The models were evaluated in each epoch using the validation dataset, early stopping was used when the accuracy tends to decrease which prevents overfitting. Different batch size of 16, 32, and 64 were used during the training. Batch size of 32 was chosen for having the highest performance. IoU and F1 Score are used as performance metrics. Binary cross entropy loss function was used for binary segmentations which help model to learn the probabilities of each class. Data augmentation techniques was applied to enhance generalization of model and to prevent overfitting by increasing the size and diversity of the training datasets adopting different geometric transformations like rotation, flipping, and rotation. The experiment was performed in Kaggle platform with its default GPU.

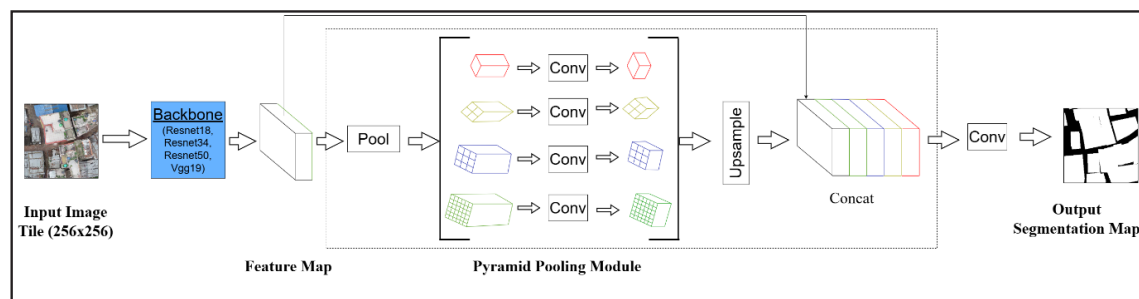


Figure 5: PSPNet Architecture

Table 1: Model Training Parameters

Parameter	Models		
	Unet	PSPNet	Linknet
Backbone	Resnet18, Resnet34, Resnet50, Vgg19		
Weight	ImageNet		
Learning Rate	Default (0.0001)		
Optimizer	Adam		
Metrics	F1-Score, IoU Score		
Loss Function	Binary Cross Entropy		
Number of Epochs	100		
Batch Size	32		
Activation Function	Sigmoid		
Data Augmentation	Horizontal Flip, Vertical Flip, Random Cropping, Random Rotation		
Callbacks	Early Stopping, Model Checkpoint		
Input shape	256*256*3 (RGB Images)		
Output	1 channel mask (Binary Segmentation)		

Initially, the models were trained and tested with the Massachusetts datasets and then again tested with the custom datasets of Bhaktapur. The performance of the models was evaluated for both Massachusetts and Bhaktapur datasets to assess their effectiveness across different geographical contexts. Subsequently, the models were trained with the Bhaktapur datasets and tested to assess performance of the models.

2.3.2 Evaluation Metrics

The performance of the models was evaluated using IoU, precision, recall, and F1 Score. IoU represents the overlap percentage between the ground truth and prediction output. Precision indicates the accuracy of positive predictions. Recall indicates sensitivity or ability to identify the true positive rates. F1 Score is the harmonic mean of the precision and recall.

Precision is the ratio of the number of correctly predicted positive samples to the number of all predicted positive samples (Norelyaqine et al., 2023).

$$\text{Precision} = \frac{TP}{TP+FP} \quad (1)$$

Recall is the ratio of the number of correctly predicted positive samples to the number of all positive samples in the test set.

$$\text{Recall} = \frac{TP}{TP+FN} \quad (2)$$

F1Score is the geometric mean between precision and recall.

$$F_1 \text{ Score} = \frac{2 \times \text{Precision} \times \text{Recall}}{\text{Precision} + \text{Recall}} \quad (3)$$

IoU is the ratio of intersection between the target and the prediction.

$$\text{IoU} = \frac{TP}{TP+FN+FP} \quad (2)$$

3. RESULTS

Qualitative and Quantitative evaluations of building footprints extraction results for Massachusetts and Bhaktapur datasets are provided in this section.

3.1 Qualitative Results

Few random images from the testing datasets are selected and segmented with different models and backbones which are then compared with ground truth. The sequence below image begins with original image followed by ground truth and then the segmentation results of Linknet, Unet and PSPNet models. Each model was tested in the series of Vgg19, Resnet18, Resnet34, and Resnet50.

Figure 6 represents the original image with its ground truth and the segmentation of building footprints generated by different models on the Massachusetts datasets. Linknet and Unet shows higher performance while PSPNet performs significantly worst. It may be due to loss of finer spatial details in PSPNet which relies on pyramid pooling module that captures global context(Yuan et al., 2022).

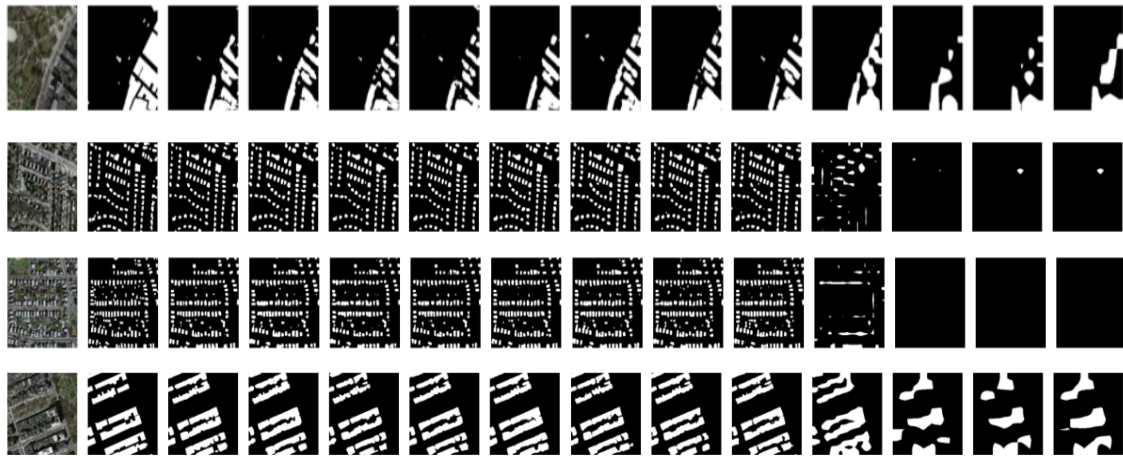


Figure 6: Performance comparison on the Massachusetts building dataset. (a) Original Image, (b) Ground Truth (c) Linknet-Vgg19, (d)Linknet-resnet18, (e)Linknet-resnet34, (f)Linknet-resnet50, (g) Unet-Vgg19, (h) Unet-resnet18, (i) Unet-resnet34, (j) Unet-resnet50, (k) PSPNet-Vgg19, (l) PSPNet-resnet18, (m) PSPNet-resnet34, and (n) PSPNet-resnet50

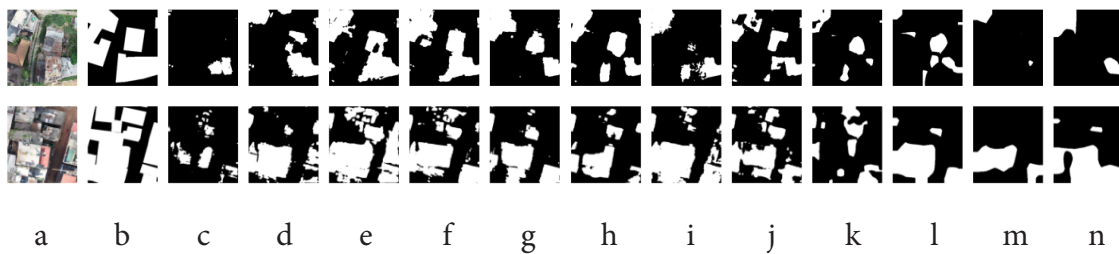


Figure 7: Performance comparison on the custom dataset with Model trained in Massachusetts. (a) Original Image, (b) Ground Truth (c) Linknet-Vgg19, (d)Linknet-resnet18, (e)Linknet-resnet34, (f)Linknet-resnet50, (g) Unet-Vgg19, (h) Unet-resnet18, (i) Unet-resnet34, (j) Unet-resnet50, (k) PSPNet-Vgg19, (l) PSPNet-resnet18, (m) PSPNet-resnet34, and (n) PSPNet-resnet50

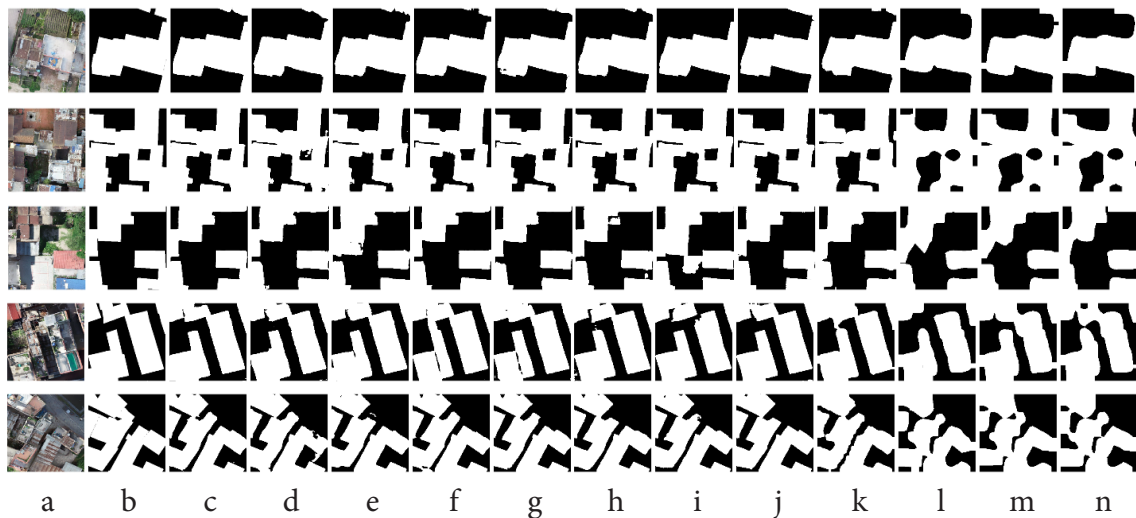


Figure 8: Performance comparison on the custom dataset (a) Original Image, (b) Ground Truth (c) Linknet-Vgg19, (d)Linknet-resnet18, (e)Linknet-resnet34, (f)Linknet-resnet50, (g) Unet-Vgg19, (h) Unet-resnet18, (i) Unet-resnet34, (j) Unet-resnet50, (k) PSPNet-Vgg19, (l) PSPNet-resnet18, (m) PSPNet-resnet34, and (n) PSPNet-resnet50

Figure 7 represents the original image with its ground truth and the segmentation of building footprints generated by various models trained on the Massachusetts datasets and tested on the Bhaktapur datasets. Almost all models perform worst results due to distinct building patterns of Bhaktapur compared to Boston areas used for training.

Figure 8 represents the original image with its ground truth and the segmentation of building footprints generated by various models on the Bhaktapur datasets. Model with Vgg19 shows better results compared to ResNet backbone due to higher number of parameters (Kamal & EZ-ZAHRAOUY, 2023).

3.2 Quantitative Results

This section represents the performance of models in various backbone architectures in terms of IoU and F1Score on Massachusetts and Bhaktapur datasets.

Table 2 represents the IoU and F1 Score for each model trained and tested with the Massachusetts dataset. Unet and Linknet perform significantly better compared to PSPNet across all backbones.

Table 2: Models Performance on Massachusetts Test Datasets

Model	Backbone	IoU	F1 Score
UNet	Resnet18	0.609	0.787
	Resnet34	0.585	0.770
	Resnet50	0.615	0.791
	Vgg19	0.606	0.787
LinkNet	Resnet18	0.590	0.774
	Resnet34	0.554	0.745
	Resnet50	0.577	0.765
	Vgg19	0.612	0.789
PSPNET	Resnet18	0.050	0.141
	Resnet34	0.061	0.166
	Resnet50	0.062	0.174
	Vgg19	0.261	0.498

Table 3 summarizes the performance of models with different backbones trained with Massachusetts datasets and tested with Bhaktapur datasets. The results on all models

plummeted significantly in performance due to difference in building pattern of Bhaktapur compared to Boston areas.

Table 3: Models trained on Massachusetts Datasets Performance Evaluation on Bhaktapur Datasets

Model	Backbone	IoU	F1 Score
UNet	Resnet18	0.109	0.239
	Resnet34	0.165	0.354
	Resnet50	0.199	0.389
	Vgg19	0.152	0.321
LinkNet	Resnet18	0.196	0.389
	Resnet34	0.395	0.659
	Resnet50	0.244	0.450
	Vgg19	0.035	0.081
PSPNET	Resnet18	0.119	0.280
	Resnet34	0.099	0.201
	Resnet50	0.097	0.237
	Vgg19	0.055	0.126

Table 4 presents the results of models on Bhaktapur datasets. The performance of all models and backbones on Bhaktapur datasets are significantly high compared to Massachusetts datasets. Unet and LinkNet has better performance compared to PSPNet. Linknet with Vgg19 backbone has best performance among all model-backbone. Overall, models using VGG19 backbone outperform every ResNet backbone.

Table 4: Models performance on Bhaktapur Test datasets

Model	Backbone	IoU	F1 Score
UNet	Resnet18	0.929	0.978
	Resnet34	0.929	0.979
	Resnet50	0.934	0.981
	Vgg19	0.939	0.982
LinkNet	Resnet18	0.916	0.975
	Resnet34	0.926	0.978
	Resnet50	0.935	0.981
	Vgg19	0.943	0.983
PSPNET	Resnet18	0.856	0.947
	Resnet34	0.866	0.952
	Resnet50	0.868	0.954
	Vgg19	0.924	0.975

4. DISCUSSION AND CONCLUSION

4.1 Discussion

The results from this research indicate that the deep learning models for building footprints extraction trained on developed countries does not generalize well for the high-density residential areas of developing countries, particularly Bhaktapur of Nepal. Models' performance improved with the introduction of the Bhaktapur datasets. Linknet with Vgg19 backbone performed best with the introduced datasets with an IoU Score of 94.29% and F1 Score of 98.29%. Linknet and Unet perform better in comparison to PSPNet due to use of skip connections emphasizing on local feature map, while UNet shows strong consistency across datasets. Models with higher number of layers in Resnet backbone has better segmentation results due to higher number of parameters.

Research by (Alsabhan & Alotaiby, 2022) demonstrated the best performance was in Unet model with Resnet50 backbone for high density residential areas using but with our introduced datasets this model ranked second highest after Linknet with Vgg19. Vgg19 backbone for all models performed well in our research which indicates that Vgg architectures are well suited for semantic segmentation that matches with previous studies like of (Norelyaqine et al., 2023), where the best results were achieved on Unet with Vgg16.

4.2 Conclusion

This study evaluated the performance of three semantic segmentation models with different backbone networks (ResNet18, ResNet34, ResNet50, and VGG19) for building footprints extraction on two location's datasets Massachusetts and Bhaktapur. The models trained solely on Massachusetts datasets performed poor while tested on the Bhaktapur datasets which highlights the limited generalizability of models trained on developed countries data to developing countries data.

All models performed significantly better results when trained and tested on Bhaktapur datasets, with LinkNet model having Vgg19 encoder had the highest accuracy in terms of IoU and F1 Score. This performance highlights the cruciality of adapting training data to the local context for accurate segmentation. The findings of this research indicate crucial role of adapting training data to the local context for accurate segmentation.

Overall, the results highlight the need of context-specific data in training segmentation models for building footprints extraction task. This research features good performance of VGG architectures when paired with UNet and LinkNet models.

REFERENCES

- Alsabhan, W., & Alotaiby, T. (2022). Automatic Building Extraction on Satellite Images Using Unet and ResNet50. *Computational Intelligence and Neuroscience*, 2022, 1–12. <https://doi.org/10.1155/2022/5008854>
- Atik, S. O., Atik, M. E., & Ipbuker, C. (2022). Comparative research on different backbone architectures of DeepLabV3+ for building segmentation. *Journal of Applied Remote Sensing*, 16(02). <https://doi.org/10.1117/1.JRS.16.024510>
- Bakirman, T., Komurcu, I., & Sertel, E. (2022). Comparative analysis of deep learning based building extraction methods with the new VHR Istanbul dataset. *Expert Systems with Applications*, 202, 117346. <https://doi.org/10.1016/j.eswa.2022.117346>
- Chen, R., Li, X., & Li, J. (2018). Object-Based Features for House Detection from RGB High-Resolution Images. *Remote Sensing*, 10(3), 451. <https://doi.org/10.3390/rs10030451>
- Feng, L., Xu, P., Tang, H., Liu, Z., & Hou, P. (2023). National-scale mapping of

- building footprints using feature super-resolution semantic segmentation of Sentinel-2 images. *GIScience & Remote Sensing*, 60(1). <https://doi.org/10.1080/15481603.2023.2196154>
- He, H., Jiang, Z., Gao, K., Fatholahi, S. N., Tan, W., Hu, B., Xu, H., Chapman, M. A., & Li, J. (2022). Waterloo building dataset: a city-scale vector building dataset for mapping building footprints using aerial orthoimagery. *Geomatica*, 75(3), 99–115. <https://doi.org/10.1139/geomat-2021-0006>
- Kamal, K., & EZ-ZAHRAOUY, H. (2023). *A comparison between the VGG16, VGG19 and ResNet50 architecture frameworks for classification of normal and CLAHE processed medical images*. <https://doi.org/10.21203/rs.3.rs-2863523/v1>
- Kang, W., Xiang, Y., Wang, F., & You, H. (2019). EU-Net: An Efficient Fully Convolutional Network for Building Extraction from Optical Remote Sensing Images. *Remote Sensing*, 11(23), 2813. <https://doi.org/10.3390/rs11232813>
- Li, W., He, C., Fang, J., Zheng, J., Fu, H., & Yu, L. (2019). Semantic Segmentation-Based Building Footprint Extraction Using Very High-Resolution Satellite Images and Multi-Source GIS Data. *Remote Sensing*, 11(4), 403. <https://doi.org/10.3390/rs11040403>
- Norelyaqine, A., Azmi, R., & Saadane, A. (2023). Architecture of Deep Convolutional Encoder-Decoder Networks for Building Footprint Semantic Segmentation. *Scientific Programming*, 2023, 1–15. <https://doi.org/10.1155/2023/8552624>
- Ok, A. O., Senaras, C., & Yuksel, B. (2013). Automated Detection of Arbitrarily Shaped Buildings in Complex Environments From Monocular VHR Optical Satellite Imagery. *IEEE Transactions on Geoscience and Remote Sensing*, 51(3), 1701–1717. <https://doi.org/10.1109/TGRS.2012.2207123>
- Rastogi, K., Bodani, P., & Sharma, S. A. (2022). Automatic building footprint extraction from very high-resolution imagery using deep learning techniques. *Geocarto International*, 37(5), 1501–1513. <https://doi.org/10.1080/10106049.2020.1778100>
- Ronneberger, O., Fischer, P., & Brox, T. (2015). *U-Net: Convolutional Networks for Biomedical Image Segmentation*.
- Vincent M, J., & P, V. (2024). Extraction of building footprint using MASK-RCNN for high resolution aerial imagery. *Environmental Research Communications*, 6(7), 075015. <https://doi.org/10.1088/2515-7620/ad5b3d>
- Wang, H., & Miao, F. (2022). Building extraction from remote sensing images using deep residual U-Net. *European Journal of Remote Sensing*, 55(1), 71–85. <https://doi.org/10.1080/22797254.2021.2018944>
- Wang, Y., Zeng, X., Liao, X., & Zhuang, D. (2022). B-FGC-Net: A Building Extraction Network from High Resolution Remote Sensing Imagery. *Remote Sensing*, 14(2), 269. <https://doi.org/10.3390/rs14020269>
- Yuan, W., Wang, J., & Xu, W. (2022). Shift Pooling PSPNet: Rethinking PSPNet for Building Extraction in Remote Sensing Images from Entire Local Feature Pooling. *Remote Sensing*, 14(19), 4889. <https://doi.org/10.3390/rs14194889>
- Ziaei, Z., Pradhan, B., & Mansor, S. Bin. (2014). A rule-based parameter aided with object-based classification approach

for extraction of building and roads from WorldView-2 images. *Geocarto International*, 29(5), 554–569. <https://doi.org/10.1080/10106049.2013.819039>

ACKNOWLEDGEMENT

We are grateful to Bhaktapur Municipality and Khwopa College of Engineering for providing the orthomosaics of Bhaktapur Municipality



Author's Information

Name	: Abin Prajapati
Academic Qualification	: MSc in Cartography and Geographical Information Engineering
Organization	: Smart Engineering Consultant Pvt. Ltd.
Current Designation	: GIS Analyst
Work Experience	: 7 years

Price of Aerial Photograph

Data	Size	NRs. Rate	Remarks
Aerial Photo (Scan Copy)	23cm X 23cm	300	

Price of Image Data

Image of Topographic Map	NRs. Rate	Remarks
Digital orthoimage (at scale 1:5000)	Rs 3125	
Digital orthoimage (at scale 1:10000)	Rs 5000	
District Map (150 dpi in JPEG file)	Rs 200	
VDC Map (150 dpi in JPEG file)	Rs 50	

Price of Land Use Digital Data

District Level Data	Unit	Rate	Local Level Data	Unit	Rate
Present Land Use	Per sq. Km.	5	Present Land Use	Per sq.Km.	50
GIS Data for Land Resource (Except Land Use Zoning Data)	Per sq. Km.	5	Soil Map Data	Per sq.Km.	50
Profile	per district	200	Land Capability Data	Per sq.Km.	50
			Profile	Per local level	1000

Price of LiDAR Data

Type	Unit	Rate	Type	Unit	Rate
Point Cloud Data	Per sq. Km.	Rs 15000	Digital Terrain Model Data	Per sq. Km.	Rs 5000
Contour Data	Per sq. Km.	Rs 3000	Orthomosaic Data (RGB)	Per sq. Km.	Rs 6000
Digital Surface Model Data	Per sq. Km.	Rs 4000	Full Data	Per sq. Km.	Rs 25000

Orthomosaic of Kathmandu Valley (39 sq. km) in RGB Rs 5000 per sheet

Price of Digital Topographic Data Layers

LAYER	Rs/Sheet	S.N	Data	Price
Administrative	100.00	1	Seamless Data whole Country	
Transportation	200.00	1.1	Digital data of all layers	Rs. 300000.00
Building	60.00	1.2	Digital data compiled at scale 1:1000000	Free
Landcover	300.00	2	Digital data of all layers compiled at scale 1:500000	Rs 1000 per sheet
Hydrographic	240.00	3	Generalized Districtwise Data Layers	
Contour	240.00	3.1	Administrative Boundary	Free
Utility	20.00	3.2	Building	Rs. 15000.00
Designated Area	20.00	3.3	Contour	Rs. 65000.00
Full Sheet	1000.00	3.4	Transportation	Rs. 60000.00
		3.5	Hydrographic	Rs. 70000.00
		3.6	Landcover	Rs. 87000.00
		3.7	Utility Line	Rs. 2000.00
		3.8	Designated Area	Rs. 1000.00
		3.9	Full Sheet	Rs. 2000.00
		4	Rural Municipality (Gaunpalika) unitwise- all layers	Rs. 1000.00
		5	Municipality (Nagarpalika) unitwise- all layers	Rs. 2000.00

Price of Printed maps

S.No	Maps	Unit	Rate (In NRs)
1	Political and Administrative Map of Nepal (2019)	Whole Nepal	150
2	Topographic Base Map (1992-2001)	Sheet	150
3	Topographic Map (1950s)	Sheet	50
4	District Map (1980s)	Sheet	50
5	Land Utilization Map (LRMP)	Sheet	50
6	Land Capability Map (LRMP)	Sheet	50
7	Land System Map (LRMP)	Sheet	50
8	Pysiographic Map of Nepal		50

Price of SOTER Data Whole Nepal NRs : 1000.00.

Evaluating Machine Learning Algorithms for Forest Cover Extraction in Kailali, Nepal

Sudarshan Kumar Gautam¹, Sanjeevan Shrestha², Subhadra Joshi³ & Jeshan Pokharel³

sudarshangtm01@gmail.com, shr.sanjeevan@gmail.com, joshisub7@gmail.com, jeshanpokharel123@gmail.com

¹ Survey Department, ² Ministry of Land Management Cooperatives and Poverty Alleviation, ³ Kathmandu University,

KEYWORDS

Forest Cover Mapping, Machine Learning, Sentinel-2, K-fold cross validation, Performance evaluation

ABSTRACT

Forest cover mapping plays a critical role in environmental monitoring, biodiversity conservation, and sustainable land-use planning, especially in ecologically diverse regions like Nepal. This study evaluates the performance of ten supervised machine learning classifiers for forest cover extraction in the Kailali District using Sentinel-2 satellite imagery. The classifiers assessed include Random Forest, Support Vector Classifier, Logistic Regression, Linear Discriminant Analysis, K-Nearest Neighbors, Decision Tree, Gaussian Naïve Bayes, AdaBoost, Quadratic Discriminant Analysis, and Gaussian Process Classifier. Feature engineering involved the derivation of 17 vegetation and water indices alongside key spectral bands, followed by correlation analysis to optimize input variables. Ground truth data were collected through field surveys and high-resolution imagery to ensure accurate model training and validation. Classifier performance was evaluated using k-fold cross-validation and standard metrics, including accuracy, precision, recall, and F1-score. Among the models, Random Forest and Gaussian Process achieved the highest classification accuracies of 91.37% and 91.31%, respectively. The study demonstrates the effectiveness of machine learning techniques in forest cover classification and provides valuable insights for enhancing remote sensing-based monitoring frameworks in support of sustainable forest management in Nepal.

1. INTRODUCTION

1.1 Background

Forest cover extraction is an essential process in remote sensing and Geographic Information Systems (GIS) that involves identifying and mapping forested areas using satellite imagery and aerial photographs. This process plays

a crucial role in environmental monitoring, conservation efforts, and sustainable land management. In Nepal, where forests contribute significantly to biodiversity and ecological stability, forest cover mapping provides valuable insights for policymakers, researchers, and conservationists. It helps in identifying biodiversity hotspots, tracking

deforestation trends, and supporting sustainable forest management initiatives (Singh & Kushwaha, 2008).

Forests offer essential ecosystem services such as carbon sequestration, water regulation, and soil conservation, playing a key role in climate change mitigation and disaster risk reduction (Moomaw et al., 2019). In Nepal, where many communities depend on forests for their livelihoods, mapping forest cover helps in planning responsible resource utilization while maintaining ecological balance (Pokharel et al., 2023). Additionally, forest cover mapping supports land-use planning by guiding decisions on afforestation, reforestation, and agricultural expansion while minimizing negative environmental impacts. It provides essential data for identifying deforested or degraded areas suitable for restoration and helps balance ecological conservation with human development needs (Muinonen et al., 2012). As a committed participant in international agreements like the UNFCCC and REDD+, Nepal actively utilizes forest cover data to meet its climate action goals and support sustainable development efforts. This data is crucial for monitoring emissions reductions, managing forest resources, and reporting on progress under its Nationally Determined Contributions (NDCs) (Maraseni et al., 2020). By continuously monitoring and updating forest cover information, Nepal can strengthen conservation strategies, reduce environmental risks, and promote long-term ecological and economic sustainability.

1.2 Significance of Machine Learning for Forest Cover Extraction

Assessing different machine learning algorithms for forest cover extraction is essential for improving classification accuracy and ensuring reliable forest mapping. Various algorithms possess unique strengths and weaknesses, making it necessary to evaluate

multiple models to determine the most effective approach. Selecting appropriate machine learning techniques enhances the precision of forest cover classification, providing dependable data for environmental monitoring and decision-making (Maxwell et al., 2018).

Accurate forest cover maps contribute to sustainable resource management by helping governments and conservation organizations plan forestry activities, monitor deforestation, and identify reforestation opportunities. Since forests play a significant role in carbon sequestration and climate regulation, improved forest mapping enables better estimation of carbon storage, analysis of deforestation trends, and assessment of land-use impacts on greenhouse gas emissions (DeFries et al., 2007).

Machine learning-based forest cover extraction is also crucial for biodiversity conservation. Detailed maps help identify critical habitats, species distribution, and biodiversity hotspots, supporting the protection of endangered species. Additionally, forest cover information aids in disaster risk management, providing insights into the vulnerability of forests to wildfires, landslides, and floods.

Governments and environmental agencies rely on forest cover data to develop policies for land use, conservation, and sustainable development (Kissinger et al., 2012). Many countries utilize satellite-based monitoring systems, which can be enhanced through machine learning techniques to provide continuous and updated forest cover information (Pacheco-Pascagaza et al., 2022).

1.3 Objectives

The primary objectives of this study are to assess the effectiveness of different machine learning algorithms for forest cover extraction using remote sensing data in Nepal. This includes comparing the algorithms based on

metrics such as accuracy, precision, recall, and F1 score to determine their performance. Additionally, the study aims to identify the most suitable algorithm for efficient and accurate forest cover mapping in Nepal, culminating in the creation of forest cover maps derived from various classification models.

2. METHODOLOGY

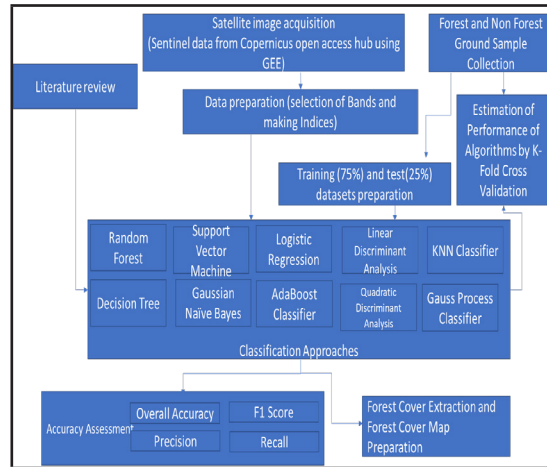


Figure 1: Overall Methodology of the Research

2.1 Study Area

The study was conducted in Kailali District, Nepal (Figure 2), covering an area of approximately 3,235 square kilometers. The district comprises diverse landscapes, from Terai plains to Siwalik foothills, making it an ideal study area for evaluating forest classification models.

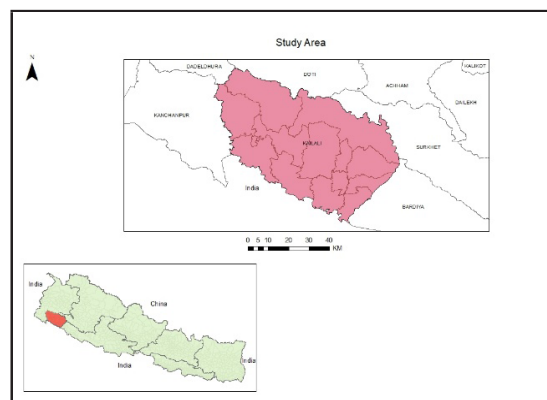


Figure 2: Study Area (Kailali District, Nepal) Map

2.2 Data Collection and Processing

2.2.1 Satellite Imagery

Sentinel-2 imagery was acquired from the Copernicus Open Access Hub. The four spectral bands (Blue Band (B2), Green Band (B3), Red Band (B4), and Near-Infrared Band (B8)) were used for classification.

2.2.2 Ground Truth Data Collection

The forest and non-forest point sample data utilized in this study forms the foundation for training and validating the machine learning algorithms employed to classify forested and non-forested regions. Ground truth data were gathered through field surveys using handheld GPS devices, along with the digitization of points from high-resolution Google Earth imagery.

2.2.3 Feature Engineering

Several spectral indices, as referenced from the Index Database, were derived from satellite bands, including vegetation indices such as NDVI, EVI2, SAVI, ARVI, OSAVI, and MSAVI2, as well as a water index (NDWI).

A total of 17 indices were computed using selected spectral bands (Red, Green, Blue, and NIR), as outlined in Table 1. When combined with the four original bands, this resulted in a total of 21 features, which were subsequently analyzed through correlation assessment. To minimize redundancy and enhance model performance, indices with high correlation values (>0.98) were excluded from further analysis (Figure 3).

Table 1: List of Indices Prepared using selected bands

Abbreviation	Full Name	Formula
NDVI	Normalized Difference Vegetation Index	$\frac{NIR - R}{NIR + R}$
EVI	Enhanced Vegetation Index	$\frac{2.5 \times (NIR - R)}{(NIR + 6 \times R - 7.5 \times B + 1)}$
SAVI	Soil-Adjusted Vegetation Index	$\frac{NIR - R}{NIR + R + L} \times (1 + L)$ Where L is a constant value (usually set to 0.5)
ARVI	Atmospherically Resistant Vegetation Index	$\frac{NIR - 2 \times R + B}{NIR + 2 \times R + B}$
OSAVI	Optimized Soil-Adjusted Vegetation Index	$\frac{NIR - R}{NIR + R + 0.16} \times 1.16$
ARVI2	Modified Atmospherically Resistant Vegetation Index	$\frac{2 \times NIR + 1 - \sqrt{(2 \times NIR + 1)^2 - 8 \times (NIR - R)}}{2}$
EVI2	Enhanced Vegetation Index 2	$\frac{2.5 \times (NIR - R)}{(NIR + 2.4 \times R + 1)}$
EVI2.2	Enhanced Vegetation Index 2.2	$G_f \times \frac{(2.5 \times (NIR - R))}{(NIR + 2.4 \times R + 1)}$ Where G_f is a gain factor (Usually set to 2.5)
MCARI2	Modified Chlorophyll Absorption Ratio Index 2	$\frac{1.5 \times (2.5 \times (NIR - R) - 1.3 \times (NIR - G))}{\sqrt{2 \times NIR + 1 + 6 \times G - 7.5 \times R}}$
BNDVI	Blue Normalized Difference Vegetation Index	$\frac{NIR - B}{NIR + B}$
GNDVI	Green Normalized Difference Vegetation Index	$\frac{NIR - G}{NIR + G}$
GOSAVI	Green Optimized Soil-Adjusted Vegetation Index	$\frac{NIR - G}{NIR + G + 0.16} \times 1.16$
NDWI	Normalized Difference Water Index	$\frac{G - NIR}{G + NIR}$
MTVI2	Modified Triangular Vegetation Index 2	$\frac{1.5 \times (1.2 \times (NIR - G) - 2.5 \times (R - G))}{\sqrt{(2 \times NIR + 1)^2 - (6 \times NIR - 5 \times \sqrt{R})} - 0.5}$
CIgreen	Green Chlorophyll Index	$\frac{NIR}{G} - 1$
GARVI	Green Atmospherically Resistant Vegetation Index	$\frac{NIR - (G - B)}{NIR + (G - B)}$
MSAVI2	Modified Soil-Adjusted Vegetation Index 2	$\frac{(2 \times NIR + 1 - \sqrt{(2 \times NIR + 1)^2 - 8 \times (NIR + R)})}{2}$

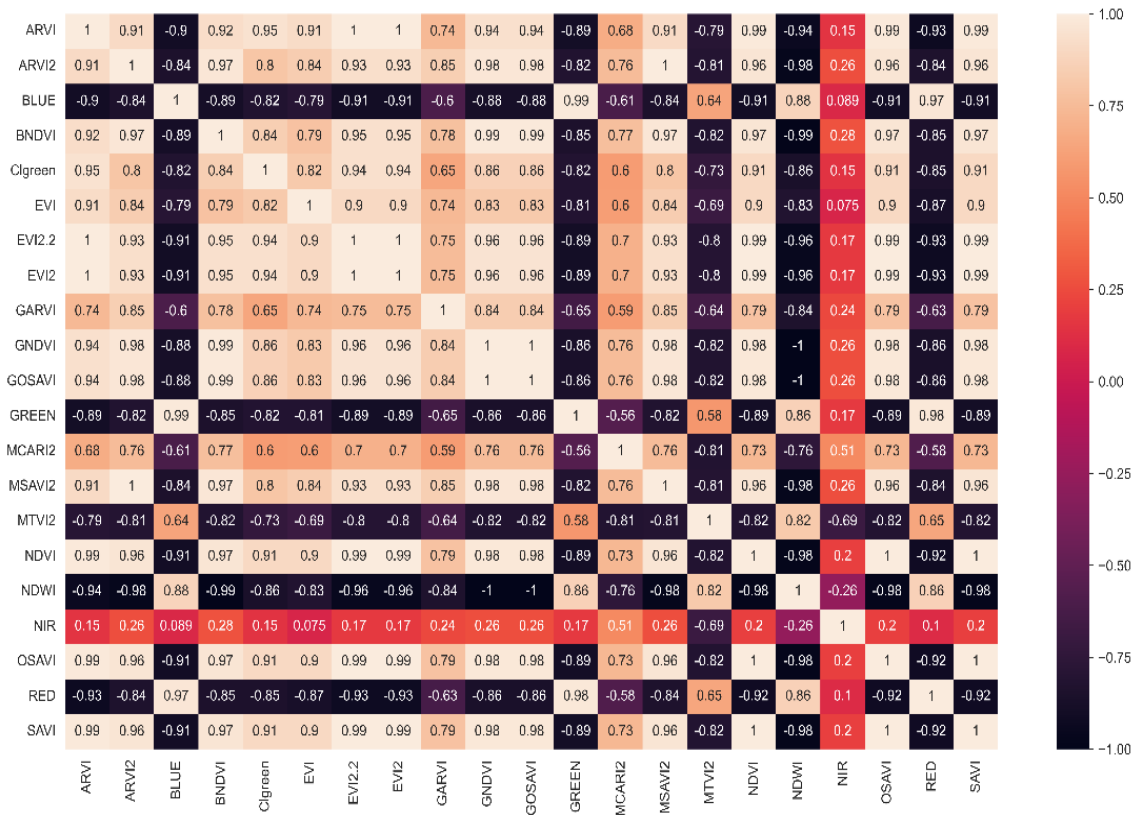
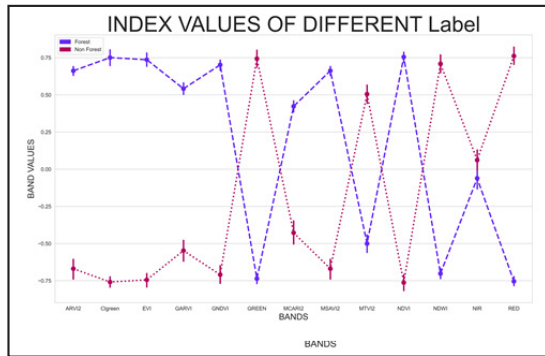


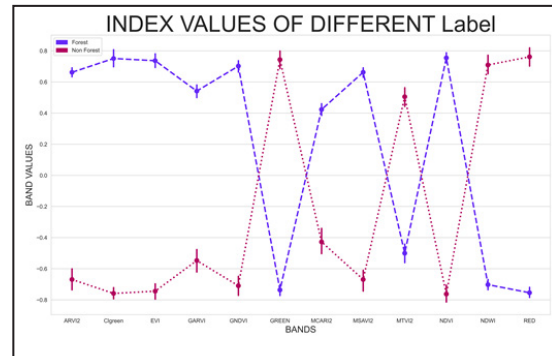
Figure 3 : Correlation Analysis between Different Vegetation Indices

The selected spectral bands and indices (ARVI2, Clgreen, EVI, GARVI, GNDVI, GREEN, MCARI2, MSAVI2, MTVI2, NDVI, NDWI, NIR, and RED) were further examined through a line plot (Figure 4(a)), illustrating their variation across forest and non-forest classes. The plot shows that the Near-Infrared

(NIR) band exhibits minimal differentiation between the two classes, suggesting limited discriminatory capability in this specific context. As a result, NIR was excluded from further analysis to streamline the process without compromising classification effectiveness.



(a)



(b)

Figure 4 : Line plot including NIR (a) and Excluding NIR (b)

2.3 Machine Learning Models

Ten supervised machine learning classifiers (as presented in Table 2) were initially assessed using 10-fold cross-validation to identify any models demonstrating weak performance that might warrant early exclusion. Among them, Random Forest and Gaussian Process Classifier achieved the highest average accuracies—91.37% and 91.31%, respectively—with low standard deviations, suggesting strong and consistent performance across folds. In contrast, the Decision Tree classifier recorded the lowest accuracy (86.59%) and showed relatively higher variability. Nevertheless, all classifiers demonstrated satisfactory performance and were retained for subsequent analysis.

Table 2 : K-Fold Cross Validation Accuracy of Machine Learning Models

Classifier	Accuracy (%)	Deviation (%)
Random Forest	91.37	2.88
Gaussian Process	91.31	2.55
Support Vector Machine	91.19	2.53
Logistic Regression	90.68	3.26
Linear Discriminant Analysis	90.62	2.69
K-Nearest Neighbors	90.68	3.28
Decision Tree	86.59	3.16
Gaussian Naïve Bayes	90.62	2.49
AdaBoost	89.92	2.82
Quadratic Discriminant Analysis	88.28	2.51

Final evaluations were performed using a standardized train-test split (75% training, 25% testing) with a fixed random state to ensure reproducibility and fair comparison across models.

3. RESULTS AND DISCUSSION

3.1 Performance of Classifiers

The performance of ten supervised machine learning classifiers was evaluated using precision, recall, F1-score, and overall accuracy. Logistic Regression and AdaBoost achieved the highest accuracy of 0.8967, followed closely by Support Vector Classifier, K-Nearest Neighbors, and Gaussian Process Classifier with accuracies around 0.89. Quadratic Discriminant Analysis had the lowest performance with an accuracy of 0.7884. The comparison highlights the strengths and weaknesses of each model for forest cover classification tasks in the study area.

Table 3 : Accuracy, Precision, Recall and F1-Score of different ML Algorithms

Classifier	Accuracy	Forest			Non-Forest		
		Precision	Recall	F1-Score	Precision	Recall	F1-Score
RF	89.17	87	92	89	92	87	89
SVC	89.42	87	92	89	92	87	89
LR	89.67	86	93	90	93	86	90
LDA	89.17	87	92	89	92	87	89
K-NN	89.42	87	92	89	92	87	90
Decision Tree	85.64	85	85	85	86	86	86
Gaussian Process	89.17	86	93	89	93	86	89
Gaussian NB	88.92	85	93	89	93	85	89
AdaBoost	89.67	86	94	90	94	85	90
QDA	78.84	80	75	77	78	82	80

3.2 Forest Cover Maps

Forest cover maps were produced by applying each of the aforementioned classifiers to the dataset, resulting in binary classifications of forest and non-forest areas. These classifications were subsequently used to generate thematic maps, providing a visual representation of the spatial distribution of

forest and non-forest regions. An example of the resulting maps is presented in Figure 5 and 6.

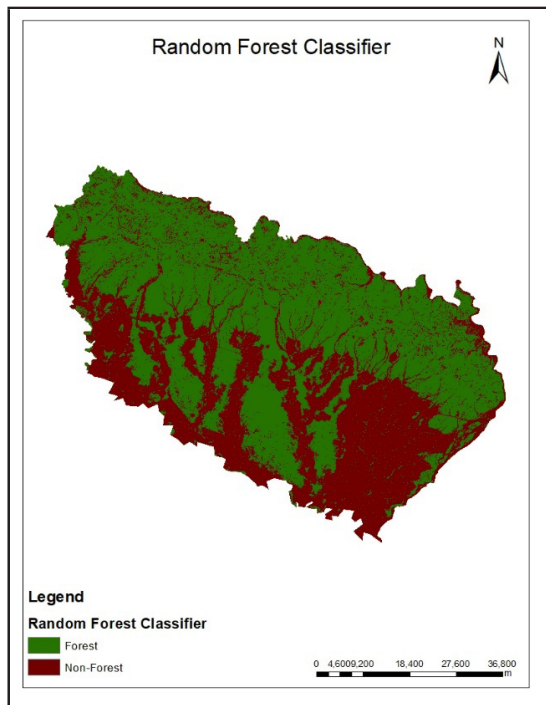


Figure 5: Forest and Non-Forest Regions of Study Area by Random Forest Classifier

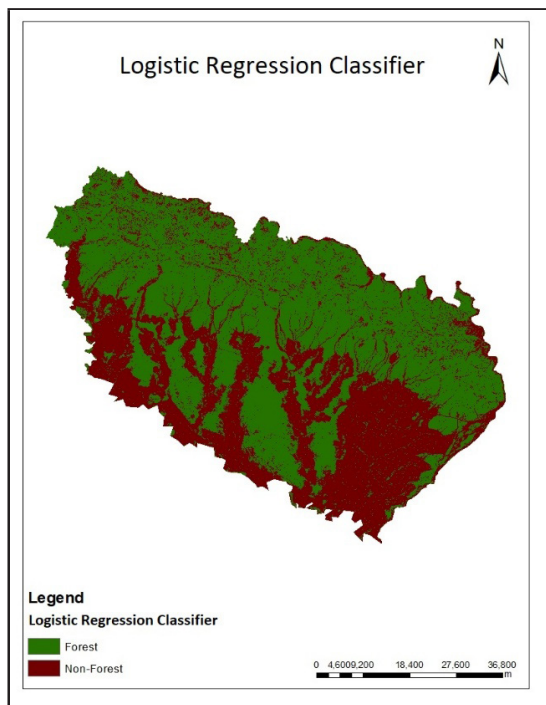


Figure 6: Forest and Non-Forest Regions of Study Area by Logistic Regression Classifier

4. CONCLUSION AND RECOMMENDATIONS

4.1 Conclusion

This study investigated the performance of ten supervised machine learning classifiers for forest cover extraction in the context of Nepal’s diverse landscape. Through rigorous evaluation using 10-fold cross-validation, the Random Forest classifier emerged as the top performer, demonstrating both high accuracy and consistency across folds. Logistic Regression, Gaussian Process, and AdaBoost classifiers also showed strong and balanced results in terms of precision and recall for both forest and non-forest classes.

On the other hand, classifiers such as Decision Tree and Quadratic Discriminant Analysis recorded relatively lower performance, which may be attributed to their limitations in modeling complex, nonlinear relationships within the data. While the Gaussian Naïve Bayes classifier achieved moderate accuracy, its reduced precision for non-forest areas indicates a potential risk of false positives in real-world applications.

4.2 Recommendations

Given their reliable performance, Logistic Regression, Gaussian Process, and AdaBoost classifiers are recommended for practical forest cover classification tasks in the study region. These models strike a favorable balance between interpretability and predictive capability, making them suitable for use in operational mapping and decision support systems.

Future research could benefit from exploring advanced ensemble techniques or hybrid approaches that integrate multiple models to further enhance classification accuracy. In addition, periodic retraining of models with updated datasets is encouraged to reflect changes in land cover and ensure continued relevance over time.

Finally, the study underscores the importance of hyperparameter optimization. Notably, fine-tuning the Random Forest classifier led to a measurable improvement in accuracy (increasing to 92%), suggesting that careful model calibration can significantly boost performance.

REFERENCES

- DeFries, R., Achard, F., Brown, S., Herold, M., Murdiyarso, D., Schlamadinger, B., & de Souza Jr, C. (2007). Earth observations for estimating greenhouse gas emissions from deforestation in developing countries. *Environmental Science & Policy*, 10(4), 385–394.
- Kissinger, G., Herold, M., & Sy, V. De. (2012). *Drivers of deforestation and forest degradation: a synthesis report for REDD+ policymakers.*
- Maraseni, T. N., Poudyal, B. H., Rana, E., Khanal, S. C., Ghimire, P. L., & Subedi, B. P. (2020). Mapping national REDD+ initiatives in the Asia-Pacific region. *Journal of Environmental Management*, 269, 110763.
- Maxwell, A. E., Warner, T. A., & Fang, F. (2018). Implementation of machine-learning classification in remote sensing: An applied review. *International Journal of Remote Sensing*, 39(9), 2784–2817.
- Moomaw, W. R., Masino, S. A., & Faison, E. K. (2019). Intact forests in the United States: Proforestation mitigates climate change and serves the greatest good. *Frontiers in Forests and Global Change*, 2, 449206.
- Muononen, E., Parikka, H., Pokharel, Y. P., Shrestha, S. M., & Eerikäinen, K. (2012). Utilizing a multi-source forest inventory technique, MODIS data and Landsat TM images in the production of forest cover and volume maps for the Terai Physiographic Zone in Nepal. *Remote Sensing*, 4(12), 3920–3947.
- Pacheco-Pascagaza, A. M., Gou, Y., Louis, V., Roberts, J. F., Rodríguez-Veiga, P., da Conceição Bispo, P., Espírito-Santo, F. D. B., Robb, C., Upton, C., & Galindo, G. (2022). Near real-time change detection system using Sentinel-2 and machine learning: A test for Mexican and Colombian forests. *Remote Sensing*, 14(3), 707.
- Pokharel, B., Chotikarn, P., & Gywali, S. (2023). Changing the perception of forest value and attitude toward management in the conservation area in Nepal and sustainable forest energy: A Review. *Asian Journal of Conservation Biology*, 12(2), 239–247.
- Singh, J. S., & Kushwaha, S. P. S. (2008). Forest biodiversity and its conservation in India. *International Forestry Review*, 10(2), 292–304. <https://doi.org/10.1505/ifer.10.2.292>



Author's Information

Name	: Sudarshan Kumar Gautam
Academic Qualification	: Masters of Engineering in Geoinformatics (Kathmandu University)
Organization	: Survey Department
Current Designation	: Survey Officer
Work Experience	: 12 years

Flood Hazard Modelling Assessment Using Deep Learning and Earth Observation

Binita Shahi¹, Arjun Poudel², Ashmeera Dahal³ & Sandesh Upadhyaya⁴
shahiii.binita@gmail.com, arjpou268@gmail.com, ashmeeradahal04@gmail.com, sandeshupadhya1@gmail.com
¹Land Management Training Center, ²Survey Office Palpa, ³Ministry of Land Management and Cooperatives and Poverty Alleviation, ⁴Survey Department

KEYWORDS

Flood Modelling, U-Net, Deep Learning, CNN and Softmax

ABSTRACT

This study explores the integration of satellite imagery with deep learning models, specifically the U-Net architecture, for flood hazard modelling and detection in flood-prone regions of Uttar Pradesh, India. The research focuses on using Sentinel-1 satellite data, combined with multispectral imagery, to develop a robust flood detection system. The methodology involves preprocessing satellite images, creating flood polygons through change detection, and training a U-Net model with a ResNet34 backbone on a dataset of 28,896 image patches. The model achieved an accuracy of 92.82% and an Area Under the Curve (AUC) score of 90%, demonstrating strong performance in identifying flooded areas. The study highlights the effectiveness of combining remote sensing and deep learning techniques for flood mapping, providing high-resolution flood maps validated against ground truth data. The results underscore the potential of AI-driven approaches in enhancing flood risk assessment, disaster response, and management strategies. In order to address class imbalance, optimizing threshold selection is necessary and incorporating additional data sources, such as LiDAR and hydrological models, can improve model performance and applicability. This research contributes to advancing flood monitoring and mitigation efforts, offering a scalable and efficient solution for flood-prone regions.

1 INTRODUCTION

Flooding in the state of Uttar Pradesh, India affected over 245,000 people in August 2022 (ReliefWeb, 2022). The Ganges was above the danger mark in at least 5 locations, including Varanasi (IMD, 2022). According to the National Emergency Response Centre (NERC) in India, flooding has affected over 1,000 villages across 22 districts in the state since 26 August 2022. Authorities had opened

386 relief camps, which, as of 29 August, were housing 16,562 evacuees. As of 31st August 2022, NERC reported 245,585 people were affected and at least 4 people died during the flood.

Satellite imageries combined with U-Net-based deep learning methods provide a powerful approach for detecting and analyzing floods (Pech-May et al., 2023). Satellites equipped with remote sensing technology capture high-

resolution images of the Earth's surface. These images can show land use, water bodies and changes over time. By taking images before, during, and after flooding events, satellites provide a temporal perspective, which is crucial for assessing the extent and impact of floods (NASA, 2020). As satellites can capture data in various spectral bands (e.g., visible, infrared), this allows for identifying water bodies and differentiating flooded areas from dry land based on their spectral signatures.

Machine learning (ML) is a subset of artificial intelligence (AI) that involves the development of algorithms and statistical models that enable computers to perform tasks without explicit programming (Ian et al., 2016). ML allows systems to learn from data, identify patterns, and make decisions with minimal human intervention (Mitchell, 1999). Unlike traditional computing methods that follow predefined rules, machine learning systems improve their performance over time as they are exposed to more data, adapting to new information and conditions.

Remote sensing involves the collection of data from a distance, typically using satellites, aircraft, or UAVs (unmanned aerial vehicles) equipped with various sensors to capture imagery of the Earth's surface (Panda et al., 2015). The data collected by these sensors can include optical, infrared, radar, and LiDAR (Light Detection and Ranging) measurements, offering a rich and complex representation of the environment (Panda et al., 2015). However, analyzing these large datasets, especially in real-time, poses a significant challenge due to the vast amount of information and the high-dimensional nature of the data. This is where machine learning comes in. ML algorithms excel at handling large volumes of data and can automatically identify patterns, classify objects, and extract meaningful information from remote sensing images (Lary et al., 2016). These capabilities are invaluable for applications such as environmental

monitoring, disaster management, urban planning, and agricultural monitoring.

Machine learning techniques can process remote sensing data more efficiently than traditional methods. For example, in the context of satellite imagery, ML algorithms can be trained to detect land use changes, classify vegetation types, or identify flood-prone areas. These automated systems can analyze vast regions and provide insights at speeds far greater than manual analysis. Moreover, machine learning can improve over time as more data is available, allowing for increasingly accurate predictions and analyses.

U-Net is a convolutional neural network designed for biomedical image segmentation, but it also excels at segmenting satellite images (Ronneberger et al., 2015). It consists of an encoder-decoder structure with skip connections, allowing for precise localization of features (Ronneberger et al., 2015). A U-Net model can be trained on labeled datasets where different classes (e.g., water, land, urban areas) are annotated. This training enables the model to learn the characteristics of flooded and non-flooded regions. Once trained, the U-Net can process new satellite images to segment and identify flooded areas by classifying every pixel as either "flood" or "non-flood". This segmentation is critical in providing detailed maps of affected regions. U-Net can help estimate the extent of flooding soon after an event using real-time satellite images, allowing for timely responses (Pech-May et al., 2023). By comparing images over time, U-Net can effectively highlight changes in land cover due to flooding, helping in damage assessment. Flood maps generated using this method can be integral for disaster response planning, risk assessment, and developing management strategies. Combining U-Net with other machine learning techniques or algorithms (like ensemble methods) can improve accuracy in detecting and classifying flooded areas (Pech-May et al., 2023). Thus,

the integration of satellite imagery with U-Net deep learning models provides a robust mechanism for effectively monitoring and managing flood events, facilitating better preparedness and response strategies.

2 MATERIALS AND METHODS

2.1 Study Area

For this study, about 1635 sq. km area was chosen that lies within the Ghazipur, Ballia, Siwan, Saran and Bhojpur districts of the Uttar Pradesh State of India, which is located in the bank of the Ganges River focusing on the high-flood areas during heavy rainfall in August and September 2022 as shown below in Figure 1.

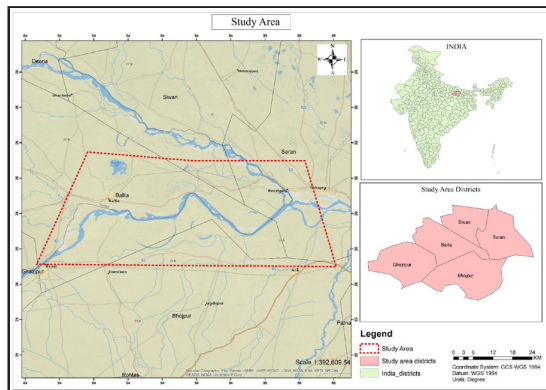


Figure 1: Study Area Map

2.2 Research Method

The methodology adopted is described as a process for flood mapping using Sentinel-1 data and Multispectral data, combining remote sensing techniques with deep learning to achieve precise flood extent detection. The process starts with the acquisition of pre- and post-flood satellite images, followed by preprocessing in the Sentinel Application Platform (SNAP). This stage involves performing subsetting, radiometric and geometric corrections, collocation of data and applying band math to differentiate water surfaces. The flood extent is then extracted through methods like thresholding, change detection and GIS-based digitization. To enhance the classification accuracy,

Multispectral optical data is incorporated. The resulting flood extent is compared to ground truth data using Area Under the Receiver Operating Characteristic Curve (AUC-ROC) analysis. If the accuracy does not meet the required threshold, a Convolutional Neural Network (CNN)-U-Net deep learning model is trained with labeled data to further refine the flood extent using AI-powered segmentation. After validation, the final flood map is generated, offering improved precision for flood assessment.

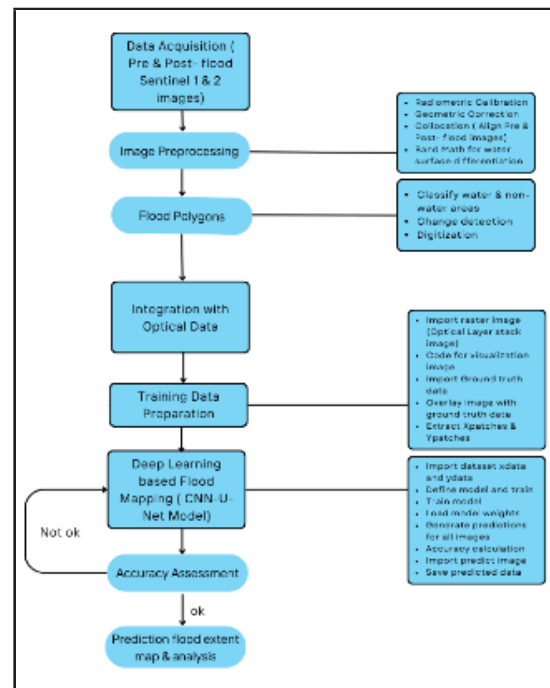


Figure 2: Methodological workflow for Flood Modelling

2.2.1 Training Data Preparation

2.2.1.1 Data Acquisition

In order to develop the ground truth data, Sentinel 1A images with a resolution of 10 meters were used. Similarly, for creating training datasets and model development, High-resolution multispectral imagery with a resolution of 3 meters was used.

2.2.1.2 Image Preprocessing

The SNAP tool was used for preprocessing images, including subsetting, radiometric

and geometric correction, multilooking, collocation as well as band math operations like Theta/Theta for master and slave images of collocated datasets.

2.2.1.3 Flood Polygons

The change detection process was carried out for the pre-flood and post-flood images after being preprocessed, depicting water and non-water areas. After that, flood areas were digitized in Quantum Geographic Information System (QGIS) environments, resulting in a vector polygon dataset called flood polygons. Each polygon was carefully delineated based on visual interpretation and the flood extent derived from Synthetic Aperture Radar (SAR) ratio calculations.

2.2.2 Integration with Optical Data (Training Sample in CNN)

Training samples are the datasets used to train the model and let it learn the features and patterns of the data (Lary et al., 2016). Without high-quality training data, even the most efficient machine learning algorithms will fail to perform (Lary et al., 2016). The need for quality, accurate, complete, and relevant data is required in the initial training process (Mohammed et al., 2022). Only if the algorithm is fed with good training data, it can easily pick up the features and find relationships that it needs to predict (Sanyal et al., 2021). The training process involves presenting the model with input data (features) along with the corresponding correct output (labels or targets), allowing the model to learn the patterns and relationships within the data (Zhao et al., 2020). The quality and quantity of training samples directly impact the performance of the trained model (Halevy et al., 2009).

Optical images from the planet website before and after the flood were imported and visualization was carried out in the Collab environment, where vector data of flood polygons were rasterized and all layers were

overlaid to define x patches and y patches of the training sample. The training samples were assigned with corresponding class labels, forming the basis for supervised classification and model training. This dataset served as a crucial input for flood mapping and accuracy assessment, enhancing the reliability of the final classification results.

2.2.3 Deep Learning based Flood Mapping (CNN-U-Net Model)

The U-Net model, a type of convolutional neural network (CNN), is widely used for flood data modeling due to its ability to perform pixel-wise segmentation (Ronneberger et al., 2015). It follows an encoder-decoder architecture, where the down-sampling (encoder) path extracts spatial features, and the up-sampling (decoder) path reconstructs the segmented image while preserving spatial details (Ronneberger et al., 2015).

For flood detection, SAR (Sentinel-1) and multispectral (Sentinel-2) images were used as input. The training dataset, created from digitized flood extent polygons, helped the U-Net learn the distinction between flooded and non-flooded areas. The activation function (e.g., ReLU) enhanced feature extraction, while the sigmoid or SoftMax function at the output layer classified flood-affected regions.

To optimize performance, hyperparameter tuning (learning rate, batch size and number of filters) was applied. Loss functions such as binary cross-entropy or Dice loss improved segmentation accuracy. The trained U-Net model effectively predicted flood-affected areas, providing high-resolution flood maps for disaster response and management.

2.2.4 Accuracy Assessment

After training, the model was tested on an unseen validation image, a georeferenced GeoTIFF file, provided by project partners. The model predicted flood-prone areas, which were binarized using a 0.50 threshold.

The predicted results were compared against digitized ground truth datasets derived from SNAP-processed imagery and validated using QGIS. Visual comparisons showed a strong spatial correlation between predicted flood areas and ground truth samples.

3 RESULTS

3.1 Flood Mapping Dataset Preparation

Initially, the layer stack of pre and post-flood multispectral images were used as an input and then, ground truth data were overlaid on layer stacked image. Then, the patch dimensions of XData obtained were (28896, 32, 32, 6) and that of YData obtained were (28896, 32, 32, 1) for model training. Then, a randomly selected patch (index 555) was visualized to examine its spectral properties and corresponding flood classification. The final dataset was stored in NumPy (.npy) format for further deep-learning applications.

3.1.1 Ground Truth Data

The ground truth flood and non-flood polygons were extracted from Sentinel 1A imagery of pre and post-flood after applying correction, band math and collocation. Then, the digitization of sample flood polygons was integrated and overlaid onto the raster for validation, which is shown in Figure 3.

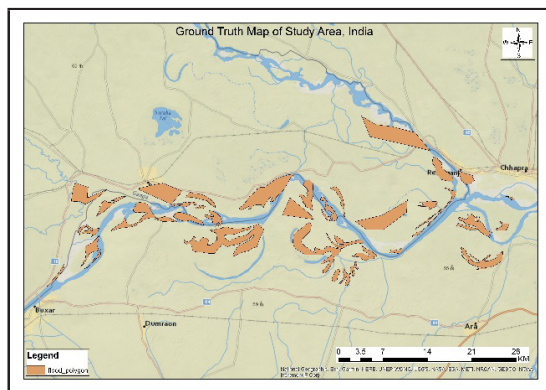


Figure 3: Ground Truth Data of Study Area

3.1.2 Input Dataset with Ground Truth Data

The multispectral images of the study area, captured before and after the flood, were used

as the input dataset after layer stacking. This dataset was defined as XData and overlaid with ground truth data, which was defined as YData which is shown in below Figure 4.

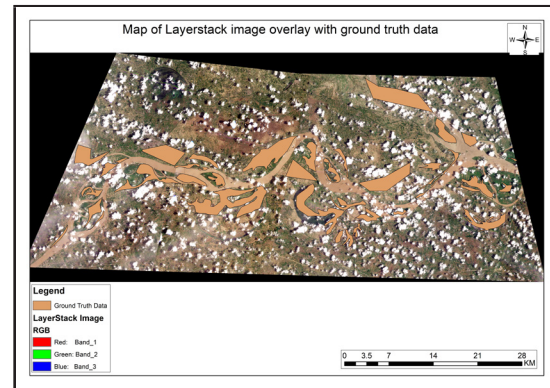


Figure 4: Layer stack image overlaid with ground truth data.

3.2 Data Modeling

In this phase, XData and YData were the input dataset. The AUC score was calculated using a weightage file where the XData and YData were split into 70% training (20,227 samples) and 30% testing (8,669 samples) and was obtained 90% and that of accuracy score was obtained 92.82%. Then, Predictions were compared with ground truth datasets from SNAP-processed imagery and validated in QGIS.

3.3 Flood Area Prediction

Now, after the model is trained, the multispectral image of another site was used for the prediction of flooded and non-flooded areas.

3.3.1 Flood Extent Map of Prediction Area

The flood extent map of the new multispectral image of Bangladesh was obtained from the above-trained model which is shown in below Figure 6, which shows non-flooded areas as “0” with the color “Cyan blue” and flooded areas as 0.998 with the color “Dark blue”.

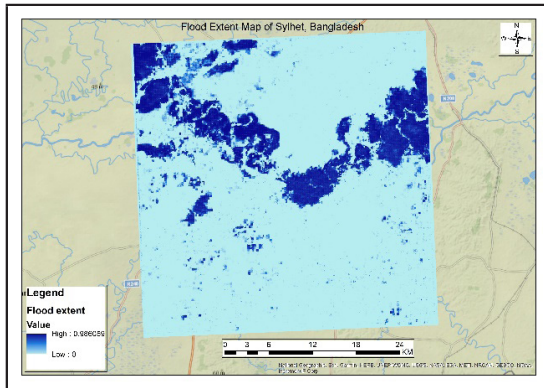


Figure 5: Flood extent map

3.3.2 Output Overlay with Prediction Image

The flooded areas as predicted from the model trained were overlaid with the prediction image which is shown in below Figure 6.

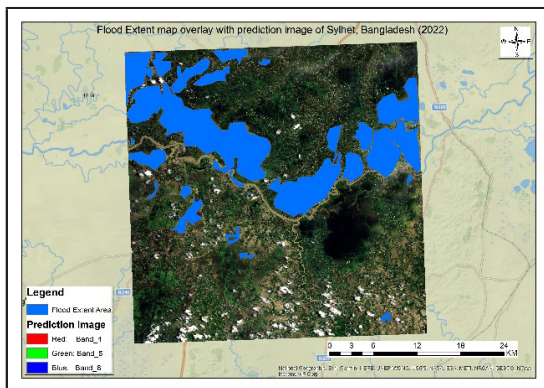


Figure 6: Predicted Flooded areas of Sylhet, Bangladesh

4 CONCLUSION

The devastating floods in Uttar Pradesh in August 2022 underscored the urgent need for advanced, rapid-response flood monitoring systems. This study addressed this challenge by developing a novel framework that uses satellite remote sensing with deep learning, especially Sentinel-1 SAR and Sentinel-2 multispectral data processed through a U-Net model. The U-Net model, trained on a dataset of 28,896 image patches, achieved an accuracy of 92.82% and an AUC score of 90%, indicating strong performance in identifying flooded areas. This approach not only

achieved high accuracy in flood detection but also demonstrated scalability by successfully mapping floods in a new region (Bangladesh), proving its potential for global applicability.

The results showed that the model could effectively segment and classify flooded areas, providing high-resolution flood maps that were validated against ground truth data. The integration of remote sensing and deep learning techniques proved to be a powerful tool for flood monitoring, offering timely and accurate information for disaster response and management. The study highlights the potential of AI-driven approaches in improving flood risk assessment and mitigation strategies.

5 RECOMMENDATION

The study's findings highlight the potential of integrating satellite imagery with deep learning models for effective flood detection and mapping. However, several areas for improvement and future work are recommended to enhance the model's performance and applicability. Firstly, if we can perform a comparative analysis in order to validate the predicted areas with that of actual flooded areas such as field data and other reliable secondary sources, the prediction through this study would be more reliable. Additionally, optimizing the binarization threshold used for flood detection could improve precision and recall, potentially leading to better overall performance. Incorporating additional data sources, such as LiDAR, weather data, or hydrological models, could further enhance the model's accuracy and provide a more comprehensive understanding of flood dynamics.

REFERENCES

- Halevy, A., Norvig, P., & Pereira, F. (2009). The Unreasonable Effectiveness of Data. *IEEE Intelligent Systems*, 24(2), 8–12. <https://doi.org/10.1109/MIS.2009.36>

- Ian, G., Bengio, Y., & Courville, A. (2016). *Deep Learning*. MIT Press. <http://www.deeplearningbook.org>
- IMD. (n.d.). *Flood Situation in Uttar Pradesh*. 2022. Retrieved March 4, 2025, from <https://mausam.imd.gov.in/>
- Lary, D. J., Alavi, A. H., Gandomi, A. H., & Walker, A. L. (2016). Machine learning in geosciences and remote sensing. *Geoscience Frontiers*, 7(1), 3–10. <https://doi.org/10.1016/j.gsf.2015.07.003>
- Mitchell, T. M. (1999). Machine learning. In *Software Testing, Verification and Reliability* (Vol. 9, Issue 3). McGraw-Hill Science/Engineering/Math. [https://doi.org/10.1002/\(SICI\)1099-1689\(199909\)9:3<191::AID-STVR184>3.0.CO;2-E](https://doi.org/10.1002/(SICI)1099-1689(199909)9:3<191::AID-STVR184>3.0.CO;2-E)
- Mohammed, S., Budach, L., Feuerpfeil, M., Ihde, N., Nathansen, A., Noack, N., Patzlaff, H., Naumann, F., & Harmouch, H. (2022). *The Effects of Data Quality on Machine Learning Performance*. 1(1). <http://arxiv.org/abs/2207.14529>
- NASA. (n.d.). *Satellite observations for disaster response and resilience*. NASA Earth Science Division. 2020. <https://appliedsciences.nasa.gov/>
- Panda, S., Rao, M., Thenkabail, P., & Fitzgerald. (2015). Remote Sensing Systems. In *Platforms and Sensors: Aerial, Satellites, UAVs, Optical, Radar, and LiDAR*.
- Pech-May, F., Sanchez-Hernández, J. V., López-Gómez, L. A., Magaña-Govea, J., & Mil-Chontal, E. M. (2023). Flooded Areas Detection through SAR Images and U-NET Deep Learning Model. *Computación y Sistemas*, 27(2). <https://doi.org/10.13053/cys-27-2-4624>
- ReliefWeb. (2022). *Floods in Uttar Pradesh displace thousands*. <https://reliefweb.int/>
- Ronneberger, O., Fischer, P., & Brox, T. (2015). *U-Net: Convolutional Networks for Biomedical Image Segmentation* (pp. 234–241). https://doi.org/10.1007/978-3-319-24574-4_28
- Sanyal, A., Chatterji, V., Vyas, N., Epstein, B., Demir, N., & Corletti, A. (2021). *Fix your Models by Fixing your Datasets*. *NeurIPS*. <http://arxiv.org/abs/2112.07844>
- Zhao, Y., Chen, J., & Oymak, S. (2020). *On the Role of Dataset Quality and Heterogeneity in Model Confidence*. 1–25. <http://arxiv.org/abs/2002.09831>



Author's Information

Name	: Binita Shahi
Academic Qualification	: Bachelor's in Geomatics Engineering
Organization	: Land Management Training Center
Current Designation	: Instructor
Work Experience	: 5 years
Published paper/article	: 2

Call for papers

The editorial board requests for papers related to geo-information science and earth observation for the publication in 25th issue of the Journal on Geoinformatics, Nepal.

Last date of submission is 30th March 2026.

For more information, please contact editorial board

Survey Department

P.O. Box 9435, Kathmandu Nepal

Tel: +977 1 4106508, 4106957, Fax: +977 1 4106757

email: info@dos.gov.np

Instruction and Guidelines for Authors Regarding Manuscript Preparation

- Editorial Board reserves the right to accept, reject or edit the article in order to conform to the journal format.
- The contents and ideas of the article are solely of authors.
- The article must be submitted in Microsoft Word by email.
- Editorial Board has no obligation to print chart/ figure/table in multi colour, in JPEG/TIFF format, the figure/picture should be scanned in a high resolution.
- Authors are also requested to send us a written intimation that the same articles is not sent for publication in other magazine/journal.

Page size: A4

Format: Single line spacing with two columns.

Margin: upper 1", left 1.15", right 1", bottom 1".

Length of manuscript: The article should be limited upto 6 pages including figures and references.

Body text font: Times New Roman "11".

Title: The title should be centrally justified appearing near top of 1st page in Cambria, "20" point (Bold).

Authors Name: Authors name should be in Times New Roman "10" with Upper and lower casing, centrally justified. There should be a gap of one lines with 11 pt between the title and author's name.

Authors Email: Authors email should be in Times New Roman "10" centrally justified. There should not be gap between the name and email.

Keywords: Four to five keywords on paper theme in Times New Roman "10" with two spacing under the Authors email left justified.

Abstract: Single line spacing after keywords, limited to around 300 words in Italic, Times New Roman "10".

Major heading (Level 1) should be flushed with the left margin in Times New Roman "10" bold font and with Upper casings. Color Dark blue. Numbering 1

Minor heading (Level 2) should be flushed with the left margin in Times New Roman "11" Bold font and with Upper and Lower Casing. Color Dark blue. Numbering 1.1

Minor heading (Level 3) should be flushed with the left margin in Times New Roman "11" Bold font, Italic and with Upper and Lower Casing. Color Dark blue. Numbering 1.1.1

Minor heading (Level 4) should be flushed with the left margin in Times New Roman "10" Italic and with Upper and Lower Casing. Color Dark blue. Numbering 1.1.1.1

BulletPoint: Use only (•).

Placement of photographs/tables: Photographs or tables should be pasted in appropriate place of manuscript pages with caption in their positions in Times new Roman "10" with Upper and lower casing.

Equations: All equations should be in Times New Roman, "11" and italic with consecutive equation numbers placed flush right throughout the paper.

References: References should be listed in alphabetical order at the end of paper in following sequence and punctuation. Author's last name, Author's initials, (Year of publication). *Title of references article in italic*, name of book or journal, volume number, country or city, name of publisher etc.

Citation: All papers are to be cited like (Rajabifarad, 2012), (Dangol & Kwak, 2014), (Zebenbergen, *et al.*, 2018). Upto two authors, the last name should be cited for both and if more than two, then cite it as *et al.*

Primary Author's Information:

Name, Academic Qualification, Organization, Current Designation, Work Experience (in years),

Published Papers/Article (Number) and scanned copy of author's passport size photo.

Note: "Author should send the picture of all the figures kept in paper as separate file."

Integrating GIS and AHP for Forest Fire Risk Mapping in Kailali, Nepal

Ganesh Pandey¹ & Daman Neupane¹
ganeshpandey362@gmail.com, damanneupane@gmail.com
¹Survey Department

KEYWORDS

Forest fire risk, AHP, GIS-MCDA, GEE, Criteria Factors

ABSTRACT

Forest are the Earth's predominant geographical phenomena distributed throughout the world and provide essential ecosystem services and products that benefit both humans and wildlife. The sustainability of the forest resources can be seriously affected by the forest fire in the dry regions covered with fire sensitive trees species. The risk of the forest fire mainly depends on the various factors such as vegetation type, topographical features, climatic parameters, socio-economic factors. Geographic Information System (GIS) and Remote Sensing (RS) technologies are frequently used for the monitoring, detection, and management of forest fires. Seven parameters: land cover, elevation, slope, aspect, land surface temperature (LST), and proximity to settlement and road were compared with each other and pair wise matrix was formed. The weight of each parameters was determined by using AHP technique. Then by using the raster calculator weighted-overlay analysis was performed to determine the final forest fire risk zone. The forest fire risk zone was categorized into five classes; very high-risk zone, high risk zone, moderate risk zone, low risk zone, and very low risk zone. The result indicated that there is a very high risk of forest fire in about 30.78%, a high risk in 34.06%, a moderate risk in 22.45%, a low risk in 9.87% and very low risk in 2.84% of total area of Kailali district.

1. INTRODUCTION

Forest is the Earth's predominant ecosystem, distributed throughout the world and produces 80% of planet's biomass (Y. Pan et al., 2013). Based on the annual report on world forest resources prepared by the Food and Agriculture Organization (FAO) in 1990, the world's total forest cover was 4.13 million hectares, but the figure diminished to 3.999 million hectares in 2015, showing a 3% reduction (FOA, 2015). Forest fires have just recently been investigated in Nepal, and the significance of these studies

is not completely recognized. Consequently, there aren't many comprehensive research on forest fires. In order to tackle fire-related issues and protect forested regions, creating a fire map is a crucial first step. Planning and managing forest conservation methods can be improved by utilizing Multi-Criteria Decision Analysis (MCDA) methodologies in conjunction with Geographic Information System (GIS) technology (Feizizadeh et al., 2015). This method enables an in-depth assessment of all the variables that affect the

risk of a fire, including topography, vegetation type, proximity to populated areas, and past fire trends (Mosadeghi et al., 2013). Through a methodical examination of these factors, policymakers can arrange resources and actions in a way that will reduce the adverse effects of fires and improve the resilience of forests as a whole. Various studies have been carried out around the world to model and assess forest fire risk and to identify the regions susceptible to fire. One of the methods widely used is Analytical Hierarchy Process (AHP) (Pourghasemi et al., 2016; Eugenio et al., 2016; Chhetri & Kayastha, 2015). The main objective of this research is to apply GIS-based MCDA, AHP for fire risk mapping. This method was chosen in this research because this had acceptable performance in various fields of study and classification problems. In particular, this study aims to prepare a forest fire risk map to prevent, manage and mitigate the incidence of fire in the Kailali, Nepal.

2. STUDY AREA

Kailali, one of the districts of Nepal, is located in the southwestern part of Terai in the Far Western Province. It has 3,235 Sq. Km area and among which 40 per cent is covered by plain terai land, 60 per cent is covered by hills of Chure range (DAO, Kailali). It is located at the latitude from 28°22' North to 29°05' North and longitude from 80°30' East to 81°18' East. It has elevation ranges from 109 m to 1950 m above sea level. This district constitutes of 13 local levels with one sub-metropolitan city, six municipalities and six rural municipalities. Dhangadhi is the district headquarter of Kailali district. Among total area of the district, 63.4 Percent of land is covered with forest and 27.8 percent land is fertile agricultural cultivated land. There are all together 229 community forest in this district. The Average Annual Rain Fall measured in this district is 1840 mm and Climate varies from tropical to sub-tropical (DAO, Kailali). The district is home to numerous religious, mythological, and

historical sites, including Ghodaghodi Lake in Ghodaghodi Municipality, which is registered in the World Ramsar list. The study area of the project is shown Figure 1 below.

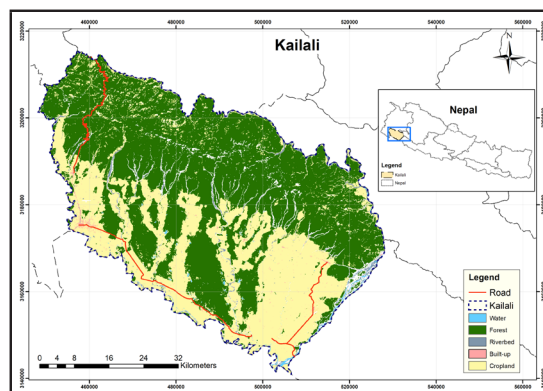


Figure 1 Study area

3. MATERIAL AND METHODS

3.1 Datasets and Software

The data used for this study are Landsat image, Digital Elevation Model (DEM), Road Network, Settlement Data, MODIS LST data, and MODIS fire hotspot data were employed for the study. GIS software was used for overall analysis and mapping purpose. Google Earth Engine (GEE) platform was used for land-cover classification.

Table 1 Datasets

S.N	Data	Data Type	Resolution	Source
1	Landsat-8 Image	Raster	30 m	USGS Earth Explorer using GEE
2	DEM	Raster	30 m	SRTM USGS Earth Explorer
3	Settlement	Point	1:25,000	OCHA Nepal
4	Road Network	Line	Vector Data	Open Street Map (OSM)
5	LST	Raster	1 km	USGS Earth Explorer using GEE (MOD11A1v061)
6	MODIS Fire Data	Point	Derived from data of 1 km resolution	Fire Information for Resource Management System (FIRMS)

3.2 Methodology

The methods include an overview of the project's methodology, covering planning, data collection and preparation, parameter selection, and weight determination for final fire risk model. The overall methodology used for fire risk mapping is shown in the Figure 2 below.

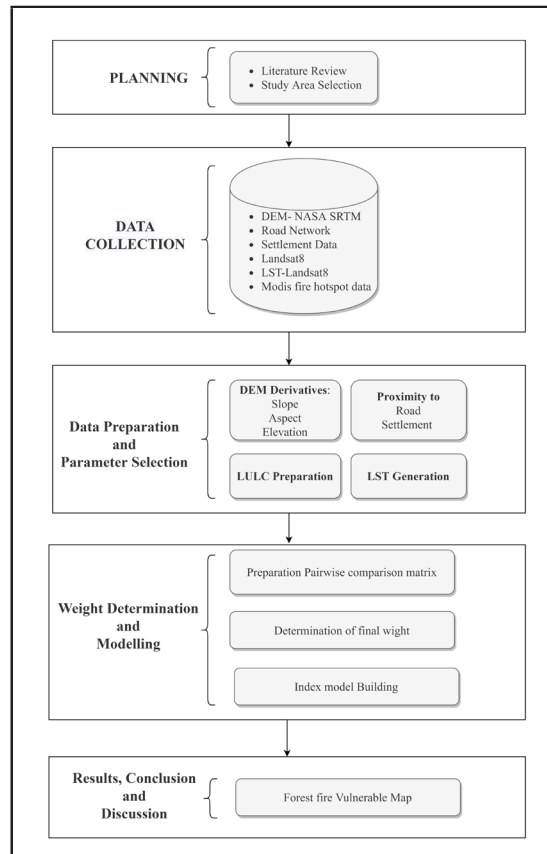


Figure 2 Work flow diagram

3.2.1 Data Collection and Data Preparation

Landsat image, DEM, Road Network, Settlement Data, LST data, and MODIS fire hotspot data were collected. Collected data were further processed with the help of GIS and GEE. DEM was used to generate slope, aspect and elevation of the study area. Land cover is considered to be the critical factor for spreading fire and has high weightage for influencing the risk. Supervised classification technique was used for image classification. Algorithm called *ee.Classifier.smileCart()*

was used. Image was classified into five different classes. Forest, cultivation, built-up, water body and sand were five classes. Accuracy assessment of the classification was also done in GEE by constructing confusion matrix. Out of total sample point 70% were used for training class and 30% were used for validation. The classified landcover map is shown in Figure 3.

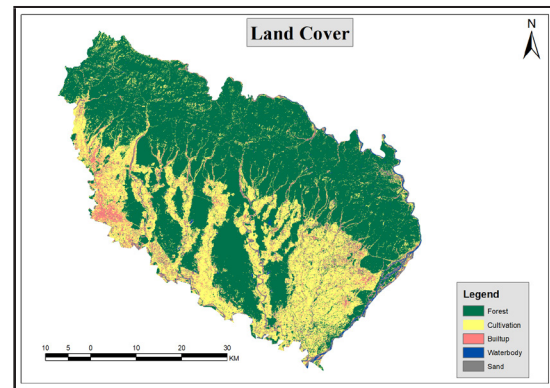


Figure 3 Landcover in Kailali

Land surface temperature can be generated from the NASA/MODIS images (Parajuli et al., 2020). In this study, monthly mean land surface temperature from 2016 to 2022 was extracted from NASA/MODIS image in GEE.

Distance to a road and settlement are used to identify the risk areas where maximum human activities occur. The fires are more common near roads and rivers because of increased movement there (Parajuli et al., 2020). So, based on the different research studies (Parajuli et al., 2020, Pourghasemi et al., 2016; Eugenio et al., 2016; Chhetri & Kayastha, 2015) road network and settlement data were used and grouped into following five categories: 0-1000m, 1000- 2000m, 2000-3000m, and above 4000m. Then multi ring buffer with 1000m interval were carried out using GIS.

3.2.2 Weight Determination and Model Preparation

The forest fire risk map was planned by using the GIS based AHP method by considering risk factors including land cover, elevation,

slope, aspect, land surface temperature, and proximity to settlement and road. AHP was first described by Myers and Alpert (1968) and then modelled by (Saaty, 1994). A set of evaluation criteria is evaluated and optimum solution among a set of alternative option is searched in the AHP method. In the process of AHP, the study area was classified into five forest fire risk classes: very low, low, moderate, high and very high. The main criteria used were land cover, elevation, slope, aspect, land surface temperature, and proximity to settlement and road. A weight of each criteria was generated by using decision maker's pairwise comparison. In order to determine the pairwise comparison matrix between the selected seven parameters different literatures were studied. References were taken from Akay & Şahi (2019), Parajuli et al., (2020), Lamat et al., (2021), and Parajuli et al., (2023) for constructing the pairwise comparison matrix. Pairwise comparison matrix is as shown in Table 2 below. After the construction of the pairwise comparison matrix, eigenvector and weighting coefficient were calculated and then consistency ratio was calculated using online based AHP weight calculator tool.

Table 2 Pairwise Comparison Matrix

Parameters	Land cover	Temperature	Proximity to Settlement	Proximity to Road	Slope	Aspect	Elevation
Land cover	1	3	5	5	5	7	7
Temperature	1/3	1	3	3	3	5	5
Proximity to Settlement	1/5	1/3	1	1	1	2	2
Proximity to Road	1/5	1/3	1	1	1	2	2
Slope	1/5	1/3	1	1	1	2	2
Aspect	1/7	1/5	1/2	1/2	12	1	1
Elevation	1/7	1/5	1/2	1/2	1/2	1	1

The eigenvector and weighting coefficient calculation and consistency ratio calculation was done using following equation (Saaty, 1994).

The eigenvector (Vp) is calculated using equation as follows:

$$Vp = \sqrt[k]{W1 * \dots * Wk} \dots\dots\dots(1)$$

Where k is the number of factors, and W is the ratings of the factor.

The weighting coefficient (Cp) is calculated using equation as follows:

$$Cp = \frac{Vp}{Vp1+\dots+Vpk} \dots\dots\dots(2)$$

The sum of Cp of all parameters of a matrix must be equal to 1. The matrix is normalized by dividing each element by the sum of the column. Then, Consistency Ratio (CR) is calculated by using equation as follows:

$$CR = \frac{CI}{RI} \dots\dots\dots(3)$$

$$CI = (\lambda_{max} - k) / (k - 1) \dots\dots\dots(4)$$

Where CI is consistency Index and λ_{max} is the maximum eigenvalue obtained as 7.06576.

CI was found to be 0.0109599. Both values of λ_{max} and CI were obtained from AHP tool. RI is the random index. RI is the average CI depending on the order k of the matrix (Kil et al., 2016) and utilizes the value given by Saaty (1994) as in Table 3. In this study total seven criteria are used namely; land cover, elevation, slope, aspect, land surface temperature, and proximity to settlement and proximity of roads, so the value of RI is 1.32.

Table 3 Random index

N	1	2	3	4	5	6	7	8	9	10
RI	0	0	0.58	0.90	1.12	1.24	1.32	1.41	1.45	1.49

As described by Saaty (1994) the value of CR should be less than 0.1 so that the judgements are reliable else the process should be repeated. In this analysis, CR is 0.0083 (less than 0.1), so the judgments are reliable. The final weight obtained using AHP method is shown in Table 4 below.

Table 4 Weight, value and rating assigned to different variable

Variable	Wt.	Class	Rank	Rating
Land cover	0.43	Forest	1	Very High
		Sand	3	Moderate
		Water Body	4	Low
		AGR	5	Very Low
		Built up	5	Very Low
LST	0.23	>36	1	Very High
		34-36	2	High
		34-32	3	Moderate
		30-32	4	Low
		29-30	5	Very Low
Proximity to settlement(m)	0.08	<1000	1	Very High
		1000-2000	2	High
		2000-3000	3	Moderate
		3000-4000	4	Low
		>4000	5	Very Low
Proximity to Road (m)	0.08	<1000	1	Very High
		1000-2000	2	High
		2000-3000	3	Moderate
		3000-4000	4	Low
		>4000	5	Very Low
Slope (Degree)	0.08	<5	5	Very Low
		5-15	4	Low
		15-25	3	Moderate
		25-35	2	High
		>35	1	Very High
Aspect	0.05	South	1	Very High
		South West	1	Very High
		South East	2	High
		West	3	Moderate
		East	3	Moderate
		North West	4	Low
		North East	4	Low
North	5	Very Low		
Elevation (m)	0.05	<200	1	Very High
		200-400	2	High
		400-600	3	Moderate
		600-800	4	Low
		>800	5	Very Low
Total	1			

4. RESULTS

4.1 Fire Risk Model

Seven parameters were used to model fire risk in Kailali district. According to weight given to each parameter and their impact on forest fire, the total area was divided into five zone. The five risk zones Very High, Moderate, Low, Very Low and Very Low risk zones are divided using GIS methodologies. By using the raster calculator final fire risk model was prepared. Total seven parameters; elevation, slope, aspect LST, land cover, proximity to road, and proximity to settlements were used. Figure 3 below shows the forest fire risk map and the area is shown in the Table 6. According to the findings, there is a very high risk of forest fire for 99788.76 hectares, a high risk for 110423.07 hectares, a moderate risk for 72771.39 hectares, a low risk for 32016.24 hectares and very low risk for 9174.78 hectares.

The expression used in raster calculator to calculate the final forest fire risk zone based on the weight used is given below.

$$FRI = 0.43 * \text{landcover} + 0.23 * \text{LST} + 0.08 * \text{Proximity to settlement} + 0.08 * \text{Proximity to road} + 0.08 * \text{Slope} + 0.05 * \text{Aspect} + 0.05 * \text{Elevation} \dots \dots \dots (7)$$

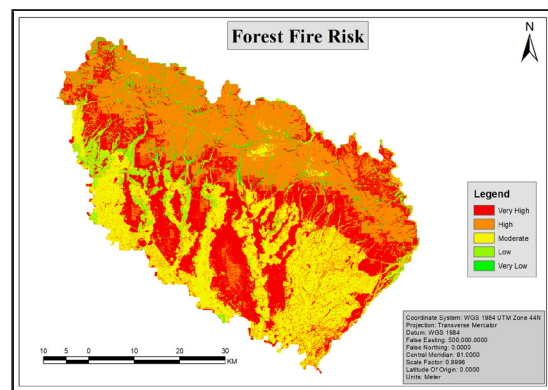


Figure 4 Forest fire risk map of Kailali

So, according to the finding there is a very high risk of forest fire in about 30.78%, a high risk in 34.06%, a moderate risk in 22.45%, a low risk in 9.87% and very low risk in 2.84% of total area.

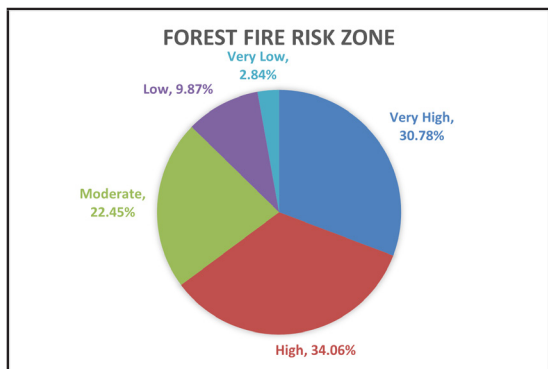


Figure 5 Pie chart showing forest fire risk zone

4.2 Validation

Fire Information for Resource Management System (FIRMS) uses satellite observations from the MODIS and Visible Infrared Imaging Radiometer Suite (VIIRS) instruments to detect active fires and thermal anomalies. Historical fire data from 2014 to 2023 were downloaded from the NASA FIRMS. From the downloaded data only point data that have confidence higher than 50 percentages were extracted for validation purpose. Out of total extracted points random 1000 points were used for overlay over risk zone. When those points were overlay over the fire risk map, 475 points were on very high risk zone, 413 on high risk zone, 84 were on moderate risk zone, 17 on low risk and 11 on the very low risk zone. This demonstrated that the risk region in Kailali district was accurately reflected on the forest fire risk map. The spatial distribution of sample points on study area is shown in figure 5 below.

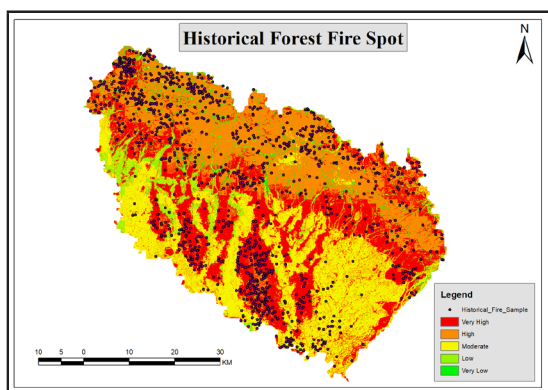


Figure 6 Spatial distribution of historical fire spots

5. CONCLUSION

GIS-based MCDA can be done for mapping forest fire risk. According to this study, there is a very high risk of forest fire for 99788.76 hectares, a high risk for 110425 hectares, a moderate risk for 72770 hectares, a low risk for 32015 hectares and very low risk for 9175 hectares approximately of Kailali district. Elevation, slope, aspects, landcover, land surface temperature, distance from road, distance form settlement area all have an impact on forest fire risk in Kailali district.

6. RECOMMENDATION

Kailali district has a lot of religious, mythological and historical places and have maximum land cover covered with forest that helps to maintain ecosystem and sustain a lot of wildlife. However, there is risk of forest fire in this district. This study recommends the following for the study area:

- i) About 62% of Kailali district is covered with forest and 30% of which is at very high risk of forest fire. A proper fire control approach such as clearing the forest floor before summer and constructing fire line should be done for reducing fire and associated damages.
- ii) District administration and related sectors should remain alert and prepared for combating wildfires, especially during the summer season.
- iii) Fire towers and alarm system should be installed where risk is high
- iv) More research related to forest fire should be encouraged and promoted that help in prevention and control of hazardous fire.

REFERENCES

- Akay, A. E., & Erdoğan, A. (2017). GIS-Based Multi-Criteria Decision Analysis for Forest Fire Risk Mapping. *ISPRS Annals of the Photogrammetry, Remote Sensing and Spatial Information Sciences, IV-4/W4*, 25–30. <https://doi.org/10.5194/isprs-annals-IV-4-W4-25-2017>
- Akay, A. E., & Erdoğan, A. (2021). Developing Validation of Forest Fire Risk Maps Based on Historical Fire Incidences. *The International Archives of the Photogrammetry, Remote Sensing and Spatial Information Sciences, XLVI-4/W5-2021*, 33–38. <https://doi.org/10.5194/isprs-archives-XLVI-4-W5-2021-33-2021>
- Akay, A. E., & Şahin, H. (2019). Forest Fire Risk Mapping by using GIS Techniques and AHP Method: A Case Study in Bodrum (Turkey). *European Journal of Forest Engineering*, 5(1), 25–35. <https://doi.org/10.33904/ejfe.579075>
- Beckley, T. M. (1998). The Nestedness of Forest Dependence: A Conceptual Framework and Empirical Exploration. *Society & Natural Resources*, 11(2), 101–120. <https://doi.org/10.1080/08941929809381066>
- Boyi Jiang. (2011). *GIS-based Multi-criteria Analysis Used in Forest Fire Estimation: A Case Study of Northernmost Gävleborg County in Sweden*.
- Carmel, Y., Paz, S., Jahshan, F., & Shoshany, M. (2009). Assessing fire risk using Monte Carlo simulations of fire spread. *Forest Ecology and Management*, 257. <https://doi.org/10.1016/j.foreco.2008.09.039>
- Chhetri, S., & Kayastha, P. (2015). Manifestation of an Analytic Hierarchy Process (AHP) Model on Fire Potential Zonation Mapping in Kathmandu Metropolitan City, Nepal. *ISPRS International Journal of Geo-Information*, 4(1), 400–417. <https://doi.org/10.3390/ijgi4010400>
- District Administration Office, Kailali. (n.d.). Retrieved April 29, 2025, from <https://daokailali.moha.gov.np>
- Eugenio, F. C., Dos Santos, A. R., Fiedler, N. C., Ribeiro, G. A., Da Silva, A. G., Dos Santos, Á. B., Paneto, G. G., & Schettino, V. R. (2016). Applying GIS to develop a model for forest fire risk: A case study in Espírito Santo, Brazil. *Journal of Environmental Management*, 173, 65–71. <https://doi.org/10.1016/j.jenvman.2016.02.021>
- FAO, F. (2016). State of the world's forests 2016. Forests and agriculture: Land-use challenges and opportunities. *FAO Report*.
- Feizizadeh, B., Omrani, K., & Aghdam, F. B. (2015). Fuzzy Analytical Hierarchical Process and Spatially Explicit Uncertainty Analysis Approach for Multiple Forest Fire Risk Mapping. *GI Forum*, 1, 72–80. <https://doi.org/10.1553/giscience2015s72>
- FOA. (2015). *Global Forest Resources Assessment 2015*.
- Gigović Ljubomir, Gordana Jakovljević, & Dragoljub Sekulović i Miodrag Regodić. (2018). GIS Multi-Criteria Analysis for Identifying and Mapping Forest Fire Hazard: Nevesinje, Bosnia and Herzegovina. *Tehnicki Vjesnik - Technical Gazette*, 25(3). <https://doi.org/10.17559/TV-20151230211722>
- Gülci, N., Akay, A. E., & Erdaş, O. (2020). Optimal planning of timber extraction methods using analytic hierarchy process. *European Journal of Forest Research*, 139(4), 647–654. <https://doi.org/10.1007/s10342-020-01275-7>

- Hong, H., Naghibi, S. A., Moradi Dashtpajardi, M., Pourghasemi, H. R., & Chen, W. (2017). A comparative assessment between linear and quadratic discriminant analyses (LDA-QDA) with frequency ratio and weights-of-evidence models for forest fire susceptibility mapping in China. *Arabian Journal of Geosciences*, *10*(7), 167. <https://doi.org/10.1007/s12517-017-2905-4>
- Jafari Goldarag, Y., Mohammadzadeh, A., & Ardakani, A. S. (2016). Fire Risk Assessment Using Neural Network and Logistic Regression. *Journal of the Indian Society of Remote Sensing*, *44*(6), 885–894. <https://doi.org/10.1007/s12524-016-0557-6>
- Kant Sharma, L., Kanga, S., Singh Nathawat, M., Sinha, S., & Chandra Pandey, P. (2012). Fuzzy AHP for forest fire risk modeling. *Disaster Prevention and Management: An International Journal*, *21*(2), 160–171. <https://doi.org/10.1108/09653561211219964>
- Khatakho, R., Gautam, D., Aryal, K. R., Pandey, V. P., Rupakhety, R., Lamichhane, S., Liu, Y.-C., Abdouli, K., Talchabhadel, R., Thapa, B. R., & Adhikari, R. (2021). Multi-Hazard Risk Assessment of Kathmandu Valley, Nepal. *Sustainability*, *13*(10), 5369. <https://doi.org/10.3390/su13105369>
- Kil, S.-H., Lee, D., Kim, J.-H., Li, M.-H., & Newman, G. (2016). Utilizing the Analytic Hierarchy Process to Establish Weighted Values for Evaluating the Stability of Slope Revegetation based on Hydroseeding Applications in South Korea. *Sustainability*, *8*(1), 58. <https://doi.org/10.3390/su8010058>
- Lamat, R., Kumar, M., Kundu, A., & Lal, D. (2021). Forest fire risk mapping using analytical hierarchy process (AHP) and earth observation datasets: A case study in the mountainous terrain of Northeast India. *SN Applied Sciences*, *3*(4), 425. <https://doi.org/10.1007/s42452-021-04391-0>
- Leal, B. E. Z., Hirakawa, A. R., & Pereira, T. D. (2016). Onboard fuzzy logic approach to active fire detection in Brazilian amazon forest. *IEEE Transactions on Aerospace and Electronic Systems*, *52*(2), 883–890. <https://doi.org/10.1109/TAES.2015.140766>
- Matin, M. A., Chitale, V. S., Murthy, M. S. R., Uddin, K., Bajracharya, B., & Pradhan, S. (2017). Understanding forest fire patterns and risk in Nepal using remote sensing, geographic information system and historical fire data. *International Journal of Wildland Fire*, *26*(4), 276. <https://doi.org/10.1071/WF16056>
- Mosadeghi, R., Warnken, J., Tomlinson, R., & Mirfenderesk, H. (2013). Uncertainty analysis in the application of multi-criteria decision-making methods in Australian strategic environmental decisions. *Journal of Environmental Planning and Management*, *56*(8), 1097–1124. <https://doi.org/10.1080/09640568.2012.717886>
- Pan, J., Wang, W., & Li, J. (2016). Building probabilistic models of fire occurrence and fire risk zoning using logistic regression in Shanxi Province, China. *Natural Hazards*, *81*(3), 1879–1899. <https://doi.org/10.1007/s11069-016-2160-0>
- Pan, Y., Birdsey, R. A., Phillips, O. L., & Jackson, R. B. (2013). The Structure, Distribution, and Biomass of the World's Forests. *Annual Review of Ecology*,

- Evolution, and Systematics*, 44(1), 593–622. <https://doi.org/10.1146/annurev-ecolsys-110512-135914>
- Parajuli, A., Gautam, A. P., Sharma, S. P., Bhujel, K. B., Sharma, G., Thapa, P. B., Bist, B. S., & Poudel, S. (2020). Forest fire risk mapping using GIS and remote sensing in two major landscapes of Nepal. *Geomatics, Natural Hazards and Risk*, 11(1), 2569–2586. <https://doi.org/10.1080/19475705.2020.1853251>
- Parajuli, A., Manzoor, S. A., & Lukac, M. (2023). Areas of the Terai Arc landscape in Nepal at risk of forest fire identified by fuzzy analytic hierarchy process. *Environmental Development*, 45, 100810. <https://doi.org/10.1016/j.envdev.2023.100810>
- Pourghasemi, H. R., Beheshtirad, M., & Pradhan, B. (2016). A comparative assessment of prediction capabilities of modified analytical hierarchy process (M-AHP) and Mamdani fuzzy logic models using Netcad-GIS for forest fire susceptibility mapping. *Geomatics, Natural Hazards and Risk*, 7(2), 861–885. <https://doi.org/10.1080/19475705.2014.984247>
- Rahimi, I., Azeez, S. N., & Ahmed, I. H. (2020). Mapping Forest-Fire Potentiality Using Remote Sensing and GIS, Case Study: Kurdistan Region-Iraq. In A. M. F. Al-Quraishi & A. M. Negm (Eds.), *Environmental Remote Sensing and GIS in Iraq* (pp. 499–513). Springer International Publishing. https://doi.org/10.1007/978-3-030-21344-2_20
- Saaty, T. L. (1994). How to Make a Decision: The Analytic Hierarchy Process. *Interfaces*, 24(6), 19–43. <https://doi.org/10.1287/inte.24.6.19>
- Scott, A. C. (2000). The Pre-Quaternary history of fire. *Palaeogeography, Palaeoclimatology, Palaeoecology*, 164(1–4), 281–329. [https://doi.org/10.1016/S0031-0182\(00\)00192-9](https://doi.org/10.1016/S0031-0182(00)00192-9)
- Vadrevu, K. P., Eaturu, A., & Badarinath, K. V. S. (2010). Fire risk evaluation using multicriteria analysis—A case study. *Environmental Monitoring and Assessment*, 166(1), 223–239. <https://doi.org/10.1007/s10661-009-0997-3>



Name	: Ganesh Pandey
Academic Qualification	: BE in Geomatics Engineering
Organization	: Survey Department
Designation	: Survey Officer
Work Experience	: 3.5 years
Published Articles/papers	: 1

CALENDAR OF INTERNATIONAL EVENTS

Photogrammetric techniques for surveillance, biometrics and biomedicine

Date: 09-11 Jun 2025

Country: Moscow, Russia

Website: <https://sites.google.com/view/psbb25/>

From Mountains to Kitchens; Remote Sensing Innovations for Water, Food & Security

Date: 16 – 19 June 2025

Country: Alberta Canada

Website: <https://crss-sct.ca/events/csrs2025lethbridge/>

The 13th International Conference on Mobile Mapping Technology

Date: 20 – 22 June 2025

Country: Xiamen, China

Website: <https://mmt2025.xmu.edu.cn/2025/>

3D underwater mapping from above and below

Date: 08-11 July 2025

Country: Vienna, Austria

Website: <https://www.tuwien.at/en/mg/geo/photo/events/3d-underwater>

FOSS4G 2025 Academic Track

Date: 14 - 20 July 2025

Country: Mostar, Bosnia-Herzegovina

Website: <https://2025.europe.foss4g.org/>

Global Smart Cities Summit 2025 cum the 4th International Conference on Urban Informatics

Date: 05-08 August 2025

Country: Hong Kong

Website: <https://www.isocui.org/icui2025/>

32nd International Cartographic Conference

Date: 18 - 22 August 2025

Country: Beijing, China

Website: <https://icc2025.com/>

9th International Workshop on Dynamic and Multi-dimensional Geospatial Information Simulation

Date: 22 - 24 August 2025

Country: Beijing, China

Website: <https://dmgis2025.scievent.com/>

3D GeoInfo & SDSC 2025

Date: 02-05 September 2025

Country: Tokyo, Japan

Website: <https://www.csis.u-tokyo.ac.jp/>

The 5th International Forum on Big Data for Sustainable Development Goals

Date: 06 – 08 September 2025

Country: Beijing, China

Website: <https://www.fbas.org.cn/fbas2025/en/index/>

The 8th ISPRS Geospatial Conference 2025

Date: 13 – 15 October 2025

Country: Tehran, Iran

Website: <https://geospatialconf2025.ut.ac.ir/>

9th International Conference on Engineering Surveying (INGEO 2025), supported by FIG Commission 6 (Engineering Surveys)

Date: 15 – 17 October 2025

Country: Brno, Czech Republic

Website: <https://www.ingeoconference.com/>

FIG Young Surveyors 2nd Americas Regional Meeting 2025.

Date: 17 -18 October 2025

Country: Minnesota, USA

Website: <https://www.ingeoconference.com/>

The 46th Asian Conference on Remote Sensing

Date: 27 – 31 October 2025

Country: Makassar, Indonesia

Website:

13th International FIG Workshop on the Land Administration Domain Model & 3D Land Administration

Date: 03 – 05 November 2025

Country: Brazil

Website: <https://figbrasil.paginas.ufsc.br/en/>

6th Symposium of the Committee on Space Research (COSPAR) Space Exploration 2025

Date: 03 – 07 November 2025

Country: Cyprus

Website: <https://cospar2025.org/>

Conference on Geoinformation 2025

Date: 25 – 28 November 2025

Country: Mexico

Website: <https://www.selper.org.mx/conferencia-de-geoinformacion-2025/>

14th EARSeL WS on Imaging Spectroscopy

Date: 02 – 04 June 2026

Country: Helsinki, Finland

Developing New National Geodetic Reference Frame of Nepal

Narayan Regmi¹, Sandesh Upadhyaya¹, Manisha Thapa¹, Shiva Prasad Lamsal¹ & Suraj Bahadur KC¹,
Suresh Shrestha¹, Sushmita Timalina¹, Dipesh Suwal¹, Mahesh Thapa¹, Shanker KC¹
nregmi2000@gmail.com, sandeshupadhyaya1@gmail.com, thapamanisha2049@gmail.com,
shivaplamsal@gmail.com, kcsuraj21@gmail.com, Shrestha.suresh@gmail.com, qust04sharma@gmail.
com, dipeshsuwal@gmail.com, mahesh100thapa@gmail.com, shankerkc01@gmail.com
¹Survey Department

KEYWORDS

Reference frame, Helmert Transformation, GNSS, ITRF, Nepal

ABSTRACT

Geodetic reference frame is fundamental geodetic infrastructure required for positioning for surveying and mapping purposes. This paper presents a method to develop national level geodetic reference frame tied to global reference frame by utilizing the long-term GNSS observations. The key to realize a national reference frame is to transform Earth-Centered Earth-Fixed (ECEF) X, Y, and Z coordinates from International Terrestrial Reference Frame (ITRF) to national reference frame by application of 14-Helmert transformation parameters. Initially, precise point positioning (PPP) provides the X, Y, and Z coordinates of reference stations with respect to ITRF, which in turn transformed to national geodetic reference frame. This paper discusses the development of 14-Helmert transformation parameter taking example of Nepal geodetic reference frame being built in near future.

1 INTRODUCTION

Geodetic reference system and frame is fundamental requirements for positioning, navigation, monitoring geological hazards and many geoscientific studies. In surveying and mapping domain, positioning is done with respect to such fundamental reference frame. Topographical and cadastral mapping, engineering surveying and others rely on geodetic reference frame. In context of Nepal, SOI datum (Survey of India) was used for topographical mapping and cadastral mapping before 1986 (KC & Acharya, 2022). In 1986, a newer geodetic datum called Nepal Datum was built and has been used for surveying and mapping activities within Nepal. Thus, Nepal Datum is the current national geodetic datum in use by Survey Department (SD).

The earth is a dynamic system and positional coordinates of reference stations anchored / fixed at its crust is a function of time due to geophysical motion. However, Nepal Datum is static in nature thus positional coordinates of 68 higher-order control points remain static. The details of development of conventional topocentric geodetic datum can be found in (Bomford, 1962).

Nepal lies at the converging boundary of Indian and Eurasian tectonic plates and tectonic motion of these two plates cause the earth crust to displace. Such crustal motion is secular in nature. The displacement accumulates at constant rate. Over the long period, the accumulated displacement will be larger than the precision of positional coordinates

referenced to conventional terrestrial datum (e.g. Nepal datum). In addition, the Gorkha earthquake of 2015 has displaced the central and eastern Nepal significantly in non systematic way. The horizontal displacement of more than 1.5m have been recorded in vicinity of Kathmadu (Shrestha, 2017). This has forced us to find the solution.

Modern geodesy is characterized by space geodetic technologies. Space geodetic techniques such as Very Long Baseline Interferometry (VLBI), Satellite Laser Ranging (SLR), Doppler Orbitography and Radiopositioning Integrated by Satellite (DORIS), and Global Navigation Satellite System (GNSS) have enabled us to build geocentric terrestrial reference frames. These technologies have made 3D ECEF Cartesian coordinate system realization possible. Moreover, among these systems, GNSS offers ease of operation and economic, and capability to build geocentric reference frame at regional, national, and global level (Soler & Snay, 2004).

The power of GNSS to build a geocentric reference frame and its ability to collect continuous observations that can provide time-dependent variations of position due to geophysical motion. Such capability of GNSS is used to build the national geodetic reference frame. At regional and national level, it has been the standard practice to establish uniformly distributed continuously operating reference stations (CORS) forming region-wide or nationwide CORS network. Then, long-term GNSS observations obtained from such CORS stations are utilized to define and develop national geodetic reference frame with respect to global reference frame.

National geodetic reference frame is defined and developed tied to global reference frame by application of 14-parameter Helmert transformation. For example, the current realization of the North American Datum of

1983 (NAD83 (2011)) is defined in terms of 14-parameter transformation from ITRF08 (Pearson & Snay, 2013). Similarly, North American Reference Frame NA12 also implements daily 7-parameters from IGS08 (Blewitt et al., 2013). At present, such global reference frame is International Terrestrial Reference Frame (ITRF). International Earth Rotation and Reference System Services (IERS) is service of International Association of Geodesy (IAG), which is a responsible organization that define, develop, and maintain the ITRF. Recent ITRF version is ITRF2020. The main idea of this paper is to present the process of determining 14-parameters of Helmert transformation to convert ITRF positional coordinates of reference stations into national geodetic reference frame.

The significance of geodetic reference frame has been acknowledged worldwide, leading to the adoption of the UN General Assembly Resolution on the Global Geodetic Reference Frame for Sustainable Development. This resolution highlights the critical need for a globally coordinated approach to geodesy. Furthermore, the necessity of newer geodetic reference frame to improve upon the limitations of existing geodetic datum; adoption of best practices of surveying and mapping techniques followed and recommended internationally; and aim to improve the accuracy of surveying and mapping and help to resolve disputes related to land boundaries, are motivations to develop national geodetic reference frame.

The new geodetic reference frame, in addition to providing stable reference frame for geoscientific studies, it is also expected to decrease time and cost of surveying and mapping activities. New geodetic reference frame being compatible with modern surveying technologies, brings quality and thus trust in surveying and mapping works.

In this paper, the first section introduces the necessity of 3D ECEF reference frame. The

second section presents the high-precision GNSS positioning focused to develop reference frame. The third section, the key section of this paper presents the mathematical aspect of realization of national geodetic reference frame taking example Nepal reference frame in coming years. Final section concludes this paper.

2 GNSS POSITIONING

Two approaches of high-precision GNSS positioning exists: 1) relative positioning, and 2) absolute positioning. Relative positioning approach implements double-differencing (DD) method to derive precise position. In this approach, two or more GNSS stations/receivers / units simultaneously make the observations. One of the station is fixed station / acts a reference /base station. The position of other/remaining GNSS stations (rover stations) is determined relative to reference stations. As reference and rover stations are closely spaced, both share identical atmospheric condition and same satellite errors, thus common errors and biases are removed in DD method, resulting highly precise relative position (Odijk & Wanninger, 2017). Absolute positioning implements precise point positioning (PPP) method, which uses un-differenced, dual frequency, pseudorange and carrier-phase observations along with precise satellite orbit and clock products, and corrections for various effects, for standalone static point positioning at millimeter level precision (Kouba et al., 2017; Zumberge et al., 1997). Compared to differential positioning approach, PPP doesn't require simultaneous observations, which is the single most, greatest advantage that PPP offers. In addition, as globally consistent satellite orbits and clocks are used in PPP processing, the consistent position of all GNSS stations worldwide or within the country in our case, are obtained in global reference frame, such as ITRF (e.g. ITRF2020). In our purpose here, to develop a national reference frame

from stations in CORS network, we consider PPP method to derive positions.

The set of homogeneous coordinates and velocities is determined by using GNSS observations collected at CORS stations using daily/weekly station position estimates and velocity estimates, long term position time series, discontinuities as well as post-seismic and co-seismic offsets. The use of long-term position time series enables a more accurate geophysical analysis of the observed site movement, particularly in understanding residual signals or non-linear motion that is linked to local geophysical events or site stability (Dawson et. al, 2009).

3 REALIZATION OF NATIONAL GEODETTIC REFERENCE FRAME 2025 (NEP25)

Defining a terrestrial reference frame means defining / fixing the origin, orientation, scale and rate of change of these parameters over time. This terrestrial reference frame is 3D Earth- ECEF – XYZ Cartesian coordinate system. IERS has taken the responsibility of defining and developing the standards of International Terrestrial Reference System (ITRS) and its physical-mathematical realization International Terrestrial Reference Frame (ITRF) (Petit and Luzum, 2010). ITRF is such 3D ECEF-XYZ coordinate system. The positional coordinates of any point on or above the surface of the Earth are described by X, Y, and Z triplets. ITRFs are updated in regular interval reflecting the dynamics of Earth system and thus positional coordinates as the function of time. A recent release of ITRF is ITRF2020, the previous being ITRF2014. These ITRFs are developed utilizing long-term space geodetic observations worldwide.

While ITRF is global reference frame (e.g. ITRF2020), national scale reference frame (e.g. NAD83 (2011)) and regional scale reference frame (e.g. NChina16) are required to cater the needs of national or regional scale requirements

such as national geodetic reference frame for surveying and mapping, crustal motion studies or geological hazards monitoring. Geodetic reference frame for surveying and mapping is fundamental infrastructure of any nation or region. Within the scope of this paper, we name such national geodetic reference frame, going to be built in near future by Geodetic Survey Division (GSD) a Nepal Reference Frame 2025 (NEP25).

In context of developing regional reference frame, long-term GNSS observations of more than 3 years from reference stations (CORS stations that qualify to be reference stations) are utilized (Wang et al., 2013). For examples, a regional reference frame of Gulf of Mexico has been developed using continuous observation of 13.5 years on average (Wang et al., 2020). Similar kind of regional reference frame of Caribbean region exists using observations of greater than 3 years period (Wang et al., 2019). Observations of more than 5 years have been used to develop reference frame of Houston, Texas (Kearns et al., 2019). Reference stations have the characteristics of 1) having good geographical distribution, 2) having long-term observations, 3) consistent daily position time series, and 4) located in stable site (Wang et al., 2013). In coming years, NEP25 is going to be developed from GNSS observations of more than 3 years period from about 30 CORS stations, being established in coming years by GSD.

A national geodetic reference frame is often developed through a simultaneous transformation from global terrestrial reference frame (Pearson & Snay, 2013; Soler & Snay, 2004; Wang et al., 2013, 2018, 2020). For example, the current realization of the North American Datum of 1983 (NAD83 (2011)) is defined in terms of 14-parameter transformation from ITRF08 (Pearson & Snay, 2013). Similarly, North American Reference Frame NA12 also implements

daily 7-parameters from IGS08 (Blewitt et al., 2013). NEP25 is going to be defined in terms of 14-parameter Helmert transformation from recently released ITRF2020. The PPP processing delivered ITRF2020 based positional coordinates are transformed to NEP25 positional coordinates by application of 14-parameter Helmert transformation (Soler & Snay, 2004; Wang et al., 2013). Helmert transformation produces distortion-free transformation of the ECEF-XYZ coordinates between two reference frames. This method transforms a set of points from one reference frame into another by translation, rotation, and scaling.

Let $x(t)_{NEP25}$, $y(t)_{NEP25}$ and $z(t)_{NEP25}$ denote the NEP25 positional coordinates for a point at any epoch (t) as expressed in a 3D ECEF cartesian coordinate system. These coordinates are expressed as a function of time to reflect the reality of the crustal motion associated with plate tectonics, land subsidence, volcanic activity, postglacial rebound and so on (Soler & Snay, 2004). Similarly, let $x(t)_{ITRF}$, $y(t)_{ITRF}$ and $z(t)_{ITRF}$ denote ITRF2020 positional coordinates for this same point at same epoch (t). Then, ITRF2020 coordinates are related to their corresponding NEP25 coordinates by a Helmert transformation that is approximated by the following equations:

$$\begin{bmatrix} x(t)_{NEP25} \\ y(t)_{NEP25} \\ z(t)_{NEP25} \end{bmatrix} = \begin{bmatrix} T_x(t) \\ T_y(t) \\ T_z(t) \end{bmatrix} + (1+s(t)) \begin{bmatrix} 1 & \omega_x(t) & -\omega_y(t) \\ -\omega_z(t) & 1 & \omega_x(t) \\ \omega_y(t) & -\omega_x(t) & 1 \end{bmatrix} \times \begin{bmatrix} x(t)_{ITRF} \\ y(t)_{ITRF} \\ z(t)_{ITRF} \end{bmatrix} \quad (1)$$

Here $T_x(t)$, $T_y(t)$, and $T_z(t)$ are translations along the X, Y, and Z axes, respectively; $w_x(t)$, $w_y(t)$ and $w_z(t)$ are counterclockwise rotations about these same three axes; and $s(t)$ is differential scale change between ITRF2020 and NEP25. These approximate equations suffice because the three rotations usually have rather small magnitudes. The differential scale change $s(t)$ can be set to zero, hence the scale factor to be unity (Soler & Snay, 2004). The function of scale factor and its value should be such that it enforces minimum

distortion of point-to-point distances between reference frames. Studies have shown that the scale factor of unity have negligible effect for coordinate transformations from a global reference frame to a regional reference frame (Wang et al., 2013). Therefore, the coordinate transformation from ITRF2020 to NEP25, with unity scale factor, can be written as (from (Wang et al., 2013)):

$$\begin{aligned} x(t)_{NEP25} &= T_x(t) + x(t)_{ITRF} + \omega_z(t) \cdot y(t)_{ITRF} - \omega_y(t) \cdot z(t)_{ITRF} \\ y(t)_{NEP25} &= T_y(t) - \omega_z(t) \cdot x(t)_{ITRF} + y(t)_{ITRF} + \omega_x(t) \cdot z(t)_{ITRF} \\ z(t)_{NEP25} &= T_z(t) + \omega_y(t) \cdot x(t)_{ITRF} - \omega_x(t) \cdot y(t)_{ITRF} + z(t)_{ITRF} \end{aligned} \quad (2)$$

where, $T_x(t)$, $T_y(t)$, $T_z(t)$, $\omega_x(t)$, $\omega_y(t)$, and $\omega_z(t)$ are the six Helmert transformation parameters at epoch (t). These parameters at a specific epoch can be calculated using positional coordinates of reference stations in both ITRF2020 and NEP25 frame.

Positional coordinates of reference stations in both frames: ITRF2020 and NEP25 at a specific epoch, can be utilized to calculate these six transformation parameters at that epoch. Two common points in both frame will provide a set of linear equations with six equations and with six unknowns. Thus unique solution of six unknowns (three translation and three rotation parameters) can be solved. However, we will have more than 30 reference stations, allowing us to use least squares method to obtain better transformation parameters, resulting better transformation from ITRF2020 to NEP25 (Wang et al., 2018). It is worth noting that NEP25 is ECEF terrestrial reference frame designed and developed to cover territory of Nepal. At certain arbitrary epoch, NEP25, national geodetic reference frame is aligned with ITRF2020. At this epoch, because both are aligned with each other, their origin, scale and axes are same. Within the scope of this paper, we chose such epoch to be ($t_0 = 2025.0$). Therefore, at this epoch about 30 reference stations will have the same XYZ coordinates with respect to both reference frame, as expressed in following equations:

$$\begin{aligned} x_{NEP25}(2025.0) &= x_{ITRF}(2025.0) \\ y_{NEP25}(2025.0) &= y_{ITRF}(2025.0) \\ z_{NEP25}(2025.0) &= z_{ITRF}(2025.0) \end{aligned} \quad (3)$$

Theoretically, a reference site should be ideally stable with respect to regional reference frame (a velocity of frame station should be minimized to zero with respect to NEP25), which means the coordinates of frame stations remain almost similar at different epochs with respect to national reference frame. Therefore, for any other epoch, let's say ($t = 2028.0$) following expression holds:

$$\begin{aligned} x_{NEP25}(2028.0) &\approx x_{NEP25}(2025.0) \\ y_{NEP25}(2028.0) &\approx y_{NEP25}(2025.0) \\ z_{NEP25}(2028.0) &\approx z_{NEP25}(2025.0) \end{aligned} \quad (4)$$

For the epoch ($t = 2028.0$), coordinates of reference stations in NEP25 can be obtained using equation (4) and (3). For the same epoch ($t = 2028.0$), coordinates of the same reference stations in ITRF2020 is obtained by PPP processing. Thus, as coordinates of about 30 common reference stations in both frames are available, the six parameters: (T_x , T_y , T_z , ω_x , ω_y , and ω_z) to transform from ITRF2020 to NEP25 at epoch ($t = 2028.0$) can be estimated from equation (2) by using least squares method to solve the inverse equation.

These six parameters are also a function of time and shows a linear relationship with time (Soler & Snay, 2004). This linear relationship can be expressed by following equations:

$$\begin{aligned} T_x(t) &= T_x(t_0) + \dot{T}_x \cdot (t - t_0) \\ T_y(t) &= T_y(t_0) + \dot{T}_y \cdot (t - t_0) \\ T_z(t) &= T_z(t_0) + \dot{T}_z \cdot (t - t_0) \\ \omega_x(t) &= [\epsilon_x(t_0) + \dot{\epsilon}_x \cdot (t - t_0)] \cdot m_r \\ \omega_y(t) &= [\epsilon_y(t_0) + \dot{\epsilon}_y \cdot (t - t_0)] \cdot m_r \\ \omega_z(t) &= [\epsilon_z(t_0) + \dot{\epsilon}_z \cdot (t - t_0)] \cdot m_r \\ s(t) &= s(t_0) + \dot{s} \cdot (t - t_0) \end{aligned} \quad (5)$$

where $(m_r = 4.84813681 \times 10^{-9})$ is conversion factor from milliarcseconds (mas) to radians. Here, (t_0) denotes a fixed time commonly called the reference epoch date (e.g. $(t_0 = 2025.0)$). Hence the seven quantities $(T_x(t_0), T_y(t_0), T_z(t_0), w_x(t_0), w_y(t_0), w_z(t_0),$ and $s(t_0)$ are all constants. The seven other quantities, $T_x, T_y, T_z, w_x, w_y, w_z,$ and \dot{s} which represents rates of change with respect to time, are also assumed to be constants.

It can be seen in above equation (5) that six parameters at any epoch can be determined. are six Helmert transformation parameters at epoch $(t_0 = 2025.0)$ and equals zero as NEP25 is aligned to ITRF2020. Taking $(t_0 = 2025.0)$ and $(t = 2028.0)$, one can determine the rate of change of these six parameters using equation (5). Rearranging equation (5) and substituting $(t_0 = 2025.0)$ and $t = 2028.0)$, we have following expression rearranged from (Wang et al., 2013) :

$$\begin{aligned} \dot{T}_x &= \frac{T_x(2028.0) - T_x(2025.0)}{(2028.0 - 2025.0)} \\ \dot{\omega}_x &= \frac{\omega_x(2028.0) - \omega_x(2025.0)}{(2028.0 - 2025.0)} \end{aligned} \quad (6)$$

The first expression in equation (6) can be used to determine rate of 3 translation parameters, and second expression can be used to determine the rate of 3 rotation parameters. Equation (6) provides the rate of six parameters required by equation (5).

Combining equation (2) and equation (5), the XYZ positional coordinates of a point / reference stations at any epoch (t) , with respect to NEP25 can be obtained using the following equations:

$$\begin{aligned} x(t)_{NEP25} &= \dot{T}_x \cdot (t - t_0) + x(t)_{ITRF} + \dot{\omega}_x \cdot (t - t_0) \cdot y(t)_{ITRF} - \dot{\omega}_y \cdot (t - t_0) \cdot z(t)_{ITRF} \\ y(t)_{NEP25} &= \dot{T}_y \cdot (t - t_0) - \dot{\omega}_x \cdot (t - t_0) \cdot x(t)_{ITRF} + y(t)_{ITRF} + \dot{\omega}_x \cdot (t - t_0) \cdot z(t)_{ITRF} \\ z(t)_{NEP25} &= \dot{T}_z \cdot (t - t_0) + \dot{\omega}_y \cdot (t - t_0) \cdot x(t)_{ITRF} - \dot{\omega}_x \cdot (t - t_0) \cdot y(t)_{ITRF} + z(t)_{ITRF} \end{aligned} \quad (7)$$

$x(t)_{ITRF}, y(t)_{ITRF},$ and $z(t)_{ITRF}$ are positional coordinates with respect to ITRF2020, which can be obtained by PPP processing. $(\dot{T}_x, \dot{T}_y, \dot{T}_z, \dot{\omega}_x, \dot{\omega}_y, \dot{\omega}_z)$ can be obtained from equation (6). Thus, the coordinate transformation of the GNSS-derived positional time series from ITRF2020 to NEP25 can be accomplished by a set of seven parameters: the epoch aligning two reference frames (t_0) , and rate of change of three translations and three rotations $(\dot{T}_x, \dot{T}_y, \dot{T}_z, \dot{\omega}_x, \dot{\omega}_y, \dot{\omega}_z)$

4 DISCUSSION

GSD is planning to establish about 30 CORS stations nationwide with the objective of defining national geodetic reference frame. Till the time of preparation of this manuscript, site selection work has been accomplished and construction of monument of these CORS station is ongoing. In future, when these CORS stations in operation and collect long-term observations, such long-term observations are utilized to define national geodetic reference frame. Such geodetic reference frame such as NEP25, can be defined / developed in terms of ITRF (e.g. current release ITRF2020) by application of 7- Helmert transformation parameters as explained in section 3. In future, NEP25 will be made accessible in forms of positional coordinates of about 30 reference stations at reference epoch, in our case $(t_0 = 2025.0)$ and rates of six parameters: $(\dot{T}_x, \dot{T}_y, \dot{T}_z, \dot{\omega}_x, \dot{\omega}_y, \dot{\omega}_z)$. Initially, user gets the positional coordinates of his/her site with respect to ITRF2020 obtained after PPP processing. Then he/she will apply transformation from ITRF2020 to NEP25 to get positional coordinates with respect to NEP25.

To better estimate rates of six parameters, GNSS observation of longer period, minimal of 3 years are required as shown by various studies (Wang et al., 2018) in order to deliver the millimeter level precision in position. National geodetic reference frame should

be updated at regular interval of years: 1) as longer period of observations will be available in future, 2) as newer release of ITRF will occur in future. In future, more / additional reference stations with longer period of observations would be beneficial such that better estimated site velocity will be obtained improving the stability of the reference frame.

5 CONCLUSIONS

With the aim of developing a national geodetic reference frame for Nepal, establishment of CORS network across the country has been initiated by GSD, SD. In this context, this paper provides an overview for the analysis and strategy to be adopted for realization of national geodetic reference frame utilizing long-term observations from nationwide established CORS stations.

REFERENCES

- Blewitt, G., Kreemer, C., Hammond, W. C., & Goldfarb, J. M. (2013). Terrestrial reference frame NA12 for crustal deformation studies in North America. *Journal of Geodynamics*, 72, 11–24. <https://doi.org/10.1016/j.jog.2013.08.004>
- Bomford, G. (1962). *Geodesy* (Second). Oxford University Press.
- KC, S., & Acharya, T. D. (2022). Advancements of Geodetic Activities in Nepal: A Review on Pre- and Post-2015 Gorkha Earthquake Eras with Future Directions. *Remote Sensing*, 14(7), 1586. <https://doi.org/10.3390/rs14071586>
- Kearns, T. J., Wang, G., Turco, M., Welch, J., Tsibanos, V., & Liu, H. (2019). Houston16: A stable geodetic reference frame for subsidence and faulting study in the Houston metropolitan area, Texas, U.S. *Geodesy and Geodynamics*, 10(5), 382–393. <https://doi.org/10.1016/j.geog.2018.05.005>
- Kouba, J., Lahaye, F., & Tétreault, P. (2017). Precise Point Positioning. In P. J. G. Teunissen & O. Montenbruck (Eds.), *Springer Handbook of Global Navigation Satellite Systems* (pp. 723–751). Springer International Publishing. https://doi.org/10.1007/978-3-319-42928-1_25
- Odijk, D., & Wanninger, L. (2017). Differential Positioning. In P. J. G. Teunissen & O. Montenbruck (Eds.), *Springer Handbook of Global Navigation Satellite Systems* (pp. 753–780). Springer International Publishing. https://doi.org/10.1007/978-3-319-42928-1_26
- Pearson, C., & Snay, R. (2013). Introducing HTDP 3.1 to transform coordinates across time and spatial reference frames. *GPS Solutions*, 17(1), 1–15. <https://doi.org/10.1007/s10291-012-0255-y>
- Shrestha, K. G. (2017). Bye-Bye EQ2015,11:56AM. *Journal on Geoinformatics, Nepal*, 14, 1–3. <https://doi.org/10.3126/njg.v14i0.16965>
- Soler, T., & Snay, R. A. (2004). Transforming Positions and Velocities between the International Terrestrial Reference Frame of 2000 and North American Datum of 1983. *Journal of Surveying Engineering*, 130(2), 49–55. [https://doi.org/10.1061/\(ASCE\)0733-9453\(2004\)130:2\(49\)](https://doi.org/10.1061/(ASCE)0733-9453(2004)130:2(49))
- Wang, G., Bao, Y., Gan, W., Geng, J., Xiao, G., & Shen, J. S. (2018). NChina16: A stable geodetic reference frame for geological hazard studies in North China. *Journal of Geodynamics*, 115, 10–22. <https://doi.org/10.1016/j.jog.2018.01.003>
- Wang, G., Liu, H., Mattioli, G. S., Miller, M. M., Feaux, K., & Braun, J. (2019). CARIB18: A Stable Geodetic Reference Frame for Geological Hazard Monitoring in the Caribbean Region.

Remote Sensing, 11(6), 680. <https://doi.org/10.3390/rs11060680>

Wang, G., Yu, J., Ortega, J., Saenz, G., Burrough, T., & Neill, R. (2013). A stable reference frame for the study of ground deformation in the Houston metropolitan area, Texas. *Journal of Geodetic Science*, 3(3). <https://doi.org/10.2478/jogs-2013-0021>

Wang, G., Zhou, X., Wang, K., Ke, X., Zhang, Y., Zhao, R., & Bao, Y. (2020). GOM20:

A Stable Geodetic Reference Frame for Subsidence, Faulting, and Sea-Level Rise Studies along the Coast of the Gulf of Mexico. *Remote Sensing*, 12(3), 350. <https://doi.org/10.3390/rs12030350>

Zumberge, J. F., Heflin, M. B., Jefferson, D. C., Watkins, M. M., & Webb, F. H. (1997). Precise point positioning for the efficient and robust analysis of GPS data from large networks. *Journal of Geophysical Research: Solid Earth*, 102(B3), 5005–5017. <https://doi.org/10.1029/96JB03860>



Author's Information

Name	: Narayan Regmi
Academic Qualification	: Masters in Geoinformation Management
Organization	: Geodetic Survey Division, Survey Department
Current Designation	: Deputy Director General
Work Experience	: 30 years
Published paper/article	: 1

Price of Maps

S.No.	Description	Scale	Coverage	No. of sheets	Price per sheet (NRs)
1.	Topo Maps	1:25 000	Terai and mid mountain region of Nepal	590	150
2.	Topo Maps	1:50 000	High Mountain and Himalayan region of Nepal	116	150
3.	Land Utilization maps	1:50 000	Whole Nepal	266	40
4.	Land Capability maps	1:50 000	Whole Nepal	266	40
5.	Land System maps	1:50 000	Whole Nepal	266	40
6.	Geological maps	1:125 000	Whole Nepal	81	40
7.	Districts maps Nepali	1:125 000	Whole Nepal	76	50
8.	Zonal maps (Nepali)	1:250 000	Whole Nepal	15	50
9.	Region maps (Nepali)	1:500 000	Whole Nepal	5	50
10.	Nepal (English)	1:500 000	Whole Nepal	3	50
11.	Nepal Map (Nepali)	1:1000 000	Nepal	1	50
12.	Nepal Map (Nepali)	1:2000 000	Nepal	1	15
13.	Nepal Map (English)	1:1000 000	Nepal	1	50
14.	Nepal Map (English)	1:2000 000	Nepal	1	15
15.	Physiographic Map	1:2000 000	Nepal	1	15
16.	Relief Map	1:2000 000	Nepal	1	15
17.	Photo Map			1	150
18.	Wall Map (loosesheet)		Nepal	1 set	50
19.	VDC/Municipality Maps (Colour)		Whole Nepal	4181	50
20.	VDC/Municipality Maps A4 Size		Whole Nepal	4181	5
21.	VDC/Municipality Maps A3 Size		Whole Nepal	4181	10
22.	Orthophoto Map		Urban Area (1:5000) and Semi Urban Area (1:10000)	-	1 000
23.	Outlined Administrative Map A4 size		Nepal	1	5

Price of Co-ordinates of Control Points

Type	Control Points	Price per point
Trig.Point	First Order	Rs 3 000.00
Trig. Point	Second Order	Rs 2 500.00
Trig. Point	Third Order	Rs 1 500.00
Trig. Point	Fourth Order	Rs 250.00
Bench Mark	First & Second Order	Rs 1 000.00
Bench Mark	Third Order	Rs 250.00
Gravity Point	-	Rs 1 000.00

Price of CORS Station Data

Type	Price
24 hr CORS Rinex data with 1 sec frequency for post processing	Rs 200
24 hr CORS Rinex data with 15 sec frequency for post processing	Rs 100
1 hr CORS Rinex data with 1 sec frequency for post processing	Rs 10
1 hr CORS Rinex data with 15 sec frequency for post processing	Rs 5
RTK Correction Service Unlimited Subscription 1 month	Rs 10000
RTK Correction Service Unlimited Subscription 3 months	Rs 27000
RTK Correction Service Unlimited Subscription 12 months	Rs 96000
GNSS Post-processing Service per point per hour data	Rs 10

Price of Geoid Data

Type	Price	Remarks
Geoid N-Separation (per point)	Rs 200	
Geoid Determined Orthometric Height (per point)	Rs 1000	
Geoid Data (per 100 sq. km)	Rs 10000	Minimum 100 sq.km and multiple of 100 sq.km



Nepal Remote Sensing and Photogrammetric Society (NRSPS)

Executive Committee

Susheel Dangol, *President*
susheeldangol@gmail.com

Er. Sanjeevan Shrestha, *Vice President*
shr.sanjeevan@gmail.com

Er. Janak Parajuli, *Secretary*
janak.parajuli1@gmail.com

Raj Kumar Thapa, *Assistant Secretary*
thapark2013@gmail.com

Er. Tina Baidar, *Treasurer*
tina.baidar13@gmail.com

Members

Dr. Chhabilal Chidi
chidichhabilal@gmail.com

Jagat Raj Poudel
jagatrajpoudel@hotmail.com

Roshani Sharma
anjaritja@gmail.com

Girija Pokharel
girija.pokhrel12@gmail.com

E-mail: nrpsociety@gmail.com

The society supported the “FIG Regional Conference 2024” organized by International Federation of Surveyors (FIG) and Nepal Institution of Chartered Surveyors (NICS) in November 14-16, 2024. Mr. Susheel Dangol, president of the society, received certificate of appreciation during the event on behalf of the society.



The society provided 3 research grants, one for the master’s level and 2 for bachelor level research under Research Grant Program.



Earth Observation Editorial Board

Susheel Dangol, *Advisor*
susheeldangol@gmail.com

Pravesh Yagol, *Chief Editor*
shrpravesh@gmail.com

Members

Prabesh Shrestha,
Shankar K.C
Thakur Lamichhane

The vice president of NRSPS, Mr. Sanjeevan Shrestha provided training on Google Earth Engine (GEE) to the students of Kathmandu University. The Training program was organized by Geomatics Engineering Society (GES) in collaboration with NRSPS on Dec 21-23, 2023



Eleventh issue of “Earth Observation” newsletter can be downloaded from www.nrps.org.np.

Multi-Modal Image Synthesis with Attention Conditional GANs: SAR, Optical, and DEM

David Nhemaphuki¹, Ajay Kumar Thapa² & Umesh Bhurtyal³

davis10ge@gmail.com, ajay.thapa@ku.edu.np, umbhurtyal@wrc.edu.np

¹ Survey Department, ² Kathmandu University, ³ Pashchimanchal Campus, Tribhuvan University

KEYWORDS

Image Synthesis, Cloud Removal, SAR, DEM, cGAN

ABSTRACT

This research addresses challenges in satellite-derived Earth observation data, such as cloud cover, atmospheric condition, seasonality and calibration inconsistencies, by leveraging Synthetic Aperture Radar for cloud penetration and Generative Adversarial Networks (GANs) for cloud removal and image synthesis. The main objective of this research is to develop conditional GAN (cGAN) models capable of synthesizing multispectral images from SAR (Sentinel-1), Optical (Sentinel-2) images and DEM (SRTM 30). The research dataset consists of above three products downloaded for 10 locations distributed across different geographical regions of Nepal from 2022-2023. Using these dataset the cGAN models are trained with different configuration. An initial cGAN model by Bermudez saw improved performance with DEM inclusion and further enhanced by integrating an attention block in the residual block. Thus, attention cGAN (A_cGAN) model was selected for further analysis. Among, the A_cGAN models the A_cGAN_SOD model performed the best which uses the dataset (SAR, DEM and optical images) while comparing the MAE, RMSE, SSIM and PSNR values. The image generated from A_cGAN_SOD model for Hetauda was used for LULC classification using random forest algorithm obtaining the overall accuracy of 89.96% which shows that the model output is applicable

1. INTRODUCTION

The rapid increase in satellite sensors with lower revisit times and higher spatial resolutions has led to the acquisition of vast remotely sensed data products, essential for Earth observation tasks like urban planning, disaster management, and weather forecasting. However, these products are often hindered by factors like cloud cover, atmospheric conditions (haze, fog, and aerosols), seasonal variability, and instrument calibration issues. These challenges create data gaps in

spatial and temporal domains, limiting their use in dynamic environmental processes such as crop monitoring, disaster response, and deforestation tracking. Cloud cover, a significant contributor to these gaps, affects around 67% of the Earth's surface, with 55% of land surfaces impacted, as demonstrated by King et al. (2013) in a study on MODIS data. Robust cloud removal and image synthesis methods are therefore crucial to ensuring consistent data availability for various applications.

Active sensors like Synthetic Aperture Radar (SAR), which can penetrate clouds, offer a typical solution to cloud-related issues but are limited by their less descriptive and complex data. To overcome these limitations, SAR data is often integrated with complementary imagery, such as near-date optical images and Digital Elevation Models (DEM), to enhance image recovery quality (Li et al., 2017). Additionally, Generative Adversarial Networks (GANs), introduced by Goodfellow et al., are a deep learning approach for generative modeling, often leveraging Convolutional Neural Network (CNN) architectures. Their objective is to learn the distribution of input data, enabling the generation of new, similar data samples. GANs consist of two neural networks: the generator, a CNN that creates realistic synthetic data, and the discriminator, a deconvolutional neural network that distinguishes between real and generated data. Conditional GANs (cGANs), as proposed by Mirza and Osindero (2014), extend traditional GANs by incorporating conditional information, making them effective in remote sensing for tasks like image synthesis and cloud removal. Studies such as Enomoto et al. (2017), Bermudez et al. (2018), and Christovam et al. (2021) have demonstrated the potential of cGANs in synthesizing high-quality, cloud-free images, enabling better applications of remote sensing data.

Attention mechanisms are pivotal in modern deep learning, enabling models to focus on critical input data while filtering out noise (Niu et al., 2021). Introduced by Bahdanau et al. (2014) in their seminal work on neural machine translation, the concept of "soft" attention allows models to dynamically assign weights to different parts of the input sequence, greatly improving alignment between source and target languages. This innovation has been widely adopted across various architectures, including Conditional Generative Adversarial Networks (cGANs),

where attention mechanisms enhance the model's ability to selectively process relevant information, leading to the generation of high-quality and coherent outputs.

The main objective of this research is to develop attention-based cGAN models capable of synthesizing multispectral images from SAR (Sentinel-1), Optical (Sentinel-2) images and DEM (SRTM 30).

2. DATASETS AND PREPROCESSING

2.1 Datasets

The dataset for this research consists of Sentinel 1 (SAR) images, Sentinel 2 (optical) images and DEM of ten locations of Nepal as mentioned in section 2.1.

Table 1: Image acquisition dates with regions

S.N	Location	Region	Image acquisition date		
			Sentinel -1	Sentinel -2 (1)	Sentinel -2 (2)
1	Taplejung	Mountain	2022-10-24	2022-10-24	2022-11-03
2	Jajarkot	Hilly	2022-12-05	2022-12-04	2022-11-19
3	Rautahat	Terai	2022-12-12	2022-12-11	2022-12-01
4	Baitadi	Hilly	2023-01-07	2023-01-06	2022-12-22
5	Banke	Terai	2023-02-03	2023-02-07	2023-01-23
6	Bhaktapur	Hilly	2023-03-13	2023-03-11	2023-02-24
7	Humla	Hilly	2023-03-27	2023-03-29	2023-04-08
8	Jhapa	Terai	2023-05-19	2023-05-14	2023-05-09
9	Kanchanpur	Terai	2023-06-12	2023-06-10	2023-06-10
10	Rupandehi	Terai	2023-10-17	2023-10-22	2023-10-20

For each location, one Sentinel-1 image and two Sentinel-2 images were acquired with acquisition dates as near as possible. The images span a time frame of one year from 2022 October to 2023 October covering the various seasons. The images have a cloud cover threshold of 5% and thus, there are no images from July, August and September as these are the heavy rainfall months. A detailed overview of the locations with the region and image acquisition dates is given in table 1 above.

2.2 Data download and pre-processing

Nepal lies in the UTM zones 44N and 45N. Among the 10 locations, 6 lie in 44N and 4 in 45N. They were spatially subset by bounding boxes of size 12km x 12km and spectral subset

was applied to S2 images to select 4 bands with 10m resolution (B4-Red, B3-Green, B2-Blue and B8-NIR) out of 12 bands. Finally, the datasets were resampled to 10m resolution and downloaded to Google Drive.

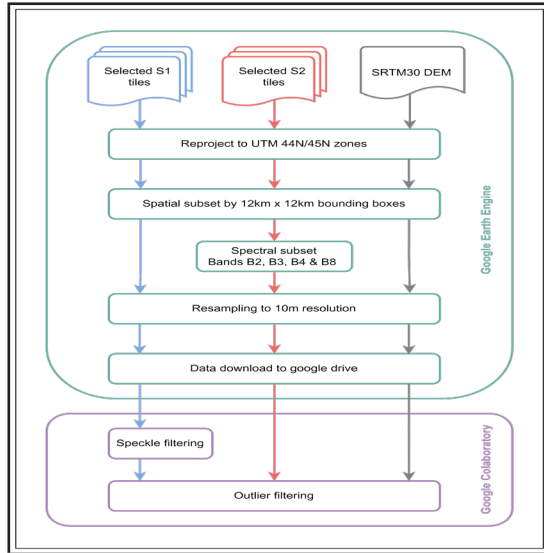


Figure 1: Data pre-processing

SAR images contain granular noise known as speckle. A median filtering that replaces each value of the pixel with the median value within the local window was used to remove speckles. Furthermore, the outliers in the pixel values for SAR, optical and DEM images are filtered out using histogram based outlier filtering. This filtering helps in reduction of noise, enhance interpretation and analysis and improve visual quality.

3. METHODOLOGY

The process begins with data collection from three primary sources: Sentinel-1, Sentinel-2, and DEM. Once collected, the data undergoes pre-processing to ensure consistency and quality for training. This stage involves noise filtering and normalization to standardize the data. Then, different datasets were prepared consisting a combination of different sources of data mentioned above and patches were extracted and divided into training, validation, and test sets.

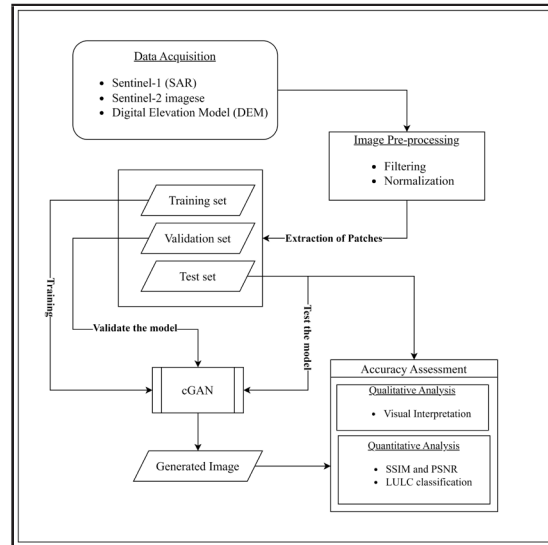


Figure 2: Research Methodology

Next step was to develop cGAN models with different settings and to train them to learn the complex relationships between SAR, optical, and DEM data. After training, the model's performance is evaluated using validation and test sets. Metrics such as MAE and RMSE were used for evaluation of model performance and the best performing model was selected for further analysis. While SSIM and PSNR were used to quantitatively evaluate the synthesized image, visual inspection was done for qualitative evaluation. SSIM is a widely used metric for measuring the similarity between two images while PSNR is a quantitative metric for assessing the quality of a reconstructed image relative to its original version. The overall flow of the proposed framework is shown in Figure 2.

3.1 Data Preparation

Data preparation involved three key steps: normalization, image concatenation, and patch extraction. Composite images were created by combining SAR, optical, and DEM data into four datasets:

- i. SAR_only (Sentinel-1),
- ii. SAR_DEM (Sentinel-1 with DEM),
- iii. SAR_OPT (Sentinel-1 with Sentinel-2) and

iv. *SAR_OPT_DEM* (Sentinel-1, Sentinel-2, and DEM)

Each datasets are paired with target Sentinel-2 optical images. Patches of size 256x256 with a 25-pixel overlap were extracted from these datasets, covering approximately 6.55 km² per patch. A total of 640 patch pairs were generated, augmented, and divided into training (80%), validation (10%), and test (10%) sets.

3.2 cGAN Model Development

The architecture design of a Conditional Generative Adversarial Network (cGAN) consists of two main components: the generator and the discriminator.

Generator: A generator takes noise and additional conditional information as inputs to generate realistic images. The model proceeds with a sequence of the encoder which progressively downsamples the input increasing feature representation. Incorporating an attention module enhances the encoder’s ability to focus on salient image regions. Following this, a series of residual blocks refine the feature maps, mitigating gradient vanishing issues. Subsequently, decoder blocks are employed to upsample the features, ultimately generating the output image. The function concludes with the compilation of the generator model, including an activation layer to finalize the output.

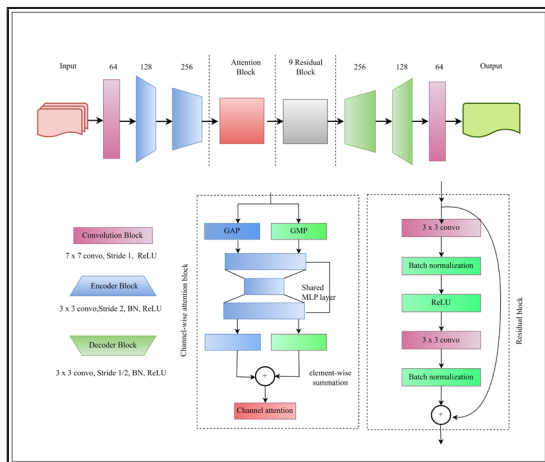


Figure 3: Generator

Discriminator: A Discriminator Model distinguishes real image and generated images by Generator. It starts with an input layer configured to match the dimension and channels of the input images. Then sequentially an encoder blocks is applied to the input image. These blocks, comprised of convolutional layers, progressively down sample the input while enhancing feature representation through activation functions such as Leaky ReLU. Following the encoder blocks, a final convolutional layer computes the logits, representing the discriminative decision for each input. An activation layer employing the sigmoid function subsequently generates the discriminator’s output, producing a probability score indicating the likelihood of the input being real or fake.

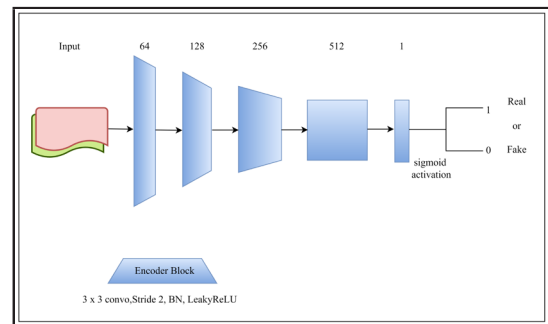


Figure 4: Discriminator

Detailed network architecture of generator and discriminator model used in the study are shown in Figure 3 and 4.

3.2 Training of the cGAN Models

A base cGAN model based on Bermudez, was trained and modified by incorporating various components as mentioned in the sub-sections below. Same hyperparameters from Table 2 were used for training in order to make uniform comparison for all the models.

Table 2: Hyperparameter used in the models

Patch Size	Training Size	Validation Size	Test Size	Epoch	Patience	Batch Size	Learning Rate
256	0.8	0.1	0.1	50	20	2	0.0002

3.2.1 Experiment I: DEM Integration

The models cGAN_S, cGAN_SD, cGAN_SO and cGAN_SOD were trained from datasets SAR only, SAR DEM, SAR OPT and SAR OPT DEM respectively. The primary goal of this experiment is to see whether adding the DEM data as additional data to the SAR and optical improves the performance of the model or not.

Table 3: Performance of cGAN models with DEM integration

S.N	cGAN_Model	MAE	RMSE
1	cGAN_S	0.270	0.361
2	cGAN_SD	0.238	0.329
3	cGAN_SO	0.059	0.084
4	cGAN_SOD	0.055	0.073

The addition of DEM data contributes in reducing errors, as evidenced by the notable improvement from cGAN S to cGAN SD. Furthermore, incorporating optical data further enhances model accuracy, leading to the lowest MAE and RMSE values in the cGAN SOD variant, which integrates SAR, optical, and DEM data. This underscores the importance of leveraging multiple types of data to improve the predictive capability of the cGAN model.

3.2.2 Experiment II: Adding Attention Block

An attention block was added to the base cGAN model architecture which helps to improve the model's ability to focus on relevant information enhancing its capacity to generate high-quality and coherent outputs. Thus, A_cGAN_S, A_cGAN SD, A_cGAN_SO and A_cGAN_SOD models were obtained.

Table 4: Attention cGAN models

S.N	cGAN_Model	MAE	RMSE
1	A_cGAN_S	0.229	0.305
2	A_cGAN_SD	0.237	0.322
3	A_cGAN_SO	0.057	0.077
4	A_cGAN_SOD	0.052	0.070

These models performed slightly better than the corresponding models in the previous experiment as it was able to achieve lower MAE and RMSE values (Table 4). A total of 8 models were trained and among them the least values of MAE 0.052 and RMSE 0.070 was observed for the model A_cGAN_SOD and was selected for the hyperparameter tuning where the parameters learning rate, batch size and patch size were tuned for the better performance of the model.

3.3 Hyperparameter Tuning

Firstly, the A_cGAN_SOD model was trained with the batch size of 1, 2, 4 and 8 while other parameters remains the same (learning rate = 0.0002 and patch size = 256). Secondly, the learning rate of 0.02, 0.002, 0.0002 and 0.0001 were taken into consideration while setting the batch size of 2 and patch size 256. Lastly, the model was then trained with the patch size of 128, 256 and 512 where batch size was set to 2 and learning rate 0.0002. The *batch size of 2, learning rate of 0.0002 and patch size of 128* demonstrates the most favorable results, exhibiting the least MAE of 0.0451 and an RMSE of 0.0632.

4. RESULT AND DISCUSSION

Table 5 summarizes the performance of various cGAN models based on SSIM and PSNR metrics, emphasizing the advantages of integrating SAR, Optical imagery, and DEM data. Models combining all three data sources outperform those using only SAR or SAR+DEM. Attention-based architectures further boost performance by emphasizing relevant features.

Table 5: Performance of cGAN models

S.N	cGAN_Model	SSIM	PSNR
1	cGAN_S	0.180	59.330
2	cGAN_SD	0.200	59.800
3	cGAN_SO	0.760	68.510
4	cGAN_SOD	0.780	68.780
5	A_cGAN_S	0.230	60.450
6	A_cGAN_SD	0.220	60.010
7	A_cGAN_SO	0.760	68.590
8	A_cGAN_SOD	0.760	68.220
9	A_cGAN_SOD(128)	0.780	68.910

The "A_cGAN_SOD (128)" model achieves the highest SSIM (0.780) and PSNR (68.910), along with low RMSE and MAE during training, demonstrating excellent learning and generalization, making it a strong candidate for practical applications. A_cGAN_SOD(128) model was used to generate the optical image for the date 2023-10-22. Then, the real Sentinel-2 image for the date 2023-10-22 and synthesized image was used for LULC classification whose results will be referred to as LULC_real and LULC_synth with an overall accuracies of 93.21% and 89.96% respectively.

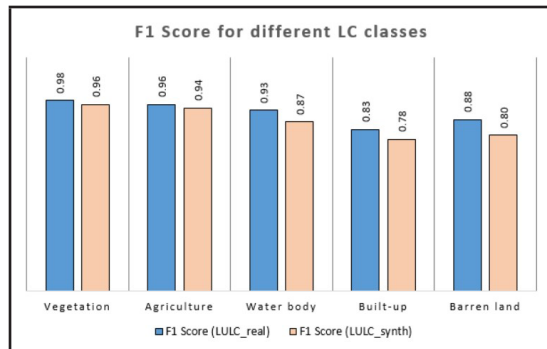


Figure 5: F1 Score for different LC classes

Figure 5 compares the F1 scores for different land cover (LC) classes between LULC_real and LULC_synth. Across all land cover classes, the F1 scores for LULC_synth are slightly lower than those for LULC_real, indicating a marginally reduced performance for the synthetic dataset. However, the scores remain within an acceptable range demonstrating the synthetic dataset's reliability for land cover classification tasks.

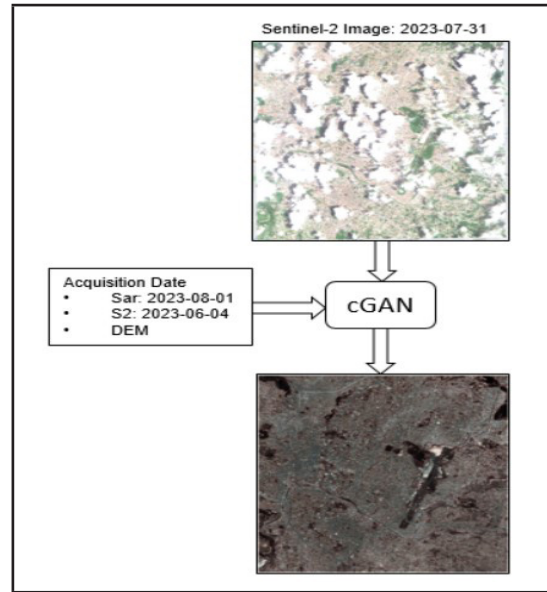


Figure 6: A_cGAN_SOD outcome

Figure 6 illustrate the outcome produced by the proposed model in the research. Initially, a Sentinel-2 image from July 31, 2023, was observed to contain significant cloud cover. To address this, the model utilized a combination of inputs: a SAR image from August 1, 2023, a cloud-free Sentinel-2 image from June 4, 2023, and a DEM. By combining these inputs, the model reconstructs a clear and usable image corresponding to July 31, 2023, overcoming the limitations caused by cloud cover in the original Sentinel-2 data.

5. CONCLUSION

Various models underwent training and testing, and models incorporating DEM data alongside SAR and optical data resulted in a marginal improvement than without it, indicating that supplementary conditioning data can enhance overall model accuracy. Also, A_cGAN_SOD, cGAN model with attention mechanism and using SAR, optical and DEM dataset, demonstrated superiority over other models, boasting the lowest RMSE and MAE values. It also achieved the highest SSIM and PSNR values showing that adding attention mechanism can generate more realistic and detailed outputs that capture important characteristics of the input data.

Moreover, the images produced by the A_cGAN_SOD model demonstrate substantial promise for geospatial analysis, effectively serving as substitutes for optical data compromised by cloud cover or other distortions. The model achieves a commendable Overall Accuracy (OA) score of 89.96% in Land Use Land Cover (LULC) classification tasks, underscoring its effectiveness in generating reliable and accurate imagery for analytical purposes.

REFERENCES

- Bahdanau, D., Cho, K., & Bengio, Y. (2014). Neural machine translation by jointly learning to align and translate. arXiv preprint arXiv:1409.0473.
- Bermudez, J., Happ, P., Oliveira, D., & Feitosa, R. (2018). Sar to optical image synthesis for cloud removal with generative adversarial networks. *ISPRS Annals of the Photogrammetry, Remote Sensing and Spatial Information Sciences*, 4, 5–11.
- Bermudez, J. D., Happ, P. N., Feitosa, R. Q., & Oliveira, D. A. (2019). Synthesis of multispectral optical images from sar/optical multitemporal data using conditional generative adversarial networks. *IEEE Geoscience and Remote Sensing Letters*, 16(8), 1220–1224.
- Christovam, L., Shimabukuro, M., Galo, M. T., & Honkavaara, E. (2021). Evaluation of SAR to optical image translation using conditional generative adversarial network for cloud removal in a crop dataset. *The International Archives of the Photogrammetry, Remote Sensing and Spatial Information Sciences*, 43, 823–828.
- Enomoto, K., Sakurada, K., Wang, W., Fukui, H., Matsuoka, M., Nakamura, R., & Kawaguchi, N. (2017). Filmy cloud removal on satellite imagery with multispectral conditional generative adversarial nets. *Proceedings of the IEEE conference on computer vision and pattern recognition workshops*, 48–56.
- Goodfellow, I., Pouget-Abadie, J., Mirza, M., Xu, B., Warde-Farley, D., Ozair, S., Courville, A., & Bengio, Y. (2014). *Generative adversarial nets. Advances in neural information processing systems*, 27.
- King, M. D., Platnick, S., Menzel, W. P., Ackerman, S. A., & Hubanks, P. A. (2013). Spatial and temporal distribution of clouds observed by modis onboard the terra and aqua satellites. *IEEE transactions on geoscience and remote sensing*, 51(7), 3826–3852.
- Li, Y., Fu, R., Meng, X., Jin, W., & Shao, F. (2020). A sar-to-optical image translation method based on conditional generation adversarial network (cgan). *IEEE Access*, 8, 60338–60343
- Mirza, M., & Osindero, S. (2014). Conditional generative adversarial nets. arXiv preprint arXiv:1411.1784.
- Niu, Z., Zhong, G., & Yu, H. (2021). A review on the attention mechanism of deep learning. *Neurocomputing*, 452, 48–62.



Author's Information

Name	: David Nhemaphuki
Academic Qualification	: MS in Geoinformatics
Organization	: Survey Department
Current Designation	: Survey Officer
Work Experience	: 9 yrs.
No. Published paper/article	: 2



Nepal Surveyor's Association (NESA)

NESA CEC Secretariate

Mr. Ambadatta Bhatta
President

Mr. Tanka Prasad Dahal
Vice President

Mr. Saroj Chalise
General Secretary

Mr. Prakash Dulal
Organization Secretary

Mr. Durga Phuyal
Secreatry

Mr. Sahadev Ghimire
Treasurer

Mr. Dilli Prasad Dahal
Member

Ram Kumar Shah
Member

Murari Tripathi
Member

Sundar Devkota
Member

Durga Prasad Upadhyaya
Member

Uttam Khadka
Member

Rajiv Prasad Shah
Member

Background

Utilizing the opportunity opened for establishing social and professional organizations in the country with the restoration of democracy in Nepal as a result of peoples movement in 1990, Survey professionals working in different sectors decided to launch a common platform named Nepal Surveyors' Association (NESA) in 1991, as the first government registered Surveyors' Organization in Nepal.

Objectives

The foremost objective of the association is to institutionalize itself as a full fledged operational common platform of the survey professionals in Nepal and the rest go as follows

- To make the people and the government aware of handling the survey profession with better care and to protect adverse effects from its mishandling.
- To upgrade the quality of service to the people suggesting the government line agencies to use modern technical tools developed in the field of surveying.
- To upgrade the quality of survey professionals by informing and providing them the opportunity of participation in different trainings, seminars, workshops and interaction with experts in the field of surveying and mapping within and outside the country
- To upgrade the quality of life of survey professionals seeking proper job opportunities and the job security in governmental and nongovernmental organizations
- To work for protecting the professional rights of surveyors in order to give and get equal opportunity to all professionals without discrimination so that one could promote his/her knowledge skill and quality of services.
- To advocate for the betterment of the quality of education and trainings in the field of surveying and mapping via seminars, interactions, workshops etc
- To wipe out the misconceptions and illimage of survey profession and to uplift the professional prestige in society by conducting awareness programs among the professionals and stakeholders
- To persuade the professional practitioners to obey professional ethics and code of conduct and to maintain high moral and integrity
- To advocate for the satification of Survey Council Act and Integrated Land Act for the better regulation of the profession and surveying and mapping activities in the country.

Organizational Structure

The Organization is nationwide expanded and it has the following structure: 14 Zonal Assemblies (ZA), 14 Zonal Executive Committees (ZEC), 5 Regional Assemblies (RA), 5 Regional Executive Committees (RAC), Central General Assembly (CGA) and a Central Executive committee (CEC).

Memberships Criteria

Any survey professional obeying professional ethics and code of conduct, with at least one year survey training can be the member of the Association. There are three types of members namely Life Member, General Member and Honorary Member. At present there are 2031 members in total.

Present Land Use and Land Use Zoning of Kushma Municipality: A Comparative Assessment with Cadastral Superimpose

Sushmita Subedi¹, Roman Pandit², Manoj G.C.³ & Indra Subedi³
subedisusmiss7@gmail.com, spcroman001@gmail.com, manoozgc@gmail.com, subediindra724@gmail.com
¹Survey Office Parbat, ²Tribhuvan University, ³Global Era Engineering Consultancy

KEYWORDS

Present Land Use, Land Use Zoning, Cadastral Superimpose, Multi-Criteria Analysis

ABSTRACT

Rapid urbanization and unplanned expansion in Nepal have necessitated a structured land use planning to balance economic growth, environmental sustainability and disaster resilience. This study conducts a comparative assessment of present land use and land use zoning in Kushma Municipality integrating cadastral data to evaluate alignment with the national land use policy. Using Geographic Information System (GIS), high-resolution satellite image and multi-criteria analysis, the research maps current land use patterns and land use zoning framework in the municipality. Results reveal agricultural dominance in present land use with 60.81% of total area followed by forest cover. Land use zoning indicates a 13.23% reduction in agricultural land, offset by substantial expansions in residential area by 10.65%. Cadastral superimposition highlights discrepancies, with agricultural parcels decreasing from 51.90% to 41.78%, while commercial areas triple in allocated space. The study underscores the need for adaptive land use policies, periodic zoning revisions and community engagement to ensure sustainable development. By integrating GIS-driven insights with participatory planning, Kushma Municipality can navigate urbanization challenges while safeguarding ecological and agricultural assets. This research contributes a replicable framework for municipalities in developing regions aiming to harmonize cadastral data, land use planning and policy implementation.

1. INTRODUCTION

Land is a fundamental and invaluable natural resource that plays a crucial role in sustaining life and supporting various human activities. However, the increasing demands for arable land, grazing areas, forestry, wildlife conservation, tourism, and urban expansion have outpaced the availability of land resources. This growing pressure on land highlights the challenges associated with its sustainable

management and equitable distribution. In Nepal, land use has been recognized as a critical sector in national development, as evidenced by various government policies, strategic plans, and official documents (Sharma, 2012). The Nepalese government has prioritized land use planning to balance competing demands while ensuring environmental sustainability and economic growth.

The use of land and its resource has been considered as one of the integral parts of sustainable development (United Nations, 2024). There is widespread agreement that sustainable agriculture plays a crucial role in achieving global sustainable development, with the need for sustainable agricultural production systems being increasingly recognized. In Nepal, however, urban centers are expanding haphazardly due to inadequate planning, despite the preparation of extensive urban development planning documents in the past (Acharya & Halden, 2018; GoN, 2015). A key focus of these plans was the management of urban areas through effective land use zoning, yet their implementation has been largely ineffective. As a result, urban growth has been disorderly and unregulated. In light of this, there is an urgent need to establish structured land use planning and zoning mechanisms to guide urban development (Dahal, 2023). A modernized land use policy is essential to ensure food security, promote environmental sustainability, create safe human settlements and foster planned urbanization alongside inclusive economic growth. While the existing policy prioritizes the protection of arable land to safeguard food security, the catastrophic earthquake of 2015 and its aftershocks have highlighted the necessity for a secure, disaster-resilient human settlement. Consequently, a comprehensive review of the current land use policy has become imperative (MoLRM, 2015).

Effective land use planning is essential for optimizing the utilization of limited land resources. It involves a systematic evaluation of land and water potential, exploration of alternative land use options, and consideration of economic and social factors to identify and implement the most suitable land use strategies (FAO, 1993). While Nepal has made sporadic efforts to implement land use planning in urban areas (GoN, 2002), comprehensive land use planning at the national level remains

largely absent. Past initiatives have focused on achieving a balanced use of natural resources through various policies and national planning endeavors. Additionally, Nepal has recently begun incorporating risk-sensitive land use planning at the municipal and rural municipal levels. However, these efforts often overlook the underlying causes and specific characteristics of geo-disasters, raising concerns about their effectiveness (Thapa, 2018).

Land use planning is typically implemented at three broad levels: national, district and local. At the local level, planning focuses on the practical execution of land-related activities, determining what actions will be undertaken, their specific locations and timing, and the entities responsible for their implementation. This process necessitates comprehensive and detailed information regarding land characteristics, population dynamics, and available services within a given locality (Oli, 2018). However, in Nepal, land use data had historically been available only at a regional scale, primarily through the Land Resource Mapping Project conducted in 1980s, which provided insights into land use, land systems, and land capability (Carson et al., 1986). Recognizing the limitations of these datasets, the Government of Nepal, through the Ministry of Land Reform and Management, established the National Land Use Project (NLUP) in the fiscal year 2057/58 with the objective of developing a comprehensive database on the country's land resources at the local level. This comprehensive digital database encompasses various spatial and thematic datasets, including current municipal land use, soil characteristics, land capability classifications, and land use zoning. Additionally, it integrates cadastral layers alongside a detailed municipal profile, which encapsulates both biophysical attributes and socio-economic parameters (Oli, 2018).

The National Land Use Policy of 2013 was formulated with a primary focus on

safeguarding arable land to ensure national food security. However, the devastating earthquake of April 25, 2015 underscored the urgent need for a more comprehensive approach to land use planning, particularly in disaster-prone areas. This disaster highlighted the necessity of enforcing regulated activities within zones susceptible to natural hazards to mitigate risks and enhance resilience. The construction of physical infrastructure henceforth must incorporate considerations of newly emerging hazards. Recognizing the evolving challenges posed by natural disasters, the Land Use Policy of 2015 was introduced as an updated framework, following a critical reassessment of the 2013 policy. This revised policy aims to address contemporary land use issues in a long-term and sustainable manner, integrating disaster risk reduction principles into national land management strategies (MoLRM, 2015).

Nepal aims to regulate land use in accordance with the Land Use Policy established by the Government of Nepal. This policy classifies land into ten distinct zones: Agricultural, Residential, Commercial, Industrial, Mines and Minerals, Cultural and Archaeological, River and Riverine, Forest, Public Use and Open Space, and Others. The delineation of these zones is based on land characteristics, capability, and requirements of the land for sustainable utilization and management (MoLRM, 2015). In order to facilitate the effective implementation of these zoning regulations, the National Land Use Policy mandates a structured institutional framework, establishing a Land Use Council at the national level, with corresponding bodies extending down to the district and municipal levels (NLUP, 2016).

2. STUDY AREA

Kushma Municipality was officially established in 2017 (2074 BS) as a local administrative unit in Nepal. It serves as the

administrative center of Parbat district within Gandaki Province, with its headquarter located in the city of Kushma. The municipality shares its eastern boundary with Modi Rural Municipality and the districts of Kaski and Syangja, while it is bordered to the west by Baglung District. To the north, it is surrounded by Jaljala Rural Municipality, Modi Rural Municipality and Phalewas Municipality, whereas Phalewas Municipality and Syangja District form its southern boundary (Kushma Municipality, 2024).

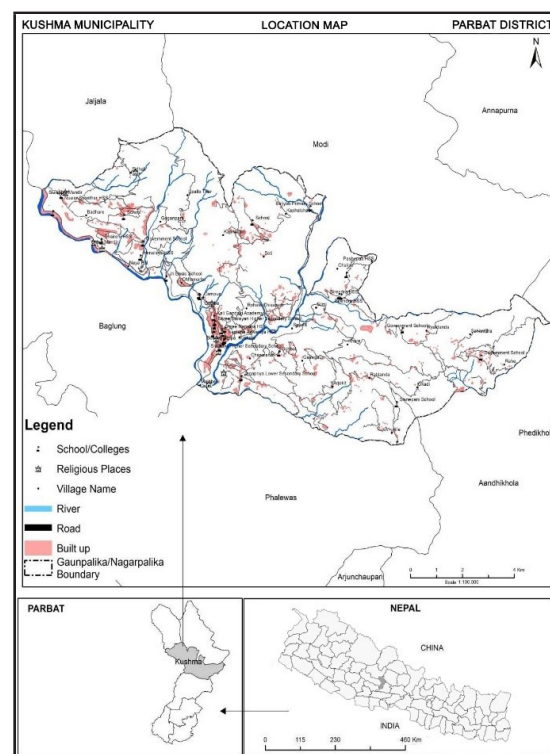


Figure 1: Location Map of Study Area

The geographical coordinates of Kushma Municipality extend from 83°36'40" to 83°48'33" east longitude and from 28°12'05" to 28°16'22" north latitude. Covering a total area of 93.18 square kilometers (36.00 square miles), the municipality recorded a population of 38,101 in the 2021 (2078 BS) Nepal Census, with a population density of approximately 409 individuals per square kilometer (CBS, 2021). Administratively, Kushma Municipality is divided into 14 wards.

3. METHODOLOGY

3.1 Preparation of Present Land Use Map

The specific approaches and methods adopted to generate the Municipality level present land use map in the project area is explained briefly with the overall work flow diagram (Figure 2). The stepwise procedure adopted to generate the present land use map of the area is the following:

3.1.1 Pan-sharpening (Image Fusion)

Pan-sharpening (resolution merge or image fusion) technique has been applied on the ZY-3 images covering the study area. This is basically done through the fusion process of high-resolution panchromatic data with lower resolution multispectral data in order to create a high-resolution multispectral data set. In this study, pan-sharpening was done using Brovey transform technique. The pan-sharpening using Brovey transform was applied to visually increase contrast in the low and high ends of the image's histogram (i.e. to provide contrast in shadows, water and high reflectance areas such as urban features).

3.1.2 Visual Image Interpretation and Classification

The desired categories of land use/ land cover were to be extracted as thematic information from the pan-sharpened ZY-3 image. In this study, knowledge-based visual interpretation was carried out. Ground reference data collected were employed in preparation of classification system.

Prior to undertaking the task of image interpretation for the identification and delineation of land use classes, two critical issues must be addressed. The first step involves establishing necessary criteria to distinguish the various feature categories present in the image. To accomplish this, the specific characteristics that define and separate the appropriate land use classes were

determined as per the classification hierarchy outlined in the Land Use Act, 2076 and the Land Use Regulation, 2079. The second key issue pertains to the selection of the minimum mapping unit (MMU) for delineating discrete areal units on photographs. In this project, the MMU for land use classification was set as one fourth of a hectare in accordance with the land use specifications for mapping at scale of 1:10,000 (NLUP, 2016). However, smaller yet significant features, particularly buildings were also mapped even if they fell below the MMU threshold.

3.1.3 Accuracy Assessment

In this study, validation of the classification result was done for the quantification and evaluation of error using a confusion matrix. A total of 457 samples points in study area were collected using GPS to be taken for the confusion matrix generation. The confusion matrix was generated based on the comparison between the classified image and the existing ground i.e. the matrix depicted the land cover classification categories in the image versus the field observed land cover types.

The error/confusion matrix was evaluated by computing the user accuracy, producer accuracy and overall accuracy which was tested statistically using the Kappa statistics. The Kappa Index of Agreement (KIA) was calculated with the following formula (Congalton 1991).

$$K = \frac{N \sum_{i=1}^r x_{ii} - \sum_{i=1}^r (x_{i+} \cdot x_{+i})}{N^2 - \sum_{i=1}^r (x_{i+} \cdot x_{+i})}$$

Where:

K = Kappa coefficient

N = Total number of observations

r = Total number of classes

x_{ii} = Number of observations correctly classified for class i (diagonal elements of the confusion matrix)

x_{i+} = Total number of observations in row i
(sum of row i)

x_{+i} = Total number of observations in column i
(sum of column i)

3.1.4 Land Use Geo-Database Creation and Mapping

Once the classification was completed and validated, a comprehensive geo-database was created in GIS environment to store and manage the land use data. Finally, a present land use map was produced to represent the current spatial distribution of each land use category within the study area.



Figure 2: Present Land Use Workflow

3.2 Preparation of Land Use Zoning Map

3.2.1 Conceptual Basis

In this particular project, the land use zoning was carried out by adopting the following concept:

- Classifying land into Agricultural area, Residential area, Commercial area, Industrial area, Mining and Mineral area, Cultural and Archaeological area, River, Lake and Water bodies area, Forest area,

Public Use area and Others as per the provision of Land Use Act, 2076 and Land Use Regulation, 2079.

- Identifying the potential zones for residential, commercial, industrial and public utility development while ensuring environmental sustainability.
- Classifying agricultural lands into sub-zones based on land quality, capability, and access to irrigation systems to optimize productivity.
- Ensuring the conservation of natural resources, including forests, shrublands, rivers, rivulets, and wetlands.
- Determining mine and mineral extraction zones with a comprehensive evaluation of their environmental and social impacts.
- Identifying public service areas, particularly open spaces to facilitate hazard mitigation strategies.
- Proposing the development of forested and public service areas in regions prone to natural hazards as a preventive measure.

The fundamental principles guiding the land use zoning of Kushma municipality are as follows:

a) Land Composition, Capability and Suitability

The primary criterion for determining land use zoning was the geographical and geological composition of the land, along with its capacity and appropriateness for specific uses.

b) Existing Land Use

Zoning decisions were based on the current land use of a given area, provided that its existing utilization aligned with its inherent composition, capability and suitability.

c) Functional Necessity

Land use zones were designated to ensure optimal utilization of land resources in accordance with the societal and economic needs.

3.2.2 General Guidelines

Based on the above criteria, the following guidelines were considered for the land use zoning:

Table 1: Guidelines for Land Use Zoning

S.N.	Zones	Guidelines
1	Agricultural Zone	<p>a) Most agricultural areas are retained, but some land is allocated for residential, commercial, industrial, and public use.</p> <p>b) Priority is given to retaining highly arable land while using marginal lands for infrastructure.</p> <p>c) Agricultural land is classified based on land capability, system, temperature, irrigation, drainage, and soil parameters.</p> <p>d) Consultation with agricultural experts is conducted for further classification.</p>
2	Forest Zone	<p>a) Existing forests remain intact.</p> <p>b) New forests or plantations are established on:</p> <ul style="list-style-type: none"> - Barren lands, wetlands, abandoned lands - Sloping land, watersheds, high mountains - Flood and erosion prone riverbanks - Marginally utilized lands - Roadside and canal areas where possible - Near industrial areas for pollution control - High and medium hazard risk lands - Suitable areas for agroforestry and timber production
3	Residential Zone	<p>a) Existing residential areas remain intact if risk-free or low-risk.</p> <p>b) New settlements are proposed based on:</p> <ul style="list-style-type: none"> - Low hazard risk land - Proximity to existing settlements - Availability of roads and infrastructure - Avoiding floodplains - Geological stability - Distance from dense forests and industrial areas - Preference for marginally productive agricultural land
4	Commercial Zone	<p>a) Existing commercial areas remain intact.</p> <p>b) New commercial/business areas, including government institutions are planned based on:</p> <ul style="list-style-type: none"> - Low hazard risk land - Proximity to residential areas and population centers - Availability of roads and infrastructure - Avoidance of floodplains - Geological stability - Distance from dense forests - Preference for marginally productive agricultural land

S.N.	Zones	Guidelines
5	Industrial Zone	a) Existing small, agriculture-based industries remain intact. b) Heavy industries affecting human settlements are relocated. c) Proposed industrial areas follow these criteria: <ul style="list-style-type: none"> - Low-hazard-risk land - Proximity to existing industrial areas (if suitable) - Distance from residential and commercial areas but accessible to markets and infrastructure - Availability of roads - Distance from rivers, ponds, and dense forests - Marginally productive agricultural land - Geological stability - Located near administrative borders for shared resources
6	Public Use Zone	a) Existing public utility and open spaces remain intact. b) New public use areas (health, education, open spaces) are placed near residential, commercial, and industrial areas. c) Planned based on local needs and participatory community discussions.
7	Mine and Minerals Zone	a) Existing mining and quarrying areas following the National Land Use Act, 2076 and Land Use Regulation, 2079. b) Potential future mining and quarrying areas are identified and prescribed.
8	Cultural and Archaeological Zone	a) Existing religious, cultural, and archaeological sites following the National Land Use Act, 2076 and Land Use Regulation, 2079. b) Cultural heritage areas are identified and planned according to master plans.
9	Riverine and Lake Zone	Existing rivers and water bodies following the National Land Use Act, 2076 and Land Use Regulation, 2079.
10	Other Zones	a) As prescribed by experts and decided by the Municipality. b) Includes land use types not covered in other categories.

3.2.3 Data

The main datasets used in land use zoning of the study area are as follows:

- Ortho-rectified High Resolution Satellite Image
- Present Land Use Map, Soil Map, Land System Map, Land Capability Map and Reports prepared by Survey Department
- Municipality Profile, Database and Reports
- Digital Topographical Datasets

- GIS Vector Data (shape file) of mainly Land Capability, Land System, Present Land Use, Administrative Boundary
- Socio-economic Data and Village Profile
- Hazard Data such as Seismicity Data, Flood Inundation Data, Industrial Risk Data, etc.

3.2.4 Methods

The specific methods used for land use zoning are the following:

3.2.4.1 Preparation

At first, a comprehensive literature review, requirement analysis and the development of a database comprising various criteria maps for land use zoning were undertaken to identify appropriate land use classifications. This process served as a foundation for generating insights into land use zoning and facilitating informed decision-making for sustainable utilization of land in the future.

3.2.4.2 Multi-criteria Analysis

Land use zoning was primarily conducted through GIS-based spatial analysis, which incorporated multiple criteria from various available datasets. The analysis utilized either GIS vector data (shapefiles) or raster data, focusing on factors like land capability, land systems, current land use and socio-economic data, which served as factor maps. A general rule for zoning was developed by applying multiple criteria derived from expert knowledge, gathered through focus group discussions with stakeholders or by using the Analytical Hierarchy Process (AHP) with pairwise comparisons. These criteria were employed to determine the most appropriate land use zones and to identify potential areas for future land use. The datasets included a range of parameters such as soil characteristics, landform, land type, arability, slope, drainage systems, topography, existing land use, crop patterns, population density and other relevant factors for zoning. A simplified rule-based approach was developed relying on expert knowledge and multiple criteria to classify land into specific zones. This approach was based on scientific principles, ensuring that the process was objective and free from individual biases.

3.2.4.3 Subjective Analysis

A subjective analysis combined with logical inference was employed for land use zoning in consultation with thematic experts and through

focus group discussions with stakeholders in order to refine the land use zones derived from multi-criteria analysis. This process was based on specific requirements and expert opinions. For instance, if a small parcel of land was deemed suitable for agricultural use but was surrounded by residential area, it would be designated as part of the residential zone. Similarly, if land suitable for agriculture was located within a river floodplain with a high risk of flooding, it would be designated for forest and plantation use to mitigate the flooding risks.

After public auditing and demarcation of land use zoning by municipal officials, experts and specialists; land use zoning guidelines were prepared in each ward which were approved by the municipal land use council. The following schematic diagram illustrates the general approach and methodology adopted for land use zoning of Kushma municipality.

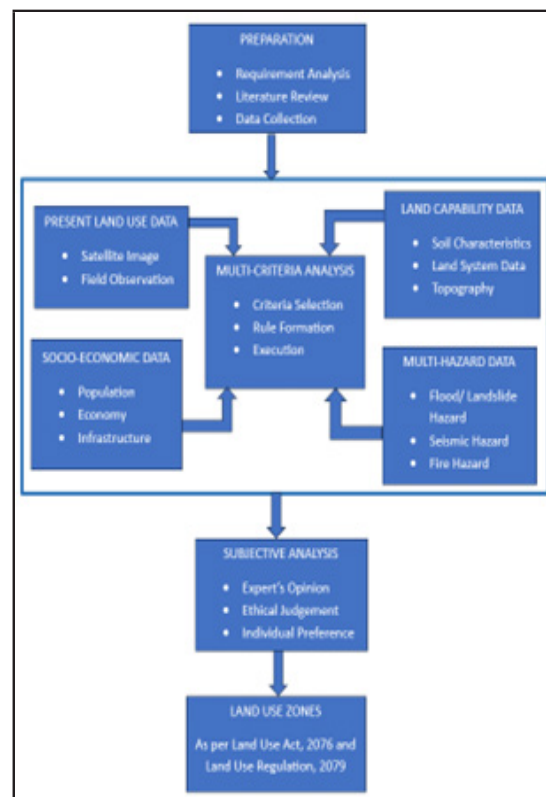


Figure 3: Land Use Zoning Workflow

3.3 Cadastral Data Superimpose

The superimpose of cadastral data was performed with both present land use and land use zoning layers for a comparative analysis in order to facilitate the effective implementation of land use policy. This process required two key components: a cadastral layer that served as the foundational dataset and a present land use/land use zoning layer to facilitate the policy enforcement. The overlay process of these data layers having same reference system led to the preparation of composite map and data. A new set of polygons with attributes were generated that explain the relations existing between the two inputs of spatial data.

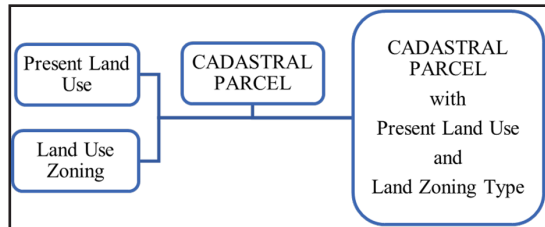


Figure 4: Cadastral Superimpose

The process of cadastral data superimpose on land use zoning was carried out in the following steps:

3.3.1 Acquisition of Cadastral Maps

The digital copies of cadastral maps of the study area were obtained from Survey Department in vector format. These maps were stored as sheet wise geodatabase with attribute database having schema as described in Table 2.

Table 2: Schema of Cadastral Parcel Feature Class

Field Name	Data Type	Description
ObjectID	Object ID	Unique object ID
Shape	Geometry (Polygon)	Geometric object type e. g. Point, Line, Polygon etc.
PARCELKEY	String (Length = 23)	Unique parcel key

Field Name	Data Type	Description
PARCELNO	Integer	Parcel number as in cadastral map
DISTRICT	Integer	District ID
GAPA_NAPA	Integer	G A P A _ N A P A Code
WARDNO	String (Length = 3)	Ward number
GRIDS1	String (Length = 9)	Grid sheet number in case of Trig sheets, and in case of island map sheet e. g. Ka, Kha etc.
PARCELTY	Integer	Parcel type code as specified by DOLIA (e.g. river, track, ravine, pine etc.)
Shape_Length	Double	N u m b e r representing perimeter of the polygon
Shape_Area	Double	N u m b e r representing area of the polygon
ParcelNote	String	

3.3.2 Scanning, Georeferencing and Digitizing

Due to the absence of certain digital cadastral maps in the database provided by Survey Department, the missing maps were obtained from Survey Office Parbat. First, the ammonia prints of these maps were acquired which were then scanned in 300 dpi using a high-quality scanner to convert into digital raster file. Then georeferencing of both digital cadastral database and scanned cadastral images were carried out with the help of ortho-rectified satellite image of the study area. This helped to establish a common geodetic framework for all related maps and data providing a common basis for overlay and other GIS operations. After georeferencing, the scanned maps were subsequently digitized to transform them to vector format, resulting in cadastral datasets stored as sheet-wise geodatabases in. gdb format.

3.3.3 Preparation of Municipality Level Seamless Cadastral Dataset Seamless cadastral datasets at both the ward and municipality levels were created through spatial analysis in a GIS environment, involving the merging of various geo-referenced cadastral map sheets. During this process, some errors such as overlaps and gaps between individual cadastral map sheets were identified. However, these errors were rectified by establishing topology within predefined thresholds. In rare instances where significant gaps or overlaps occurred, they were addressed accordingly.

3.3.4 Superimpose of Seamless Cadastral Dataset on Land Use Zoning Map

The superimpose of cadastral dataset on land use zoning map of the same area, same scale and same georeferenced framework was performed functions in GIS environment. During the overlay procedure, careful attention was given to preserving topology by adhering to key principles such as preventing overlaps, avoiding intersections and ensuring that no topological function was entirely contained within another.

3.3.5 Linking Attribute of Land Use Zoning with Cadastral Parcel

The process of connecting land use zoning map with seamless cadastral datasets involved querying the attribute table of cadastral datasets at the VDC level with the land use zoning class datasets. This linkage associated geographic objects in a vector map with one or more tables, specifying the driver database to be utilized. In a geometry file, each parcel category number was linked to a corresponding row in the attribute table. The system's practical functionality enabled the integration of thematically distinct yet topologically interconnected objects within a single map. Additionally, the table was linked to subsequent layers for further analysis and integration.

3.3.6 Production of Data, Map and Report

The process described in this section resulted in the creation of a composite data base, map and report. The overall method adopted for cadastral superimpose on land use zoning of Kushma municipality is illustrated in Figure 5.

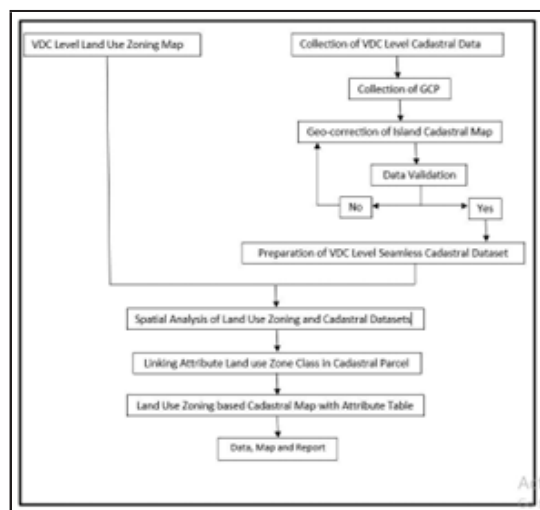


Figure 5: Method Adopted for Cadastral Superimpose

4. RESULTS AND DISCUSSION

4.1 Present Land Use

The present land use map of Kushma municipality demonstrates that agriculture land has dominated the land use class in this area. The present land use area in hectares for the municipality, broken down by wards, reveals varying distributions across different regions. In Ward 1, agricultural land dominates with 513.02 hectares, while Ward 2 has the highest agricultural area at 736.54 hectares. Ward 3 follows closely with 770.49 hectares allocated for agriculture. Commercial activities are limited across all wards, with Ward 5 having the highest commercial land use at 14.37 hectares. Cultural and archaeological sites are relatively small in all wards, with Ward 3 having the highest at 0.83 hectares. Forested areas vary significantly, with Ward 2 having the highest forest cover at 496.96 hectares, while Ward 6 has only

0.52 hectares. Industrial areas are minimal in most wards, with Ward 1 having the highest at 13.73 hectares. Mine and mineral areas are concentrated in Ward 13, accounting for 3.11 hectares. Public use spaces are distributed across wards, with Ward 10 having the largest area at 31.74 hectares. Residential areas are relatively consistent across wards, with Ward 5 having the highest at 28.17 hectares. Ward 1 has the most significant riverine, lake, and marsh area at 39.79 hectares, while Ward 5 has the lowest at 11.67 hectares. This detailed

breakdown by wards offers insights into the unique land use patterns within each region of Kushma Municipality, aiding in localized planning and development initiatives.

The distribution of present land use pattern of Kushma municipality is presented Figure 6 and ward-wise details are provided in Table 3. Table 4 depicts the confusion matrix generated for the validation of classification results. The overall accuracy of present land use classification was 95.62% and the Kappa Coefficient was computed as 0.94.

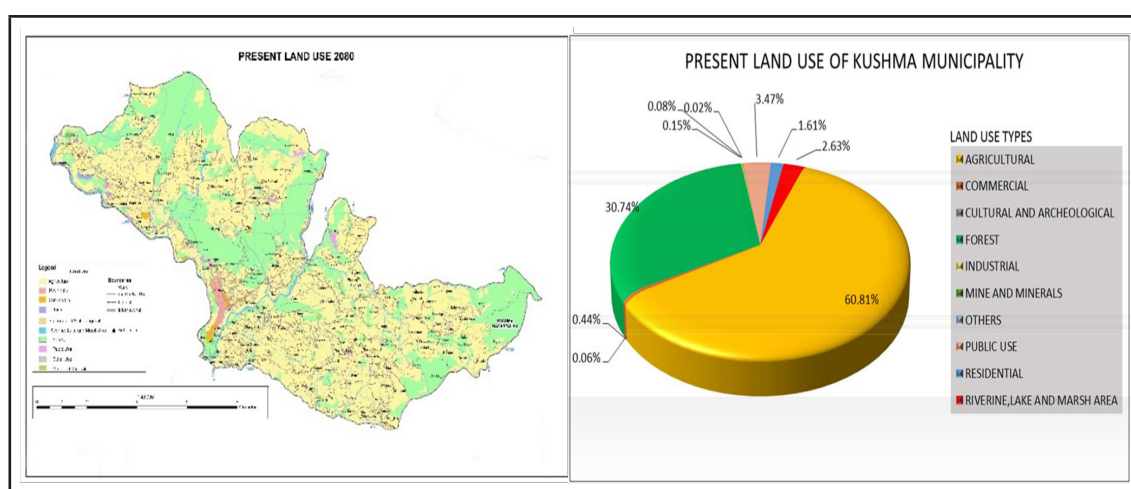


Figure 6: Present Land Use 2080

Table 3: Present Land Use 2080

LAND USE TYPE	PRESENT LAND USE 2080 (AREA IN HECTARES)														Grand Total
	WARD NO.														
	1	2	3	4	5	6	7	8	9	10	11	12	13	14	
AGRICULTURAL	513.02	736.54	770.49	162.42	36.54	14.70	104.02	173.57	239.33	637.91	522.56	533.31	484.56	737.17	5666.14
COMMERCIAL	0.64	5.56	2.74	6.75	14.37	4.51	3.93	1.16	0.17	0.04	0.03	0.39	0.04	0.31	40.66
CULTURAL AND ARCHEOLOGICAL	1.37	0.32	0.49	0.49	0.81	0.25	0.05	0.11	0.20	0.17	0.17	0.07	0.53	0.83	5.86
FOREST	253.38	496.96	401.02	255.10	49.31	0.52	78.29	295.20	20.51	61.80	171.75	72.28	104.12	603.55	2863.77
INDUSTRIAL	13.73	0.05	0.00	0.05	0.00	0.00	0.00	0.52	0.00	0.03	0.00	0.00	0.00	0.00	14.38
MINE AND MINERALS	0.20	0.00	0.04	0.00	0.00	0.00	0.00	0.00	0.00	0.00	0.00	3.11	0.00	3.69	7.03
OTHERS	0.00	0.25	0.00	0.00	0.00	0.00	0.00	0.00	0.00	0.98	0.00	0.01	0.04	0.78	2.05
PUBLIC USE	30.94	39.96	34.02	26.21	11.39	5.16	11.96	17.04	13.65	28.60	31.74	24.79	20.44	27.23	323.14
RESIDENTIAL	13.49	14.46	17.16	9.66	28.17	9.32	4.16	6.78	9.05	8.14	8.39	6.78	5.55	8.84	149.94
RIVERINE, LAKE AND MARSH AREA	39.79	34.46	22.98	14.36	11.67	3.84	9.31	24.82	11.51	17.27	20.54	7.70	11.77	14.61	244.63
Grand Total	866.57	1328.55	1248.93	475.04	152.26	38.30	211.72	519.21	294.42	755.02	755.19	648.45	627.04	1397.00	9317.69

Table 4: Accuracy Assessment of Present Land Use 2080

		GROUND VERIFICATION											
Land Use	Categories	Agriculture	Forest	Residential	Commercial	Industrial	Public	Minerals	Cultural and Archeological	River, Lake and Marsh	Other	Total	User's Accuracy
		Agriculture	98	0	1	0	0	1	0	1	0	1	102
Forest	1	53	0	0	0	1	0	1	0	0	56	94.64%	
Residential	0	0	55	2	0	0	0	1	0	0	58	94.83%	
Commercial	0	0	0	33	1	0	0	0	0	0	34	97.06%	
Industrial	1	0	0	0	22	0	0	0	0	0	23	95.65%	
Public	0	0	1	0	0	80	0	2	0	0	83	96.39%	
Minerals	0	0	0	0	0	1	15	0	0	0	16	93.75%	
Cultural and Archeological	0	0	1	0	0	0	0	35	0	0	36	97.22%	
River, Lake and Marsh	1	1	0	0	0	0	0	0	34	0	36	94.44%	
Other	1	0	0	0	0	0	0	0	0	12	13	92.31%	
Total		102	54	58	35	23	83	15	40	34	457		
Producer's Accuracy		96.08%	98.15%	94.83%	94.29%	95.65%	96.39%	100.00%	87.50%	100.00%	92.31%		

4.2 Land Use Zones

Across Kushma Municipality, agricultural zones dominate the land use, spanning a total 4433.05 hectares, indicating a strong emphasis on farming and cultivation activities. Significant forest cover of 2832.94 hectares in the municipality highlights conservation efforts, while residential zones covering 1142.46 hectares suggest the areas designated for housing and habitation. The commercial zones occupy 136.46 hectares, cultural and archaeological zones encompass 5.86 hectares,

and public use zones provide recreational spaces over 503.04 hectares. Industrial and mine/minerals zones are relatively small, covering 14.09 hectares and 6.90 hectares, respectively. Riverine, lake, and marsh areas contribute 242.88 hectares to the overall landscape, reflecting the diverse natural features within the municipality.

The distribution pattern of land use zoning in Kushma municipality is presented in Figure 7 and ward-wise details are provided in Table 5.

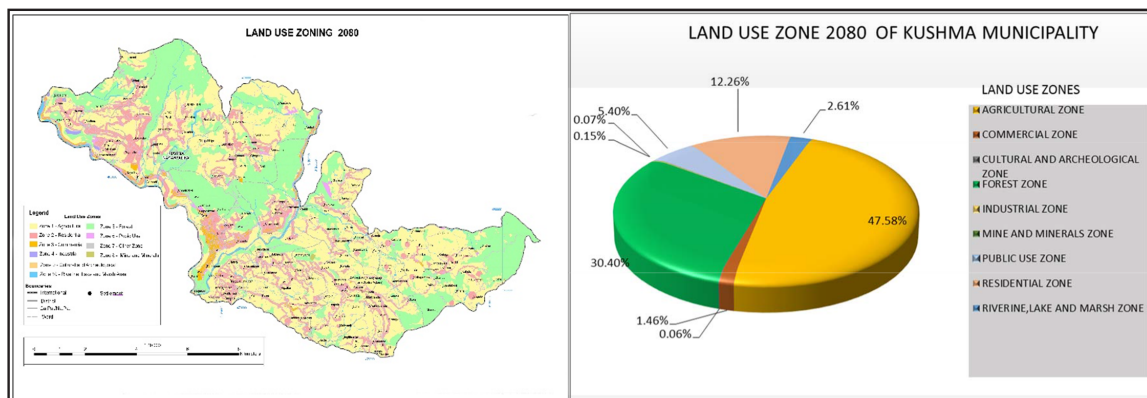


Figure 7: Land Use Zoning 2080

Table 5: Land Use Zoning 2080

LAND USE ZONES	LAND USE ZONE 2080 (AREA IN HECTARES)														Grand Total
	WARD NO.														
	1	2	3	4	5	6	7	8	9	10	11	12	13	14	
AGRICULTURAL ZONE	338.52	526.27	655.20	90.12	32.41	11.69	60.69	90.57	155.56	495.64	448.98	452.00	406.69	668.70	4433.05
COMMERCIAL ZONE	18.07	14.61	5.22	21.16	38.49	11.26	7.56	12.32	1.76	3.61	0.03	0.39	0.04	1.95	136.46
CULTURAL AND ARCHEOLOGICAL ZONE	1.37	0.32	0.49	0.49	0.81	0.25	0.05	0.11	0.20	0.17	0.17	0.07	0.53	0.83	5.86
FOREST ZONE	248.52	494.44	396.88	251.11	47.37	0.52	76.45	292.90	20.27	60.45	170.17	71.07	103.22	599.57	2832.94
INDUSTRIAL ZONE	13.47	0.05	0.00	0.05	0.00	0.00	0.00	0.51	0.00	0.01	0.00	0.00	0.00	0.00	14.09
MINE AND MINERALS ZONE	0.20	0.00	0.04	0.00	0.00	0.00	0.00	0.00	0.00	0.00	0.00	3.11	0.00	3.56	6.90
PUBLIC USE ZONE	57.66	60.72	49.59	40.24	19.55	7.34	19.87	33.67	22.53	42.32	43.35	35.80	29.04	41.35	503.04
RESIDENTIAL ZONE	148.61	197.94	118.72	57.73	1.95	3.41	37.85	64.82	82.75	135.76	72.05	78.49	75.93	66.45	1142.46
RIVERINE, LAKE AND MARSH AREA	40.15	34.20	22.79	14.14	11.67	3.83	9.25	24.29	11.36	17.07	20.43	7.52	11.59	14.59	242.88
GRAND TOTAL	866.57	1328.55	1248.93	475.04	152.26	38.30	211.72	519.21	294.42	755.02	755.19	648.44	627.04	1397.00	9317.69

4.3 Comparison Between Present Land Use 2080 and Land Use Zone 2080

Comparing the data between Present Land Use 2080 and Land Use Zoning 2080 for Kushma Municipality reveals significant shifts in land allocation across various categories. Presently, agricultural land spans 5666.14 hectares, constituting 60.81% of total land use, yet it is projected to decrease by 13.23% to 4433.05 hectares in Land Use Zoning 2080. Conversely, commercial areas, currently occupying 40.66 hectares (0.44%), are slated to expand by 1.03% to 136.46 hectares. Forested areas, accounting for 2863.77 hectares (30.74%), are projected to shrink by 0.33% to 2832.94

hectares. While industrial and mine areas remain stable at 14.38 hectares (0.15%) and 7.03 hectares (0.08%) respectively, residential zones are expected to surge by 10.65% from 149.94 hectares (1.61%) to 1142.46 hectares (12.26%). Public use areas are set to rise by 1.93% from 323.14 hectares (3.47%) to 503.04 hectares (5.40%). However, riverine, lake, and marsh areas may experience a slight reduction from 244.63 hectares (2.63%) to 242.88 hectares (2.61%), underscoring the complex interplay of urban development and environmental conservation in Kushma Municipality's future land use planning.

Table 6: Comparison Between Present Land

Use 2080 and Land Use Zone 2080

LAND USE TYPES	Present Land Use 2080		Land Use Zoning 2080		Change in Area (hectare)	Rate of Change (Percentage)
	Area (Hectare)	Percentage	Area (Hectare)	Percentage		
Agricultural	5666.14	60.81 %	4432.33	47.58 %	-1233.81	-13.23%
Commercial	40.66	0.44 %	137.09	1.46 %	96.43	1.03%
Cultural And Archeological	5.86	0.06 %	5.86	0.06 %	0	0.00%
Forest	2863.77	30.74 %	2832.94	30.40 %	-30.83	-0.33%
Industrial	14.38	0.15 %	14.09	0.15 %	-0.29	0.00%
Mine And Minerals	7.03	0.08 %	6.90	0.07 %	-0.13	0.00%
Others	2.05	0.02 %	0.00	0.00 %	-2.05	-0.02%
Public Use	323.14	3.47 %	503.04	5.40 %	179.9	1.93%
Residential	149.94	1.61 %	1142.55	12.26%	992.61	10.65%
Riverine, Lake and Marsh Area	244.63	2.63 %	242.88	2.61 %	-1.75	-0.02%
TOTAL	9317.69	100.00 %	9317.69	100.00%		

4.4 Comparison between Cadastral Parcel Superimpose on Present Land Use and Cadastral Parcel Superimpose on Land Use Zone

A comparison between the Cadastral Superimposed on Present Land Use 2080 and Cadastral Superimposed on Land Use Zone 2080 data reveals notable shifts in land utilization within Kushma Municipality. In terms of agriculture, there's a notable decrease in parcel count from 88,550 to 65,634 and in area from 4,747.36 to 3,821.62 hectares, resulting a decline in percentage from 51.90% to 41.78%. Conversely, commercial land use experiences a substantial increase, with parcel count rising from 1,599 to 5,516 and area expanding from 65.48 to 209.65 hectares, leading to an increase in percentage from 0.72% to 2.29%. Cultural and archeological sites witness a decrease in parcel count from 140 to 115 and in area from 18.73 to 8.98 hectares, with a corresponding decline in percentage from 0.20% to 0.10%. Forest areas show a slight reduction in both parcel count, from 501 to 487, and area, from 2,823.90 to 2,769.57 hectares, resulting in a decrease in percentage from 30.87% to 30.28%. Industrial areas experience a decrease in parcel count from 125 to 114 and in area from 19.10 to 9.23 hectares, leading to a decrease in percentage from 0.21% to 0.10%. Notably, the "Others" category undergoes complete elimination in the land use zone scenario, with parcel count dropping from 50 to 0 and area from 11.64 to 0 hectares. These changes underscore a significant alteration in land use allocation patterns, with some categories exhibiting minor fluctuations while others undergo more substantial shifts within the municipality.



Figure 8: Cadastral Superimpose on Present Land Use

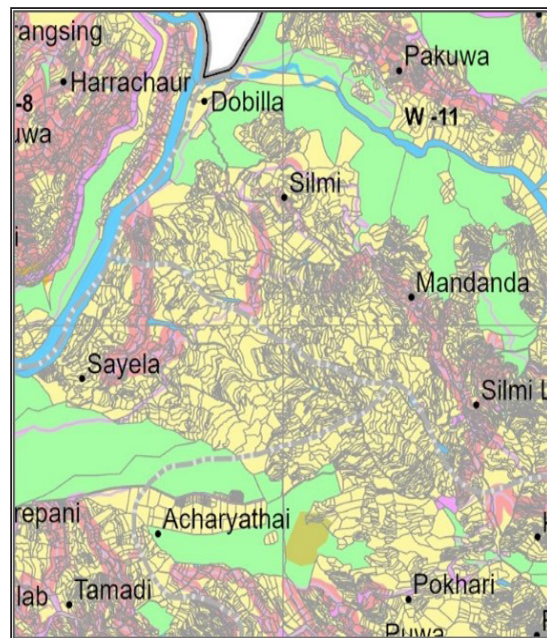


Figure 9: Cadastral Superimpose on Land use Zone

Table 7: Cadastral Parcel Superimpose on Present Land Use Vs Cadastral Parcel Superimpose on Land Use Zone

LAND USE TYPES	CADASTRAL SUPERIMPOSED ON PRESENT LAND USE 2080			CADASTRAL SUPERIMPOSED ON LAND USE ZONE 2080			RATE OF CHANGE
	No. of Parcel	Area (Hectare)	Percentage	No. of Parcel	Area (Hectare)	Percentage	
Agriculture	88550	4747.36	51.90%	65634	3821.62	41.78%	-10.12%
Commercial	1599	65.48	0.72%	5516	209.65	2.29%	1.57%
Cultural & Archeological	140	18.73	0.20%	115	8.98	0.10%	-0.10%
Forest	501	2823.90	30.87%	487	2769.57	30.28%	-0.59%
Industrial	125	19.10	0.21%	114	9.23	0.10%	-0.11%
Mine and Minerals	21	3.15	0.03%	22	3.54	0.04%	0.01%
Others	50	11.64	0.13%	0	0	0.00%	-0.13%
Public Use	3072	262.29	2.87%	3608	294.11	3.22%	0.35%
Residential	16061	1074.82	11.75%	34489	1829.7	20.0%	8.25%
Riverine, Lake & Marsh	434	120.05	1.31%	568	200.12	2.19%	0.88%
Grand Total	110553	9146.51	100.00%	110553	9146.51	100.00%	

5. CONCLUSION AND RECOMMENDATION

In conclusion, the land use zone mapping in Kushma municipality reflects a purposeful and community-centric urban development strategy. Overall, there is a clear trend towards urbanization and residential expansion, as evidenced by the notable increase in parcel count and area for residential land use. Commercial development also sees substantial growth, with an increase in both parcel count and area. However, this growth is accompanied by a decrease in agricultural land use, indicating a shift away from agricultural activities. Furthermore, while some land use categories, such as cultural and archeological sites, forest, industrial areas, and mine and minerals show minor fluctuations, others like the "Others" category witness complete elimination in the land use zone scenario. This suggests a notable restructuring of land use allocation, potentially reflecting changes in societal needs, economic priorities and environmental conservation efforts. Overall, these findings emphasize the dynamic nature of land use planning and the importance of adaptive strategies to address evolving societal and environmental challenges in urban and rural landscapes. These comparisons underscore dynamic shifts in land use patterns within Kushma Municipality, reflecting evolving urbanization, economic activities, and environmental considerations.

To realize the goals of land use policy, several key recommendations can be proposed based on land use zoning of Kushma municipality. Firstly, zoning refinement should be conducted periodically to adapt to the evolving needs. Sustainable development must be prioritized particularly in agricultural and forest zones. Infrastructure planning should be strategically aligned with residential and commercial expansion and cultural preservation efforts must safeguard significant archaeological and heritage sites. Additionally, industrial zone management should focus on eco-friendly practices through periodic assessment and revision of zoning regulations. Active community engagement is essential for inclusive decision-making and a structured monitoring and evaluation framework should be established to assess and refine land use policies regularly. Furthermore, water resource management should emphasize conservation efforts in riverine, lake, and marsh areas. An adaptive planning approach is crucial for enhancing resilience to environmental and socio-economic changes while data-driven decision-making should be supported by investments in advanced data collection tools to enable evidence-based planning. Lastly, collaboration and partnerships with key stakeholders must be fostered to ensure a holistic and well-coordinated approach to development. These recommendations

collectively aim to guide Kushma Municipality toward sustainable, resilient, and community-centered growth.

REFERENCES

- Dahal, K. (2023). Peri-urban development: Discussion with land use zoning, statutory provision, and issues inside Katahari Rural Municipality, Nepal. *Journal of Geographical Research*, 6(1), 1–16.
- MoLRM. (2015). *Land use policy 2015*. Government of Nepal.
- NLUP. (2016). *Preparation of VDC level land resource maps*.
- Sharma, R. K. (2012). Evolution of land use policy in Nepal. *Journal on Geoinformatics, Nepal*, 11, 16–21.
- United Nations. (2024). *Sustainable Development Goals*. United Nations. <https://sdgs.un.org/>
- Acharya, K. K., & Halden, R. U. (2018). *Urban planning and development in Nepal: Challenges and opportunities*. Kathmandu: Nepal Institute of Urban and Regional Studies.
- Government of Nepal. (2015). *National Urban Development Strategy*. Ministry of Urban Development.
- Food and Agriculture Organization. (1993). *Guidelines for land-use planning*. FAO Development Series 1. Rome: FAO.
- Government of Nepal. (2002). *Urban Development Policy 2002*. Ministry of Physical Planning and Works.
- Thapa, P. B. (2018). Geo-disaster and risk sensitive land use planning in Nepal. *Bulletin of Nepal Geological Society*, 35, 167–170.
- Carson, B., Shah, P. B., & Maharjan, P. L. (1986). *Land Resource Mapping Project, land systems report: The soil landscapes of Nepal*. Kenting Earth Sciences Limited.
- Oli, P. P. (2018). *Land use zoning towards the fulfillment of the 2030 agenda for sustainable development*. FIG Congress 2018, Istanbul, Turkey.
- Central Bureau of Statistics Nepal. (2021). *Population and housing census 2021: Kushma Municipality, Parbat District*. Census Nepal.
- Kushma Municipality. (2024). *Introduction to Kushma Municipality*. Kushma Municipality Office.
- Congalton, R. G. (1991). *A review of assessing the accuracy of classifications of remotely sensed data*. *Remote Sensing of Environment*, 37(1), 35–46. [https://doi.org/10.1016/0034-4257\(91\)90048-B](https://doi.org/10.1016/0034-4257(91)90048-B)



Author's Information

Name	: Er. Sushmita Subedi
Academic Qualification	: Copernicus Master in Digital Earth (MSc)
Organization	: Survey Office Parbat
Current Designation	: Survey Officer
Work Experience	: 7 years
No. Published paper/article	: 5

Remeasuring Annapurna I: Geospatial Innovation and the Quest for Precision

Er. Khim Lal Gautam¹ & Suraj Bahadur K.C.¹
gautamkhimlal@gmail.com, kcsuraj21@gmail.com
¹ Survey Department,

KEYWORDS

Mount Annapurna I, Height Remeasurement, Space Geodetic Survey, Mountain Expedition.

ABSTRACT

Mount Annapurna I, the world's tenth-highest peak and a geographic jewel of Nepal, has long captivated scientists, mountaineers, and mapmakers. Despite its significance, the mountain's officially recognized elevation- 8,091 meters—has been derived from legacy survey that vary in accuracy and methodology. In light of recent advances in geodetic science, tectonic shifts, and climate-induced landscape changes, a modern remeasurement of Annapurna I is both timely and necessary. This article explores the historical context of its elevation estimates, the scientific and technological rationale for remeasurement, and the broader geophysical, cartographic, and cultural implications. It argues that a new measurement campaign, leveraging Global Navigation Satellite System (GNSS), satellite gravimetry, and aerial photogrammetry, would enhance national geospatial data infrastructure, support environmental monitoring, and reaffirm Annapurna's place in global geoscientific research.

1. INTRODUCTION

Situated in the North-central region of Nepal, Mount *Annapurna I* is the tenth-highest mountain in the world. (Hutchinson, 2020). *Annapurna I* is the only peak which is above 8000 meters in the 55 kilometers long Annapurna Massif (Shrestha, 2021) which contains 13 peaks above 7000 meters and 16 peaks above 6000 meters (Discovery World Trekking, n.d.). It is also one of the most dangerous mountain because of changing terrain, violent windstorms, and frequent avalanches (Firth et al., 2008). *Annapurna I* was named after hindu goddess of food and nourishment (Nepal Himal Peak Profile, n.d.). The word *Annapurna Is* derived from Sanskrit word where Anna means food and purna means 'filled with'. Therefore, the designation

can be interpreted as "The Deity Abundant in Nourishment" or, in simpler terms, as "The Supplier" (Baume, 1978).



Figure 1: Mt. Annapurna I from North Base Camp (Photo: Nima Rinji Sherpa, youngest and fastest climber of all 8,000-meter peaks.)

Although 10th highest in the world and the 8th highest mountain of Nepal, it is one of the most well-known mountains. *Annapurna I* is located within the Annapurna Conservation Area Nepal largest protected region, covering 7929 Km² (NTNC, n.d.) one of the regions of Nepal attracting hordes of trekkers from all around the world. Despite its fame among mountaineers for being one of the most dangerous peaks to climb, its precise elevation has long been taken for granted (Prajwalol, 2023). In the face of advancing geodetic technology, increased tectonic activity in the region, and the growing need for accurate geospatial data (KC & Acharya, 2022), re-measuring Annapurna has become a matter of geodetic pride and scientific necessity.

2. EXPEDITIONS IN ANNAPURNA

Maurice Herzog and Louis Lachenal successfully summited Annapurna I on June 3, 1950, marking the first ascent of an 8,000-meter peak (Huey & Eguskitza, 2001). Sherpa climber Ang Tharke was the Guide for this expedition. However, Tharke couldn't make it to the summit because of frostbite at the last camp (Herzog, 1951).

This achievement was a significant milestone in the history of mountaineering. Herzog later wrote a book titled "Annapurna" detailing their expedition, the challenges they faced, and the triumph of reaching the summit. The success on Annapurna I was a remarkable feat in the early exploration of high-altitude peaks.

Sonam Wolang Sherpa made history as the first Nepali to make it to the peak of Annapurna I on October 13, 1977. Till 2022 summer 407 summiteers (some of them repeated scale) have successfully scaled this mountain. (Department of Tourism, 2023, 335)

Annapurna I is notorious as the 'Killer Mountain' due to its challenging ascent (NCESC, n.d.). The Himalaya Database reveals a daunting statistic—1 in 4 climbers

attempting to scale the mountain have perished. In the 2021 season, over 50 climbers conquered the peak, bringing joy as, remarkably, no fatalities occurred among the successful ascents that year. (Himalayan Database, 2021). In recent years, the fatality rate has decreased owing to factors such as sophisticated climbing equipment, tools, and accurate weather forecasts.

Recent expeditions have increasingly incorporated geodetic instruments such as handheld GNSS receivers and altimeters, though these are often limited in accuracy. What remains missing is a comprehensive, scientifically robust remeasurement campaign that integrates modern surveying techniques with high-altitude logistics. A well-equipped expedition, combining professional mountaineers and geodetic experts, could yield critical data not only for validating Annapurna's current elevation but also for understanding how tectonic and climatic forces continue to reshape this iconic massif.

3. FROM BATTLE TO TRIANGULATION

The British rulers, understanding the importance of safeguarding and expanding their colonies, knew the significance of having a plan. Whether for development or waging wars, a map was deemed essential. This awareness became more pronounced after the East India Company lost three wars with Haider Ali, the King of Mysore, and his son Tipu Sultan between 1767 and 1791 AD. The British, resorting to various conspiracies and diplomatic maneuvers, launched another attack on Mysore in 1798 after exploring different strategies. After a long, bloody battle in 1799, they successfully unfurled the British flag in Mysore (Kochhar, 2013). After the victory over Mysore in 1799, the Britishers reflected on the reasons behind their repeated defeats in previous wars. They concluded that their defeats resulted from waging wars without

organized plans. Recognizing the importance of a map, they understood that organized warfare was challenging without one.

For this, in May 1799, Lord Sir Richard Belesli ordered Lieutenant Colonel William Lambton to survey and prepare a map of India. Lambton was also a surveyor and an Army officer injured in the Mysore war. The British also wanted to know how much land they had conquered following the victory over the Mysore war. Following the lord's order, Lambton commenced planning for the map, working on astronomical observation. Lambton came up with a plan within seven months by November, which the lord approved. With this, some basic works of surveys had also been completed by then. He eventually started the geographical and mathematical survey after three years in 1802 AD (Roy, 1986). It was during this survey that it was known that Annapurna I towered over 8000 meters. The record shows that the peak was initially registered in the field book as Peak XXXIX.

4. ANNAPURNA I-THE PEAK XXXIX

On April 10, 1802, the British formally commenced the trigonometrical survey with the measurement of the baseline, spanning 12.1 kilometers along the Madras seashore (present-day Chennai). From 1818, it was officially named the Great Trigonometrical Survey of India (Kumar, 2012). It was headed by Colonel William Lambton. Thanks to this mega-project, many of the highest mountains of Nepal including Sagarmatha (Mt. Everest) were identified as the world's highest peak.

During the British rule, the surveyors of Survey of India conducted trigonometric surveys and mapping the Himalaya from the Chomolhari Himal in Bhutan to Nanda Devi in Garhwal, covering 79 major peaks to determine their positions and elevations (Phillimore, 1958). As the local names of all the Himalayan peaks were not known, they temporarily named them using Roman numerals. Just like the world's

highest peak was called peak XV, Annapurna I was referred to as Peak XXXIX in Roman numerals. The calculation of Annapurna I elevation from sea level, performed at the East India Survey Department headquarters in Dehradun, showed it to be 26,492 feet (8,075 meters) tall (Tilman 1951). This standard was established by triangulation stations at eight points near the Nepal-India border. The long distance and the length of the summit range made it harder to accurately pinpoint the exact position. In trigonometric surveys, the precision of height measurement relies on accurately gauging the distance from the observation point to the summit.

It was only known after a very long time that the Peak XXXIX, which the British surveyors had measured, was actually *Annapurna I*. Later, in 1929, the British Survey of India prepared the map of this region in the scale of 1 inch to 4 miles, and that map showed *Annapurna I*'s elevation as 8078 meters. However, in the 1963 map, the peak's elevation is noted as 8,091 meters.

Table 1: Table 1: List of Mountain peak with coordinate and height. Source: Burrard, S. G., & Hayden, H. H. (1908).

SN	Name of Peak	Ht in feet	Latitude	Longitude	Location
1	T ⁴⁵	26867	28°5'32"	86°36'51"	Nepal Himalaya
2	Dhaulagiri	26795	28°41'48"	86°29'42"	Nepal Himalaya
3	XXX	26658	28°33'0"	84°33'43"	Nepal Himalaya
4	Naga parbat I	26620	35°14'21"	74°35'24"	Punjab Himalaya
5	XXXIX	26492	28°35'44"	84°49'19"	Nepal Himalaya
6	K ⁶ or Gasherbrum I	26470	35°43'30"	76°41'48"	Karakoram
12	K ⁴ or Gasherbrum II	26360	35°45'31"	76°39'15"	Karakoram
7	Gosainthan	26291	28°21'07"	85°46'55"	Nepal Himalaya
8	K ^{3a} or Gasherbrum III	26090	35°45'36"	76°38'33"	Karakoram
9	XXXIV	26041	28°32'5"	84°7'26"	Nepal Himalaya
10	K ³ or Gasherbrum IV	26000	35°45'38"	76°37'2"	Karakoram

(*The values of longitude are based upon the determination of the difference between Greenwich and Madras Made in 1894-96 and are not those hitherto accepted by Survey of India at that time)

It can be seen that the elevation is different from the ones calculated by the Great Trigonometrical Survey. It can be understood that the field observation was an effort for greater accuracy in their data. Before making the map, the Survey of India had secretly sent their surveyors to various places in Nepal for field verification (Pradhananga, 2007), as Nepal is officially close to foreigner before 1950 (Adhikari, 2018)

Some books written on peaks above 8000 meters have also discussed the confusion and uncertainty on the part of the Survey of India regarding the exact height of Annapurna because the viewpoint for the triangulation survey was prone to errors due to distance and the need to cover a long mountain range for observation. 'To the Third Pole,' by Dyhrenfurth (1955), a book published in London in 1955, has delved into this issue. The book, translated from German to English, notes 8078 meters (26504 feet) as the height of *Annapurna I*. Here is an excerpt from Chapter Six of the book which states:

“The official readings of 26,811 feet (8172 metres) For Dhaulagiri and 26,504 feet (8078 metres) for Annapurna, are minima which probably need adjusting upwards by 130 to 170 feet.” (Dyhrenfurth,1955)

The Survey of India, based on aerial surveys between December 1957 to June 1958 and subsequent ground verification (1959-60), published a map in 1963. On map sheet number 62 p/14, a point broadly identified as 'Annapurna Himal' is noted at 26545 feet (8091 meters). However, the map makes no mention of Annapurna I (Survey of India, 1963).

The map published by Nepal, following field verification in 2001, also lists the height of Annapurna I as 8091 meters. It is evident that Nepal's survey, considering the similarity in elevation and location details to our original map, may have derived the height from the

Survey of India's map, even though the latter does not explicitly mention the name.



Figure 3: Map published by Survey of India in 1963 with the scale of 1 inch equal to 1 mile

In 2014, a specialized aircraft from the German Space Agency (DLR) was employed to create a digital elevation model and GIS map of the Annapurna range, covering area of radius 6 to 8 km. The primary objective was to assess the parameters of their newly developed three-dimensional aerial camera system, known as MACS (Modular Airborne Camera System).

The aim of DLR was to check the various parameters of the MACS aerial photogrammetric camera and to create different GIS products like a topographic map which can be helpful to study different topographical phenomena of the region like the study of landslide susceptibility as the region is most prone to landslide (KC, 2018).



Figure 4: Summit of Annapurna I (left) and Machhapuchhre (right,) in front DLR motorized glider with special 3D camera,

Some unofficial sources claim that the summit of Annapurna I stands at a height of 8097.47 meters, calculated from aerial photos taken from the special airplane, which needs further verification.

The base map of Nepal was prepared based on Indian topographical map series (Baidar et al., 2023). Except Mt Everest, the Survey Department has not conducted direct field observation to determine the elevations of any prominent mountains. Observing variations in the heights of Annapurna I over time, it's now crucial for us to conduct a detailed scientific study. This emphasizes the importance of accurately measuring the heights of all peaks, especially those exceeding 8,000 meters.

6. WHY REMEASUREMENT

The Annapurna region, despite being a popular Himalaya tourist destination, remains relatively underexplored in terms of comprehensive scientific research.

The Annapurna region, despite being a well-known destination for trekkers and climbers, remains relatively underexplored from a scientific research perspective. While numerous national and international institutions focus on accurately measuring the peak of Sagarmatha and surroundings, there is a notable lack of interest in measuring Annapurna I (Manandhar, 2017).

The region is famous for its stunning scenery and many tourists and scientists visit the region and are curious about the height of this peak. Conducting GNSS measurements not only provides accurate geo information and height but also significantly contributes to various Earth science research endeavors (Abdelazeem et al., 2024).

Annapurna range has large glaciers that are melting due to climate change which can cause the region prone to avalanches and landslides (Khadka et al., 2023). Geospatial and geodetic data collected from the Annapurna region are

invaluable for research on tectonic activity and geohazards, as they provide critical insights into the region's structural evolution and seismic hazards (Bilham et al., 1997).

Past measurements relied on traditional surveying. Now there has been huge technical improvement in precision surveying. Using modern methods like GNSS improves the precision of measurement. GNSS gives precise position and ellipsoidal height. With the advancement in gravity measurement techniques from satellite, airborne and terrestrial, we now have access to high resolution and accurate gravity data which can be used to refine elevation with respect to mean sea level by creating geoid model. The accurate height measurement resolves the doubt in inconsistent previous measurements (Bolkas et al., 2016). This project not only determines the orthometric height of the peak but also contributes to enhancing the geodetic network in Nepal's Mid-Himalaya region around Pokhara City (Oli, 2007).

7. TECHNOLOGICAL METHODOLOGY

Height determination integrates precise ground GNSS surveys and applying corrections and geoid models for accurate elevation data. (Dangol et al., 2021). The proposed methodological framework should include the following components:

7.1 Review of Existing Horizontal and Vertical Control Networks and Gravity Data.

The proposed activity includes

- Densifying the existing network using modern GNSS and leveling instruments for both horizontal and vertical control points, as well as gravity points.
- Updating coordinates and evaluate shifts from tectonic activity, especially post-2015 Gorkha earthquake.

7.2 Establishment of CORS and GNSS Observation

Continuous Operating Reference Stations (CORS) station can be established and used as stable base station. These stations can provide a precise and stable reference framework for GNSS observations necessary for accurate coordinate determination.

7.3 Precise Levelling and Gravity Survey

The primary objective of this task is to establish accurate vertical control and define a precise local geoid model. Key activities include:

- Conducting precise leveling to transfer orthometric heights from existing leveling benchmarks to the CORS stations and perform trigonometric leveling using CORS as base station to provide independent validation.
- Carrying out dense and uniformly distributed relative gravity observations using relative gravimeter. The observations can be tied to the nearest absolute gravity station.
- Conducting GNSS observations at leveling benchmarks and gravity stations to for geoid determination.

7.4 Summit Observation

At least two surveyors will deploy high-precision GNSS instruments along with Ground Penetrating Radar (GPR) devices at the summit. An adequate number of reference stations will be established around the Annapurna Massif to ensure accurate summit positioning.

7.5 Data Processing Validation and Height Determination

CORS and GNSS data can be processed incorporating data from International GNSS Service (IGS) stations. The final precise height will be published following the completion of data processing.

Surface Gravity data can be processed and combined with airborne gravity data, Digital Terrain Model, and the Global Gravity Models (GGMs). Incorporating the latest GGM will further enhance the accuracy of the geoid model.

7.6 Photogrammetry and 3D Modeling

To know more details about summit morphology and to provide secondary reference for height estimation, 3D modelling can be conducted using aircraft or UAV.

8. COLLABORATORS AND STAKEHOLDERS

The success of re-measuring Mount Annapurna requires a **multi-disciplinary, cross-institutional partnership** involving expertise in **geodesy, remote sensing, climate science, mountaineering, and local government**. Key collaborators and stakeholders might be :

- Department of Tourism, the National Mountain Administration Agency of Nepal under Ministry of Culture, tourism and Civil Aviation.
- Ministry of Forest and Environment of Nepal.
- National/ international universities and research institutes.
- Space agencies (NASA, ESA, DLR)
- International Development Partners, given that Annapurna I was first climbed by a French expedition, there's an interesting historical link that could be leveraged. The *Agence Française de Développement* (AFD) or other international development agencies might have interest in supporting scientific and cultural projects in Nepal. Also, we should collaborate with German Aerospace Centre (DLR), as they conducted aerial survey over Annapurna massif in 2014.

- Gandaki Providence
- Mountaineering and expedition agencies.
- Survey Equipment and Technology Providers such as Trimble, Leica, Geosystem,

9. EXPECTED OUTCOMES

Re-measuring Annapurna using state-of-the-art geodetic and remote sensing techniques will result in multiple scientific, cartographic, and societal benefits. The key expected outcomes include:

- **Accurate, Up-to-Date Elevation of the summit of Annapurna I**
- strengthening the geodetic network of the region.
- Scientific Insights into Tectonic and Climatic Processes,
- Improved National and Global Mapping Infrastructure,
- Capacity Building and Research Collaboration
- Long-Term Monitoring Framework
- Public Awareness and Educational Outreach.

10. OPPORTUNITIES AND CHALLENGES

Nepal's Survey Department measured Sagarmatha using its own resources, producing number of skilled geodesists. They gained experience with handy tools, and the department can complete this project efficiently. However, to materialize the idea, one of the important aspects is funding.

Opportunity and challenges are two sides of a coin. With every opportunity comes challenges. The most important and daunting challenge of this mission is to climb one of the technically challenging peaks, conduct summit observation, and gather accurate data. Other

challenges include raising ample resources for the expedition, obtaining necessary gears and technological devices, managing the expenses required for manpower for ground survey, and addressing possible technical difficulties of working in harsh geographical areas.

It would be a matter of pride for the Survey department to measure Annapurna I, the first eight-thousand peak to be scaled—with its own human resources based on its own data.

11. CONCLUSION

Nepal is home to eight peaks towering above 8000 meters, which attract a significant number of foreign tourists every year. Among them, Annapurna I stands as an unparalleled gem in the realm of global mountaineering. While other countries in Asia also have mountains, Nepal's peaks remain unmatched in their breathtaking beauty. Nepal's mountains are not just natural wonders—they are cultural, economic, and geographic assets. Therefore, it is imperative to tell the world about these mountains, advertise their majestic beauty and explore various unknown and unexplored facts related to them.

Annapurna I is a mountain full of mysteries and suspense. Many world-renowned climbers come to Annapurna to climb the peak and seek glory. The peak also holds several environmental and religious importance. Despite its fame, Annapurna remains understudied in comparison to Everest and other Himalaya giants. Re-measuring Annapurna I is not just about correcting numbers—it's about deepening our understanding of Himalaya geology, climate impacts, and geohazards. Successful remeasurement not only gives precise height but the initiative contributes to broader geoscientific goals. It will refine regional geoid model, quantify crustal deformation, and bolster hazard assessment across Nepal's central Himalaya. Ultimately, this work underscores the critical role of

high-precision geodesy in supporting national development strategies and advancing global Earth observation efforts and inspiring future research in the region.

The study presents a comprehensive framework for the remeasurement of *Mount Annapurna I*, building upon the methodological precedent established during the recent Sagarmatha height measurement campaign completed in 2020. This study integrates cutting-edge geospatial technologies, such as GNSS, gravity observations, and precise leveling to improve the accuracy of topographic data in tectonically active regions.

REFERENCES

- Abdelazeem, M., Abazeed, A., Kamal, H. A., & Mohamed, M. O. A. (2024). Towards an accurate real-time digital elevation model using various GNSS techniques. *Sensors*, 24(24), 8147. <https://doi.org/10.3390/s24248147>
- Adhikari, D. R. (2018). A small state between two major powers: Nepal's foreign policy since 1816. *Journal of International Affairs*, 1(1), 19–38. Retrieved from <https://nepjol.info/index.php/joia/article/view/22575>
- Armchair Mountaineer. (n.d.). Annapurna: The first 8000-meter peak. The Armchair Mountaineer. Retrieved April 22, 2025, from <https://armchairmountaineer.com/annapurna>
- Baidar, T., Lama, B., Gyawali, R., & Pokhrel, G. (2023). Topographic base map update in Nepal: Overview, accomplishments and way forward. *Nepalese Journal of Geoinformatics*, 22(1), 69–78. <https://doi.org/10.3126/njg.v22i1.55129>
- Baume, L. C. (1978). Sivalaya: The 8000-metre peaks of the Himalaya – a chronicle and bibliography of exploration.
- Bilham, R., Larson, K., & Freymueller, J. (1997). GPS measurements of present-day convergence across the Nepal Himalaya. *Nature*, 386(6620), 61–64. <https://doi.org/10.1038/386061a0>
- Bolkas, D., Fotopoulos, G., Braun, A., & Tziavos, I. N. (2016). Assessing digital elevation model uncertainty using GPS survey data. *Journal of Surveying Engineering*, 142(3), 04016001. [https://doi.org/10.1061/\(ASCE\)SU.1943-5428.0000169](https://doi.org/10.1061/(ASCE)SU.1943-5428.0000169)
- Burrard, S. G., & Hayden, H. H. (1908). A sketch of the geography and geology of the Himalaya Mountains and Tibet. Calcutta: Superintendent of Government Printing, India.
- Dangol, S., Joshi, P., KC, S.B., Thapa, M., Banjara, B., KC, S., & Bhandari, S. (2021). Measurement of the height of Mt. Sagarmatha (Everest) – Methodology and results. *Nepalese Journal of Geoinformatics*, 20, 59–66.
- Discovery World Trekking. (n.d.). Annapurna Mountain Range and Conservation Area. Discovery World Trekking blog. Retrieved April 22, 2025, from <https://www.discoveryworldtrekking.com/blog/annapurna-mountain-range>
- Dyhrenfurth, G. O. (1955). To the Third Pole: The History of the High Himalaya. London: Werner Laurie (English edition).
- Firth, P. G., Zheng, H., Windsor, J. S., Sutherland, A. I., Imray, C. H., Moore, G. W. K., Semple, J. L., Roach, R. C., & Salisbury, R. A. (2008). Mortality on Mount Everest, 1921–2006. *BMJ*, 337, a2654. <https://doi.org/10.1136/bmj.a2654>
- Gautam, P. (n.d.). Mountains' Mysteries: Unraveling the mystical allure of Mount Everest and Mount Annapurna. [Unpublished manuscript or article].

- Herzog, M. (1951). Annapurna. *The Alpine Journal*, 58, 155–168. Retrieved from the Alpine Journal Archive: https://www.alpinejournal.org.uk/Contents/Contents_1951_files/AJ58%201951%20155-168%20Herzog%20Annapurna.pdf
- Huey, R. B., & Eguskitza, X. (2001). Limits to human performance: Elevated risks on high mountains. *Journal of Experimental Biology*, 204(18), 3115–3119. (Discusses the physiological challenges at altitude; context for 1950 climb.)
- Hutchinson, J. L. (2020). Climate change, “Everestification,” and the future of mountaineering on Annapurna I (Master’s thesis, Evergreen State College). Olympia, WA: Evergreen State College Archives.
- KC, S. B. (2018). Photogrammetric surface reconstruction from oblique and nadir looking aerial images in the extreme environment of the Himalayan area “Sabche Cirque” (Master’s thesis). German Aerospace Center (DLR) – Institute of Optical Sensor Systems. Retrieved from <https://elib.dlr.de/124099>
- KC, S., & Acharya, T. D. (2022). Advancements of geodetic activities in Nepal: A review of pre- and post-2015 Gorkha earthquake eras with future directions. *Remote Sensing*, 14(7), 1586. <https://doi.org/10.3390/rs14071586>
- Khadka, N., Chen, X., Sharma, S., & Shrestha, B. (2023). Climate change and its impacts on glaciers and glacial lakes in Nepal Himalayas. *Regional Environmental Change*, 23(143), 1–14. <https://doi.org/10.1007/s10113-023-02142-y>
- Kochhar, R. (2013). Natural history in India during the 18th and 19th centuries. *Journal of Biosciences*, 38(2), 201–224. <https://doi.org/10.1007/s12038-013-9303-4>
- Kumar, D. (2012). Policies for scientific expansion. In P. Petitjean, C. Jami, & A. M. Moulin (Eds.), *Science and Empires: Historical studies about scientific development and European expansion* (Vol. 136, pp. 269–271). Dordrecht: Springer.
- Lavé, J., Guérin, C., Valla, P. G., Guillou, V., Rigaudier, T., Benedetti, L., France-Lanord, C., Gajurel, A. P., Morin, G., Dumoulin, J. P., Moreau, C., & Galy, V. (2023). Medieval demise of a Himalayan giant summit induced by mega-landslide. *Nature*, 619(7968), 94–101. <https://doi.org/10.1038/s41586-023-06086-4>
- Manandhar, N. (2022). Concept in determining the height of Mount Everest (Sagarmatha). *Nepalese Journal of Geoinformatics*, 21, 1–10. <https://doi.org/10.3126/njg.v21i1.45113>
- NCESC, (n.d.). Why is Annapurna so dangerous? NCESC Geographic Pedia. Retrieved 2025, from <https://www.ncesc.com/geographic-pedia/why-is-annapurna-so-dangerous/>
- Nepal Himal Peak Profile. (n.d.). Annapurna I – Nepal Himal Peak Profile. Retrieved from <https://nepalhimalpeakprofile.org/annapurna-i>
- National Trust for Nature Conservation (NTNC). (n.d.). Annapurna Conservation Area Project (ACAP). Retrieved from <https://ntnc.org.np/project/annapurna-conservation-area-project-acap>
- Oli, P. P. (2007). Astronomy and gravity surveying in Nepal. *Nepalese Journal of Geoinformatics*, 6(1), 16–24. <https://doi.org/10.3126/njg.v6i1.51219>
- Phillimore, R. H. (1958). Historical Records of the Survey of India, Vol. V (1844–1861). Dehradun: Survey of India.

- Prajwalol, (2023,). Mount Annapurna: The majesty of Nepal’s Himalayas. Nepal Database. Retrieved from <https://www.nepaldatabase.com>
- Pradhananga, T. B. (2007). Surveying and mapping in Nepalese context. *Nepalese Journal of Geoinformatics*, 6(1), 106–110.
- Roy, R. (1986). Science and politics: Understanding colonial science. In P. Petitjean, C. Jami, & A. M. Moulin (Eds.), *Science and Empires: Historical studies about scientific development and European expansion* (pp. 269–271). Dordrecht: Springer.
- Shrestha, S. (2021). Impact of climate change on snow cover and tourism in Annapurna region of Nepal (Master’s thesis). (Publication No. 28451354) ProQuest Dissertations Publishing.
- SoI, (1929). Topographic Map – Annapurna Himal (1 inch to 4 miles) [Map]. Dehradun: Survey of India.
- SoI. (1963). Topographic Map Sheet No. 62 P/14: Annapurna Himal [Map]. Dehradun: Government of India.
- Thapalia, B. (2025). Annapurna Massif: Majestic peaks, treks, and climbing routes. *MysticAdventureHolidaysBlog*. Retrieved from <https://mysticadventureholidays.com> (General information on Annapurna region, tourism.)
- Tilman, H. W. (1951). Annapurna Himal and south side of Everest. *The Alpine Journal*, 58, 101–110. (Mentions early survey heights of Annapurna I as computed by Survey of India.)
- DoT, (2023). *Mountaineering in Nepal: Facts & Figures 2023*. Kathmandu: Government of Nepal, Ministry of Culture, Tourism & Civil Aviation. (Includes statistics on Annapurna I summiteers up to 2022; see p. 335.)
- Himalayan Database. (n.d.). Annapurna I – Expedition Archives. The Himalayan Database (E. Hawley & R. Salisbury, compilers). Retrieved 2025, from <http://www.himalayandatabase.com>



Author's Information

Name : ER Khim Lal Gautam
 Academic Qualification : M. Sc. GIS
 Organization : Survey Department
 Current Designation : Chief Survey Officer
 Work Experience : 20 years



Nepal Geomatics Engineering Society (NGES)

website: www.nges.org.np

email: contactgeomatics@gmail.com

Executive Committee

President

Er. Mahesh Thapa

Vice-President

Er. Bhuwan Singh Bisht

Secretary

Er. Ashok Shrestha

Joint-Secretary

Er. Pranjali Basnet

Treasurer

Er. Susmina Manandhar

Executive Members

Er. Binod Prasad Bhatta

Er. Gorkah Nath Pandey

Er. Samrat Acharya

Er. Sanisha Gharti Pun

Er. Vibek Dumre

Er. Dristi Bajimaya

Er. Sushil Subedi

Er. Kriti Kajol Chudal

Photo Feature

[Participant closely examining maps during the mapping competition]



[A glimpse of talk program on Nepal's addressing system]



About NGES

Geomatics Engineering was introduced in Nepal over two decades ago in response to the growing need for professionals specializing in geospatial information. Currently, Geomatics Engineering programs are offered at Purbanchal University, Kathmandu University, and Tribhuvan University. To date, more than 850 Geomatics Engineers are registered with the Nepal Engineering Council.

Nepal Geomatics Engineering Society (NGES) was established on August 16, 2015, to foster the development of the geomatics engineering discipline in Nepal. Serving as an umbrella organization for Geomatics Engineers across the country, NGES aims to connect geomatics professionals, promote the application of geospatial technologies, enhance professional skills, and safeguard the rights of its members, all while contributing to national progress.

KEY EVENTS

Talk Program Addressing System in Nepal

Nepal Geomatics Engineering Society (NGES), in collaboration with RUPSON and supported by the Asia Foundation's Data for Development Program, organized an event on September 19, 2023, focused on the addressing system in Nepal. The event brought together experts, government officials, and private sector representatives. Participants highlighted the absence of a definitive regulatory body for the addressing system in Nepal and emphasized the urgent need to establish standardized methods to support effective governance and service delivery.

Talk program on Disaster Risk Reduction

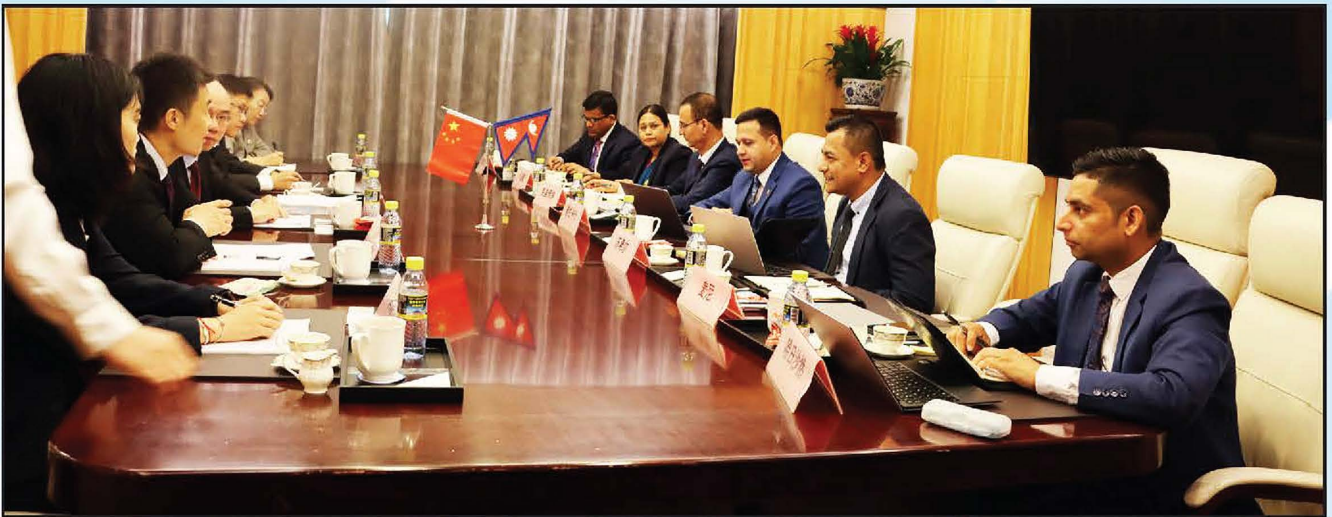
NGES organized a virtual talk on "Geospatial Technologies for Disaster Risk Reduction" on October 13, 2022, in observance of International Disaster Risk Reduction Day. The program emphasized the crucial role of geospatial technologies in acquiring and analyzing spatial data throughout all phases of the disaster management cycle. It also highlighted the use of collaborative platforms such as OpenStreetMap, which enables communities and disaster management agencies to collectively map critical infrastructure and local features, thereby improving risk assessment, early warning, and disaster response efforts.

Mapping Competition

Nepal Geomatics Engineering Society (NGES) organized the "Map Design Competition, Slogan Competition, and Talk Program" on November 16, 2022, in celebration of GIS Day. The event was held at the Survey Department hall and saw participation from over 50 contestants.

GEO-SERIES

Nepal Geomatics Engineering Society (NGES) has aired 15 episodes of "Geo-Series," a well-known virtual program that brings together national and international leaders in the geospatial field. These experts have generously shared invaluable knowledge and experiences, significantly empowering geo-professionals. Geo-Series serves as a dynamic platform for sharing insights and advancing understanding across a wide range of topics—from career advice to cutting-edge developments in geo-information technology.



Nepali delegation team led by Director General of Survey Department Mr. Prakash Joshi in JEG meeting, at Beijing China.



Director General Mr. Prakash Joshi and Director Mr. Tanka Prasad Dahal participating in UNGGIM AP plenary meeting, Delhi 29 Nov. 2024



Director Tanka Prasad Dahal participating in "Evolving Role of National Mapping Agencies: Transitioning towards Geospatial Knowledge Infrastructure (GKI) from 30 November-5th December 2024, Hyderabad, India.

Making Sense of Geo-spatial data for total solution in National and Local Development Activities

Available Maps and Data

- ❖ Geodetic Control Data
- ❖ CORS Station Data
- ❖ Geoid Data
- ❖ Aerial Photographs
- ❖ Topographic Base Maps
 - ❖ Terai and middle mountain at the scale of 1:25,000
 - ❖ High hills and Himalayas at the scale of 1:50,000
- ❖ Land Use Maps
- ❖ LiDAR Data
- ❖ Political and Administrative Map of Nepal
- ❖ Digital Topographic Data at scales 1:25,000 & 1:50,000
- ❖ Cadastral Plans
- ❖ Orthophoto Maps
- ❖ Image Data
- ❖ SOTER Data
- ❖ Topographic Digital Data at scales 1:100,000 1:250,000 1:500,000 1:1,000,000

Available Services

- ❖ Establishment of control points for various purposes of Surveying and Mapping
- ❖ Cadastral Surveying
- ❖ Surveying and mapping for development activities
- ❖ Topographic and large scale mapping
- ❖ Digital geo-spatial database support
- ❖ GIS Development

Price of some of the publications of Survey Department

- List of Geographical Names, Volume I to V – NRs 600/- per volume.
- The Population and Socio - Economic Atlas of Nepal, 2011 (HardCopy) NRs.2,500.00 (In Nepal), €200.00 (Outside Nepal)
- The Population and Socio - Economic Atlas of Nepal, 2011 (CDVersion) NRs.250/-

Contact Address:

SURVEY DEPARTMENT

Min Bhawan, Kathmandu, Nepal
Phone: +977-1 -4106508, Fax: +977-1 -4106757
E-mail: info@dos.gov.np
website: www.dos.gov.np

